UNIVERSITY OF TURKU

The need and validation of a HER2 positive Breast cancer spheroid models for antibody drug conjugate research and development

Drug Discovery and Development

Institute of Biomedicine

Master's thesis

Orion pharma, Oncology R&D, ADC research team

Author:

BSc Joakim Gustafsson, Joakim.p.gustafsson@utu.fi

Supervisors:

PhD Antti Arjonen, antti.arjonen@orionpharma.com

MSc Reetta Riikonen, reetta.riikonen@orionpharma.com

PhD Ullamari Pesonen, ullamari.pesonen@utu.fi

16.10.2025

Turku

Master's thesis

Subject: Drug discovery and development
Author: Joakim Gustafsson
Title: The need and validation of HER2 positive Breast cancer spheroid models for antibody drug conjugate research and development
Supervisors: Senior scientist, PhD, Antti Arjonen; Senior scientist, MSc Reetta Riikonen and Professor, PhD, Ullamari Pesonen
Number of pages: 82 pages
Date: 16.10.2025

Abstract

Antibody drug conjugates (ADCs) are a relatively new drug modality, where instead of using antibodies to inhibit the function of overexpressed oncogenic tyrosine kinase receptors on the cell surface, ADCs can target any protein on the cell membrane and via internalization of the target protein, deliver a cytotoxic payload into the cancer cell.

Enhertu (T-DXd) and Kadcyla (T-DM1) are FDA and EMA approved ADCs for the treatment of HER2 positive breast cancer. Enhertu has been shown to have better responses in the clinics compared to Kadcyla. However, similar difference in efficacy, has not been able to be demonstrated in the standard dose-response studies with *in vitro* monolayer (2D) cell cultures.

It is known that ADCs suffer from weak penetration into the tumor tissue in patients. The efficacy of Enhertu is likely due to the high antibody to drug ratio and the bystander effect of the payload Deruxtecan (DXd) compensating for the lower ADC exposure caused by the weak penetration. These characteristics require a three-dimensional (3D) model like a spheroid to observe their advantages.

Two HER2+ Breast cancer spheroid models and one HER2-negative spheroid model were developed, and their antibody internalization and ADC cytotoxicity dose-response were studied, and the results were compared to their corresponding 2D results.

We found that there were noticeable differences in the cumulative intake of trastuzumab between 2D and 3D culture formats. The HER2+ models showed increased insensitivity to Topoisomerase 1 inhibitors, which lead to a reduced cell killing with T-DXd, DXd and Exatecan. T-MMAF and T-DM1 showed the same relative efficacy ranking across both 2D and 3D culture formats. The 2D culture format with HCC1954 cell line was observed to overestimate the efficacy of all ADCs in comparison to the 3D culture format.

Immunofluorescent staining and confocal imaging were successfully conducted to assess the ADC penetration and payload distribution of T-DXd inside a spheroid.

Key words: Antibody drug conjugate, ADC penetration, Breast cancer, Bystander effect, Confocal imaging, Dose-response, HER2-targeted therapy, Internalization, Spheroid

Table of contents

1 Introduction

1.1 Breast cancer

Breast cancer (BC) is ranked second leading cause of death worldwide (Siegel et al., 2025). According to the latest cancer statistics, the projection for female cancer cases in 2025 estimates 988,660 new cases and 294,220 deaths. Among these figures, BC is expected to account for 316,950 new cases and 42,170 deaths (Siegel et al., 2025). The incidence rate has increased annually for 1,6% during 2017-2021 to the point where currently one of every eight women will develop BC during their lifetime (Siegel et al., 2025). Thanks to the advances in cancer therapies and proactive screening for tumours, the BC five-year relative survival rate has been 91% for women of all races during 2014-2020. But the five-year survival rate for metastasized BCs is only 32% which is 6% of all BC cases (Siegel et al., 2025).

BC arises from the mammary glands, which are composed of adipose and glandular tissue. Glandular tissue is the functional component, which consists of approximately 15 to 25 lobes. Each lobe is further divided into several lobules, which house 10 to 100 alveoli. These alveoli are responsible for secreting milk into the lumen, where it is subsequently stored. The lumen of different alveoli are connected via lactiferous ducts, which merge to form a lactiferous sinus (Figure 1.)(Biswas et al., 2022). BCs can be histologically divided into a variety of different subtypes of which invasive ductal carcinoma and invasive lobular carcinoma are the most common subtypes. Invasive ductal carcinoma also known as ”no special type”, is the most common subtype consisting of 40-80% of cases (Erber and Hartmann, 2020). These tumors originate from the lactiferous ducts and exhibit a diverse range of morphologies that lack the characteristics of any specific subtype. Their growth patterns may manifest as tubules with good ductal differentiation, in a trabecular arrangement, or in a solid form with nests or cords. Invasive lobular carcinoma accounts for 5-15% of all cancer cases (Erber and Hartmann, 2020). They originate from the terminal end buds and are distinguished by a unique single-file growth pattern and discohesive cell formation with a reduction in E-cadherin expression (Batra et al., 2023; Erber and Hartmann, 2020).

The carcinogenesis of BC is not completely understood, but there are widely accepted theories like “sporadic clonal evolution model” and “cancer stem cell model”. The sporadic clonal evolution model suggests that the cumulation of random mutations and epigenetic changes can lead to any breast epithelial cell to initiate tumor genesis. The cancer stem cell model implies, that the tumor initiation happens when a stem cell or a progenitor cell gains the ability to divide without restrictions (Bombonati and Sgroi, 2011; Economopoulou et al., 2012). It has been hypothesized, that the reality could be a combination of both, where the accumulation of sporadic mutations and epigenetic alterations in stem cells lead to an evolutionary selection of the fittest leading to cancer initiation (Bombonati and Sgroi, 2011).

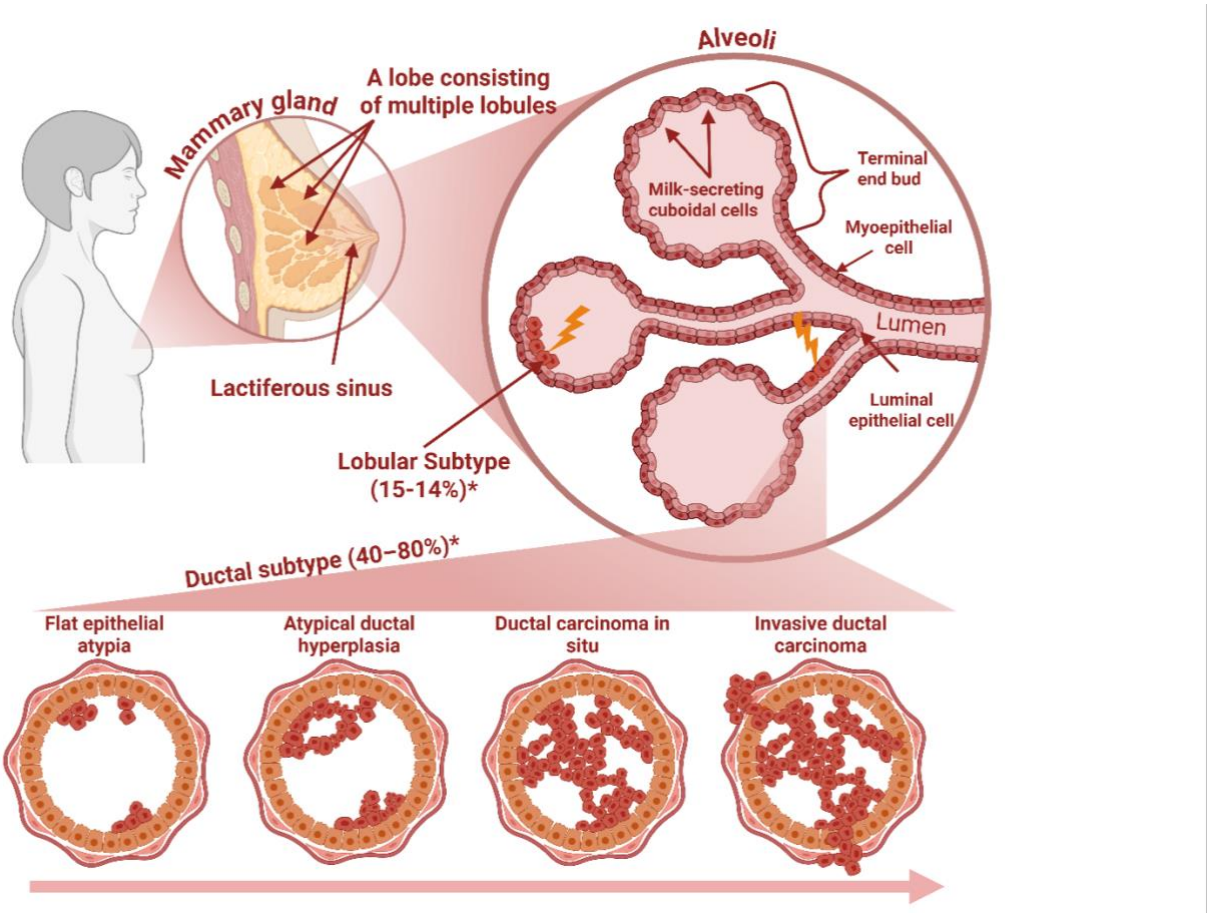

Figure 1. The anatomy of the mammary gland and carcinogenesis

The mammary gland comprises of multiple lobes, which consists of multiple alveoli. The terminal end buds are the functional units responsible for producing milk. Lobules are connected via Lactiferous ducts, which merge into Lactiferous sinuses. The most common invasive BC subtypes are Invasive ductal carcinoma (40-80%*) and lobular invasive carcinoma (5-15%*). Flat epithelial atypia, Atypical ductal hyperplasia, Ductal carcinoma in situ and invasive ductal carcinoma create an evolutionary continuum (Bombonati and Sgroi, 2011)(Erber and Hartmann, 2020)***.** Created with BioRender.com

BC progresses from normal glandular tissue, undergoing several stages of genetic alterations before becoming invasive. The grading process involves evaluating the histological characteristics of the tumor, which are scored using the Elston and Ellis-modified Scarff-Bloom-Richardson system (Harbeck et al., 2019).

There are multiple risk factors, like genetic predisposition, hormonal factors and lifestyle factors that will increase the likelihood of developing BC. Genetic predisposition has the biggest impact with germline mutations in tumor suppressive genes like BRCA1/2, CHEK2, PALB2, and TP53 making the cells more susceptible to the effects of a second somatic mutation to the remaining gene. This is known as the two-hit model (Xiong et al., 2025; Knudson, 1971). Hormonal factors include estrogen replacement therapy, contraception, nulliparity, not breastfeeding, early menarche and late menopause, all of which revolve around estrogen exposure to the cells. The physiology of breast tissue is very sensitive to changes in estrogen and progesterone concentrations caused by the menstrual cycles. During the menstrual

cycles, an imbalance between estrogen and progesterone can lead to increased cell proliferation. Increased cell proliferation leads to higher rates of DNA replication, raising the probability of replication errors. If not repaired, these errors can accumulate as mutations, contributing to genomic instability and increasing the risk of cancer (Harbeck et al., 2019).

1.1.1 Molecular classification of BC

As mentioned earlier, BC can be histologically categorized to different subtypes, which correlate with prognosis, recurrence patterns, and treatment responses. But histological assessment alone can't sufficiently predict the underlying tumor biology, needed for targeted therapies, leading to the creation of molecular classification (Erber and Hartmann, 2020).
In the year 2000, Perou et al. classified various clinical BC samples using microarray gene expression data into four molecular subtypes: Luminal, HER2-enriched, breast-like, and basal-like (Perou et al., 2000). Subsequent research enabled the division of the Luminal subgroup into Luminal A and B (Sørlie et al., 2001). The normal breast-like subtype has since been excluded, as it is believed to reflect sample contamination from normal mammary glands (Łukasiewicz et al., 2021). Later, the claudin-low subtype was recognized as the fifth intrinsic subtype, identified through an integrated analysis of human and murine mammary tumors (Herschkowitz et al., 2007). In 2009, Parker et al. introduced a 50-gene signature for subtype classification, referred to as PAM50, which could accurately classify specific BC cases into the primary intrinsic subtypes with an accuracy of 93% (Parker et al., 2009). The four main subtypes were subsequently validated through consensus clustering analysis conducted on mRNA gene expression from 466 primary tumors, which were comprehensively profiled at the DNA, RNA, and protein levels (The Cancer Genome Atlas Network, 2012).

Luminal A tumours are defined by the presence of estrogen receptors (ER) and/or progesterone receptors (PR), along with the absence of human epidermal growth factor receptor 2 (HER2). These tumours are classified as low-grade tumours which express low levels of genes associated with cell proliferation, typically resulting in a favourable prognosis. In contrast, Luminal B tumours are of a higher grade and are associated with a worse prognosis. They are ER positive and may be PR negative and/or HER2 positive, also displaying elevated expression of genes related to proliferation, such as MKI-67 and AURKA. Additionally, Luminal B tumours show reduced expression of genes linked to luminal epithelial cells compared to Luminal A tumours, making them more poorly differentiated. The expression of ER is comparable in both Luminal A and B subtypes, serving as a key factor in differentiating luminal tumours from the other non-luminal subtypes. Together they account for nearly 70% of all BC cases in Western populations (Łukasiewicz et al., 2021).
The HER2-enriched subgroup constitutes approximately 10–15% of BC cases. HER2-enriched subtype is distinguished by elevated levels of HER2 expression, coupled with the lack of ER

and PR activity. HER2-enriched tumors exhibit a more rapid growth rate compared to luminal subtypes and historically it had the worst prognosis among BC subtypes prior to the advance of HER2-targeted treatment options (Łukasiewicz et al., 2021).

The remaining two subtypes “basal-like” and “Claudin-low” are a bit more controversial as they both have been categorized by a low expression of ER, PR and HER2 also known as triple-negative breast cancer (TNBC), leading to an overlap in molecular profiling. TNBCs are primarily characterized by their aggressive nature compared to the other molecular subtypes and by their tendency to affect younger individuals, particularly those under the age of 50. The difference between the two is that basal-like expresses various genes and proteins typically associated with 'basal' or myoepithelial cells found in normal breast tissue. These proteins includes high-molecular-weight cytokeratins (such as CK5/6, CK14, and CK17), P-cadherin, caveolins 1 and 2, nestin, αB crystallin, CD109, and EGFR (Badve et al., 2011).

Claudin-low subtype is categorized by a reduced expression of genes that play a role in cell-cell adhesion, such as claudins 3, 4, and 7, occludin, and E-cadherin, while having an elevated expression of N-cadherin and vimentin, which are usual features of mesenchymal cells, making the subtype highly metastatic (Rädler et al., 2021).

In conventional diagnostic protocols, the molecular subtyping of BC is performed by evaluating the expression of ER, PR, HER2 and Ki-67 (Table 1.) using immunohistochemistry (IHC). IHC staining is not able to distinguish between different TNBC subtypes, due to the similar expression profile. The HER2 staining results classify the sample into categories of IHC 1+, 2+, or 3+. An IHC 1+ result is deemed negative, whereas an IHC 3+ result is classified as positive. An IHC 2+ result is considered borderline and requires additional evaluation through in situ hybridization (ISH) to verify the HER2 status, which is required for the targeted therapies (Erber and Hartmann, 2020). Among the various subtypes of BCs, HER2 enriched and luminal B HER2+ tumors can be treated with HER2 targeted therapies.

Table 1. Molecular subtyping (WHO Classification of Tumours Editorial Board, 2019; Goldhirsch et al., 2013)

	ER +/-	PR +/-	HER2 +/-	Ki-67
Luminal A	Positive	High (≥20%)	Negative	Low (typically <14%)
Luminal B (HER-)	Positive	Low (<20%) or Negative	Negative	High (≥14–20%)
Luminal B (HER+)	Positive	Any	Positive (IHC 3+ or FISH+)	Any
HER2-enriched	Negative	Negative	Positive (IHC 3+ or FISH+)	Any
TNBC (Basal-like)	Negative	Negative	Negative	Any

1.1.2 BC treatment

For early-stage BC, the conventional approach involves either breast-conserving surgery combined with radiotherapy or mastectomy, where the whole breast is removed. Surgery is often combined with adjuvant therapy, which is done to decrease the size of the tumor prior the surgery, to make the operation easier. The decision to administer adjuvant systemic therapy, is based upon the evaluation of lymph node status, hormone receptor presence, and the status of HER2. Treatment modalities for BC include surgery, chemotherapy, radiotherapy, endocrine therapy, targeted therapy, and immunotherapy. Chemotherapy treatments generally attack the rapid proliferation rate of cancer, causing DNA damage, which kills the cancer cells. Radiotherapy causes reactive oxidative radicals through precise radioactive beams, which again damage the DNA. Endocrine therapy, like selective estrogen receptor modulators, are used when the cancer growth is driven by hormones like estrogen, to block its activity. Targeted therapy implies to kinase inhibitors, which are used to block overly active cell signaling pathways responsible for growth and various other functions. Immunotherapies target the immune system evasiveness of cancer, making the tumor cells again vulnerable for immune cells (Wang and Wu, 2023).

Non-metastatic BC, treatment typically centers around surgical intervention, with preoperative systemic chemotherapy being utilized to decrease the tumor size, allowing preservation of breast tissue, and reducing the necessity for axillary lymph nodes dissection (Wang and Wu, 2023). Axillary lymph nodes are the nearest lymph nodes for breasts near the armpit. Axillary lymph nodes are responsible for draining the lymphatic fluid from the arm and breast. The quantity of axillary lymph nodes affected by metastases has been utilized to evaluate the cancer stage, and it has proven to be an effective biomarker for the aggressive phenotype (Jatoi et al., 1999).

In cases of metastatic BC, where the cancer cells have invaded the nearby tissue and surgical intervention is no longer an option, usually the primary objective for treatment is to extend survival and enhance the quality of life for patients also known as palliative care. Generally, treatments that spread throughout the body are favored, with surgical options reserved for palliative care only in select patients with tumors causing discomfort like obstruction of the urinary tract or bowel (Wang and Wu, 2023).

1.1.3 Currently approved HER2-targeted treatments

The identification of HER2 overexpression as a key factor in the progression of HER2+ advanced BC, along with the creation of targeted therapies, has resulted in an overall survival rate exceeding 90% (Wang and Wu, 2023). HER2 is receptor tyrosine kinase (RTK), which is usually activated by heterodimerization of another monomer of its receptor family (EGFR,

HER3 or HER4). Dimerization is usually mediated through ligand binding to one of the RTKs of the HER family as HER2 does not have a ligand binding pocket itself. There are multiple different ligands that can activate the different HER family receptors such as Epidermal growth factor (EGF), Transforming growth factor alfa (TGFα) and Neuregulin1 (NRG1), just to name a few. The dimerization of HER2 or any of HER family counterparts leads to transphosphorylation of their intracellular domains, and the activation of the downstream pathways like phosphatidylinositol 3' kinase (PI3K)/Akt pathway (Moasser, 2007). When the expression of HER2 increases like in the case of HER2+ BC, the HER2 monomers are expressed in such high manner, that the monomers start to spontaneously homodimerize without the need for a ligand. The spontaneous dimerization applies also for the other HER family receptors, which leads to the continuous activation of the HER2 pathway and the other HER family RTKs. This, in turn, activates a range of distinct intracellular oncogenic signaling pathways that promote cell proliferation, survival, and metastasis (Moasser, 2007).

Currently, there are eight therapies targeting HER2 for BC (Table 2.), that have received approval from the Federal drug administration (FDA) and European medicines agency (EMA). Among these, three are classified as monoclonal antibodies, two are ADCs, and three are small molecule tyrosine kinase inhibitors (TKI) (Swain et al., 2023). Additionally, there is one more tyrosine kinase inhibitor, Pyrotinib, which has been approved solely in China (Blair, 2018). Monoclonal antibodies (mABs), such as Herceptin (trastuzumab), which received approval in 1998 as the first monoclonal antibody for HER2 treatment, function by attaching to the extracellular domain (ECD) IV of HER2. The binding inhibits HER2 signalling and facilitates antibody-dependent cell-mediated cytotoxicity (ADCC), complement-dependant cytotoxicity (CDC) and antibody-dependent cell-mediated phagocytosis (Petricevic et al., 2013). Trastuzumab was first approved for metastatic BC, but later it has been approved for both early-stage and metastatic settings, often in combination with chemotherapy (Swain et al., 2023).

TKIs like Lapatinib, function by binding to the intracellular kinase domain of HER2, inhibiting the activation of the downstream pathways of HER2 signalling. TKI can diffuse through blood brain barrier, allowing to target brain metastases and they can be used if the target epitope of HER2 mutates making the antibodies ineffective (Swain et al., 2023). TKIs are also usually used as adjuvant therapies with antibodies or chemotherapy (Swain et al., 2023).

ADCs are usually employed when the previously mentioned treatments cease to be effective, and the cancer keeps progressing. They have also been utilized in early setting to avoid residual disease, where a small portion of cells survive the initial therapy. One of the ADCs (Enhertu), have also proven to be effective in HER2-low tumors allowing for broader patient populations (Modi et al., 2022). More of Enhertu in chapter 1.2.4.

Table 2. FDA Approved HER2-targeted therapies against BC

Modality	Drug name	Brand name	Mechanism of action
ADC	Trastuzumab deruxtecan	Enhertu	ADC with Top1 inhibitor, which induces formation of DSB via Top1cc
ADC	Trastuzumab emantasine	Kadcyla	ADC with a Tubulin inhibitor, which disrupts mitosis and tubulin exoskeleton
mAB	Trastuzumab	Herceptin	Binds to HER2 receptor, blocking its signal, while activating ADCC and CDC
mAB	Pertuzumab	Perjeta	Blocks HER2 dimerization, blocking its signalling while activating ADCC
mAB	Margetuximab	Margenza	Binds to HER2 receptor, blocking its signal. Modified Fc region to increase ADCC
TKI	Lapatinib	Tykerb	Binds to the kinase domain of HER2 and EGFR, blocking HER2/EGFR signalling
TKI	Neratinib	Nerlynx	Binds to the kinase domain of HER2 and HER4, blocking HER2/HER4 signalling
TKI	Tucatinib	Tukysa	Binds to the kinase domain of HER2 and HER3, blocking HER2/HER3 signalling

1.1.4 Internalization of HER2 receptor

Internalization is a broad term that refers the process of reorganizing molecules from the cell surface into the cell. In this context, internalization refers to different endocytosis pathways. Endocytosis plays a vital role in managing numerous cellular functions, including the maintenance of essential surface proteins and transporters, such as glucose transporters that help regulate serum glucose levels. It also regulates signalling from surface receptors, including G-protein coupled receptors and RTKs, as well as modulating cell–cell and cell–matrix interactions through the uptake of integrins and adhesion molecules (Elkin et al., 2016).
The internalization of HER2 has been debated for a while, with studies showing that HER2 does not get internalized (Haslekås et al., 2005) while other studies show that it does, but only to a small degree combined with rapid recycling (Austin et al., 2004a). It is probable that discrepancies in quantitative techniques and analyses contribute to the substantial differences observed in the reported internalization rates (Leyton, 2020). HER2 is usually internalized either as a homodimer or in combination with EGFR, HER3, and HER4 as a heterodimer, but not as a monomer (Bertelsen and Stang, 2014). The dimerization partner might affect the recycling and degradation of HER2 (Meijer and Van Leeuwen, 2011). With the successful development of HER2 targeting ADCs like Kadcyla and Enhertu, it has been validated that

HER2 is being internalized (LoRusso et al., 2011; Ogitani et al., 2016a). The internalization can be mediated through multiple different pathways. The most common and well characterized endocytosis pathway is clathrin mediated endocytosis (CME) but there are also clathrin independent endocytosis pathways like caveolae mediated endocytosis (CavME) (Elkin et al., 2016).

CME is a complex, multistage process that involves a variety of factors, including clathrin heavy and light chains, adaptor protein-2, the cargo being internalized, dynamin, and other endosomal accessory proteins (EAP). Collectively, these components play crucial roles in the initiation, stabilization, and maturation of clathrin-coated pits, ultimately resulting in membrane fission by dynamin, which leads to the formation of clathrin-coated vesicles (Mettlen et al., 2018).

CavME is less well known than CME. The present knowledge regarding caveolae biogenesis suggests that the process initiates at the endoplasmic reticulum, where caveolin-2 interacts with caveolin-1 to form hetero-oligomeric complexes. Subsequently, the caveolin-1/caveolin-2 heterooligomers are transported to the Golgi apparatus, where the complexes associate with cholesterol to generate 'caveolae precursors'. These small caveolae precursors, also referred to as 'exocytic caveolar carriers', are then trafficked to the plasma membrane. Upon reaching the plasma membrane, PTRF-cavin, which is believed to function as a coat protein for caveolae, is recruited to the membrane that contains oligomerized caveolins, cholesterol and sphingolipids. This recruitment stabilizes the membrane curvature and contributes to the characteristic flask shape of caveolae. The incision of the caveolae during endocytosis is facilitated by dynamin like in CME (Fridolfsson et al., 2014; Kiss and Botos, 2009).

The binding of the cargo is enabled by AP2 in CME and via caveolin-1 in CavME. It remains uncertain whether both pathways operate in parallel and converge at the early endosomes, or if caveolae take their own path and merge to form multi-caveolar structures referred to as "Caveosomes", which are believed to be equivalents of early endosomes (Sharma et al., 2003; Mettlen et al., 2018; Kiss and Botos, 2009). Additionally, a recently identified pathway involving clathrin-independent carriers (CLICs) and glycophosphatidylinositol-anchored protein-enriched endosomal compartments (GEEC), termed the CLIC/GEEC pathway, was discovered by inhibiting both CME and CavME pathways, and it has been observed to mediate endocytosis for HER2 (Kirkham et al., 2005; Barr et al., 2008).

Internalized surface proteins can experience various outcomes after they enter the early endosome. They may be recycled to the plasma membrane, or in polarized cells, transported across the cell via a mechanism known as transcytosis, or directed to the lysosomes for degradation through late endosomes. The maturation of endosomal compartments from early to late endosomes occurs through a process that includes a decrease in luminal pH, modification

of essential phosphatidylinositol lipids regulated by lipid kinases and phosphatases, and the recruitment and activation of Rab-family GTPases (Elkin et al., 2016).

There are still debates about the dominating internalization pathway. There are several compelling studies that indicate that HER2, similar to other members of the HER family and Transferrin receptor (TfR, CD71), undergoes primarily CME (Pedersen et al., 2008; Gilboa et al., 1995). However, there is also compelling evidence suggesting that the internalization of HER2 primarily occurs through CavME (Hammood et al., 2021). Sequences for AP-2 and Caveolin-1 binding has been characterized on HER2 (Gilboa et al., 1995; Zhao et al., 1999). The knockdown of clathrin heavy chain has been observed to inhibit the endocytosis of HER2 (Pedersen et al., 2008). The expression levels of HER2 and caveolin-1 were found to be inversely related. When caveolin-1 expression was reduced, especially in cell lines exhibiting high levels of expression, there was an increase in both the level of HER2 and its retention time at the cell surface. In contrast, the forced overexpression of caveolin-1 led to a decrease in the presence of HER2 at the cell surface (Pereira et al., 2018). A number of studies are concentrating on various mechanisms that stabilize HER2 at the plasma membrane, such as Endo A2, Flotillins, and HSP90, and how changes in their expression can mediate resistance to internalization (Baldassarre et al., 2017; Pust et al., 2013; Austin et al., 2004b). The endocytosis pathway could be influenced by the dimerization partner and also fluctuate based on the cell line and the cargo concentration (Hammood et al., 2021). The degree of HER2 expression has been shown to serve as an indicator of the trafficking behaviour of antibody-HER2 complexes in cancer cells (Ram et al., 2014). Ram et al. found that trastuzumab is effectively recycled in HER2-high cells, with only a minor portion of the antibody-HER2 complexes being directed to the lysosomes. In contrast, trastuzumab recycling is not observable in HER2-low cells under the assay conditions, and the internalized antibody-HER2 complexes proceed to the lysosomes (Ram et al., 2014). In a panel of cell lines exhibiting varying levels of HER2 expression, the cell surface levels of trastuzumab decreased by approximately 15% within the initial 60 minutes. After 18 hours, the original cell surface levels of HER2 were restored in cells with high HER2 expression, whereas in cells with low to intermediate HER2 expression levels, the cell surface levels of HER2 continued to decline to about 15% and 50% of the original HER2 levels (Ram et al., 2014). This could indicate that the internalized ADC-receptor complexes in HER2-low cell lines are more likely to undergo lysosomal degradation of the ADC, leading to the cleavage of the linker and the release of the ADC payload. However, it has been observed that the efficacy of T-DM1 is dependent on the level of HER2 expression in cancer cells, and it is established that patients with high HER2 expression, as defined by IHC3+ exhibit more frequent responses compared to those with lower levels (LoRusso et al., 2011). Interestingly enough, the more recently approved HER2 ADC T-DXd has been approved also for HER2-low BC (Modi et al., 2022).

There have been various efforts to maximize the amount of ADC-receptor complexes entering the lysosomes to achieve the linker cleavage and efficient payload release (Cheng et al., 2020; Li et al., 2016; Kang et al., 2019; Paul et al., 2023). There have been efforts to minimize the recycling of the HER2 receptor in the endosomes through utilization of a tetravalent biparatopic antibody binding to domain IV (trastuzumab epitope) and domain II (Pertuzumab epitope). A tetravalent biparatopic antibody is an antibody that has two pairs of binding arms, with each pair binding to distinct, non-overlapping epitopes on the same antigen. Trastuzumab was found to dissociate from HER2 in 2 h, enabling the receptor to recycle, whereas the tetravalent biparatopic anti-HER2 stayed associated with the receptor throughout the entire endocytic pathway, promoting receptor ubiquitination, trafficking to the lysosomes, and efficient degradation (Cheng et al., 2020). Same principle has been used to ADCs, which have resulted in better efficacy compared to T-DM1 (Li et al., 2016). The tetravalent biparatopic ADC developed by Li et al. was observed to cause a substantial increase in internalization. Studies revealed that the antibodies cross-linking ability triggered a specific and fast endocytosis of the receptor, independent of clathrin and dynamin. The cross-linking of multiple receptor-antibody complexes resulted in activation of aggregation dependent endocytosis (ADE) pathway. ADE is an actin-driven process, which morphologically resembles macropinocytosis. This was further confirmed using Cytochalasin D and EIPA, which are widely recognized agents for inhibiting macropinocytosis. Together these inhibitors suppressed the internalization of the tetravalent biparatopic ADC. Activation of the ADE pathway was reliant on the high HER2 expression level, as sparsely localized HER2 receptors did not allow for sufficient cross-linking (Paul et al., 2023).

Additionally, there are effort of engineering the antibody to dissociate from HER2 in the endosomes, allowing HER2 to be recycled to the cell surface, while the antibody is directed to lysosomes (Kang et al., 2019).

As additional knowledge becomes available regarding HER2 endocytosis and recycling, therapies can be developed to leverage the most efficient underlying mechanisms.

1.2 Antibody drug conjugates

Antibody drug conjugates (ADC) are biological drugs that combine the potency of chemotherapeutic agents with the specificity of antibodies to form targeted chemotherapy (Figure 2.). Biological drugs are generally large complex molecules produced with living organism such as animals or micro-organisms. Currently, the FDA has approved 15 ADCs for various types of cancer, with two of them indicated for BC. ADCs work by utilizing an antibody to specifically target tumour specific antigens or tumour-associated antigens on the surface of cancer cells to deliver chemotherapeutic agents directly to the cancer cells via

internalization and cleavage of the antigen-ADC complex. Each component has a significant impact on the efficacy, safety and kinetics of the ADC (Metrangolo and Engelholm, 2024).

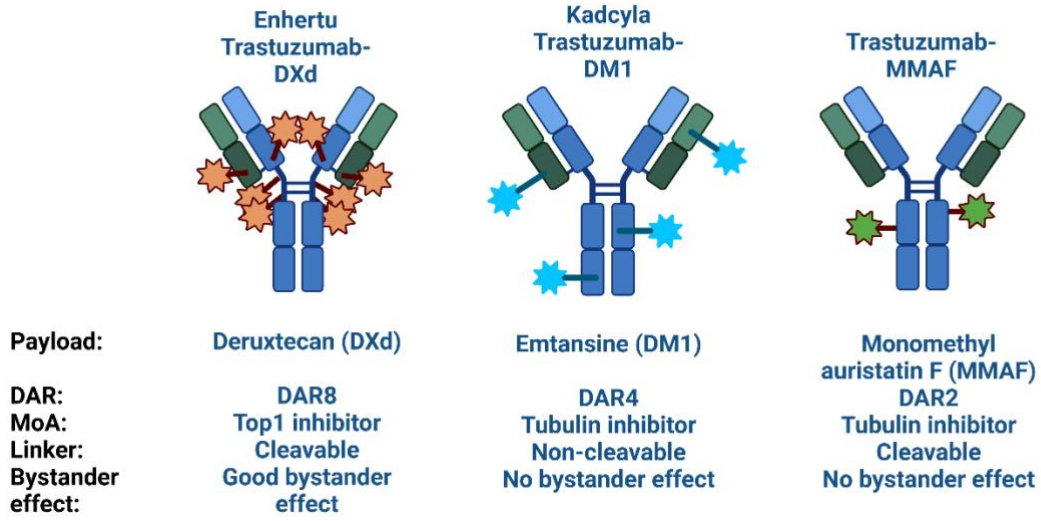

Figure 2. Antibody drug conjugates

The figure shows three ADCs, of which Enhertu and Kadcyla are both FDA and EMA approved for the treatment of advanced BC. The third one is a research purposed ADC used in the experiments. The figure shows the general characteristics of the ADCs, which will affect how they act in different models.
Created with BioRender.com

1.2.1 Monoclonal Antibody

The antibody is a crucial component of the ADC since it guides the payload to the right place. Antibodies are large (150 kDa) proteins consisting of constant domains, which include heavy chains ($C_{H1\text{-}H3}$) and light chains C_L, that give antibodies their Y-shape structure (Figure 3.). Located at the ends of both arms of antibodies are the variable regions ($V_{H \text{ and } L}$), which are responsible of the specific binding to a target (Ryman and Meibohm, 2017). Antibodies form the backbone of the ADCs. Majority of ADCs utilize an IgG1 type antibody, but there is also one with an IgG4 type antibody currently approved. Antibodies should be hydrophilic and low in immunogenicity to avoid aggregation in plasma, which would increase the clearance of the antibodies (Metrangolo and Engelholm, 2024).

ADC targets primarily include membrane proteins such as receptors or adhesion molecules, since antibodies are unable pass through a cell membrane due to their substantial size (Metrangolo and Engelholm, 2024). Antibodies must have a good affinity for the selected target. Affinity refers to the strength of a single binding interaction between the target and the antibody. ADC targets are usually highly expressed since heterogeneous or low antigen expression may lead to cells not internalizing sufficient amount of ADCs, leading to a poor response (Harper et al., 2013). However, there are exceptions, such as CD33 in Acute Myeloid Leukemia, which exhibits a relatively low target expression of 10,380 receptors per cell,

whereas HER2 in BC is expressed in the hundreds of thousands per cell. Differences in acceptable target expressions highlights the significance of target expression in relation to healthy tissue in order to reduce off-target effects of the ADC (Molica et al., 2021). Ideally, the target should possess a function that cancer cells rely on to reduce resistance and enhance responses, similar to HER2 ADCs, where the antibody itself induces ADCC, CDC and inhibits the HER2 signalling (Samantasinghar et al., 2023).

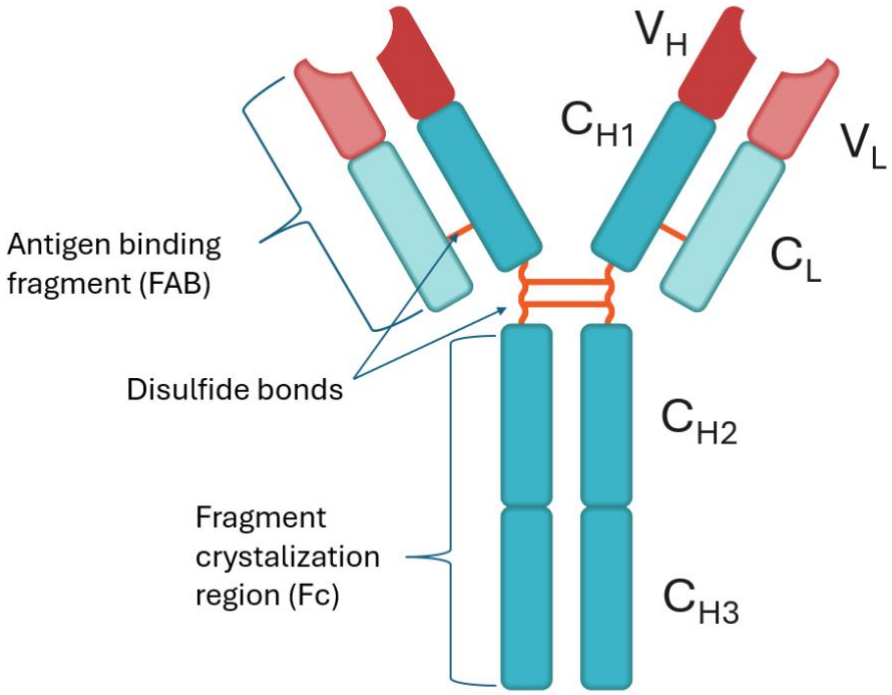

Figure 3. Structure of an IgG1 Monoclonal antibody

The affinity of the antibody affects multiple aspects of the ADC kinetics inside a solid tumour. A low affinity to a target antigen allows the antibody to penetrate deeper into the tumour, as the low affinity allows the antibody to dissociate from the target and diffuse deeper. However, the lower affinity could affect the internalization rate, leading to low amounts of released payload (Thurber et al., 2008; Xu, 2015; Ritchie et al., 2013). As mentioned earlier, the internalization of cell membrane proteins targeted with antibodies is usually mediated through clathrin-dependent processes, like receptor-mediated endocytosis. Alternatively, internalization can occur through less common clathrin-independent pathways like phagocytosis, macropinocytosis, caveolin-dependent endocytosis and aggregation-dependant endocytosis (Ritchie et al., 2013; Paul et al., 2023). The internalization of the ADC may also be influenced by the epitope to which the antibody binds, potentially resulting in a complete failure of the internalization process (Jin et al., 2022).

A high affinity for the target antigen guarantees that the antibody remains bound to the antigen until internalization is triggered. However, a high affinity often leads to reduced penetration, as it enables the unbound antibody to infiltrate deeper into the tumor only after all available receptors have been occupied (Thurber et al., 2008). The binding site barrier effect is a

phenomenon characterized by reduced antibody penetration, caused by the combined effect of the antibody size, strong affinity for the target, high target expression, and a high internalization rate of the target-ADC complex (Thurber et al., 2008). The longer it takes for the ADC to be internalized, the more time there will be for all targets to be occupied, leading to more time for the ADC to diffuse deeper into the tumour. A higher affinity can lead to a more rapid internalization of the antigen-ADC complex (Rudnick et al., 2011). A rapid internalization rate and recycling of the target back to the cell membrane enhances the binding site barrier effect. The antigen expression does also affect the penetration of the ADC. The lower the antigen expression is, the less time and less antibody it takes to saturate the available targets, allowing more antibody to diffuse further into deeper layers. A bigger dose creates a bigger concentration difference driving the diffusion further, while having more antibody to saturate more layers of the spheroids allowing again deeper penetration (Thurber et al., 2008).
A better tumour penetration could also be achieved with smaller antibodies like antigen binding fragments (FABs) or single chain variable fragments. However these smaller antibodies usually suffer from lower tumour retention meaning that the fragments will not accumulate into the tumours (Thurber et al., 2008; Wu, 2021).
The clearance of proteins is generally facilitated through three mechanisms. For small proteins (<60 kDa) prominent pathway is typically the non-metabolic elimination pathway, such as renal or biliary excretion. The second mechanism involves a “non-specific metabolic” pathway, including proteolysis that occurs in the extracellular environment or within cells, such as Kupffer cells, following pinocytosis. The third pathway consist of “specific metabolic” processes that involve receptor-mediated endocytosis and subsequent degradation (Li et al., 2017). Due to the substantial size of antibodies, renal clearance is not applicable for them. Additionally, the “non-specific metabolic” route is decreased due to the recycling through the neonatal Fc receptor (FcRn) binding mediated by the Fc region of the antibody. Consequently, “the specific metabolic” pathway emerges as the primary route for clearance, resulting in an extended half-life (Li et al., 2017). FABs and single chain variable fragments are missing the Fc region of the IgG, which is responsible for utilizing the FcRn mediated recycling of the antibodies, leading to a massive decrease in half-life (Ryman and Meibohm, 2017). Due to smaller size (approx. 50 kDa) FABs get cleared systemically through kidneys, which further decreases the half-life, making the utilization of FABs challenging for any therapeutic applications (Li et al., 2017).

1.2.2 Linker

The linker of the ADC is the component responsible for the release of the payload at the tumor site. Linkers can be divided into cleavable and non-cleavable linkers based on the mechanism

of payload release once the ADC-antigen complex gets internalized. Currently most of the ADCs approved by the FDA (by 2025) have utilized a cleavable linker instead of a non-cleavable linker (Metrangolo and Engelholm, 2024).

Cleavable linkers can be divided into protease-, pH- and glutathione-sensitive groups based on the mechanism of release. The protease-sensitive approach leverages tumor specific proteases inside the lysosomes to cleave a specific peptide sequence within the linker, like cathepsin B. The pH-sensitive method takes advantage of the pH changes between the cytosol (pH = 7,4) and the acidic environment of endosomal (pH = 5–6) and lysosomal (pH = 4.8) compartments, to initiate the hydrolysis of an acid-labile group in the linker, such as a hydrazone. The third strategy capitalizes on the elevated levels of intracellular glutathione compared to plasma, facilitating the release of the payload through reduction of the linkers disulfide bridge by glutathione (Jain et al., 2015).

Non-cleavable linkers require a complete degradation of the ADC in lysosome for the payload to be released. Non-cleavable linkers have been considered safer since the stability of the linker in plasma is greater compared to the cleavable linkers. Instability of the linker could lead to premature release of the payload and subsequent increased systemic exposure to the drug (Jain et al., 2015). In an attempt to optimize the linker stability, the conjugation site to the antibody, the linker length and steric hinderance of the cleavage site have been studied (Samantasinghar et al., 2023).

As previously mentioned in the antibody chapter 1.2.1, the hydrophobicity of the linker-payload motif can affect the solubility of the ADC, leading to aggregates. The linker-payload motifs are usually conjugated to lysine or cysteine residues of the antibody. Conjugation via lysine residues can lead to increased variance in the drug-to-antibody ratio (DAR) and in the location of the conjugations, since the conjugation could take place in any of the estimated 30 lysines available for conjugation in an IgG1 based antibody (Jain et al., 2015). Conjugation via cysteine residues, conversely, is accomplished through the regulated reduction of interchain disulfide bridges. An IgG1 molecule contains only four interchain disulfide bridges, which provides only eight potential sites for conjugation. This limitation in conjugation sites contributes to a reduced heterogeneity in the DAR. The amount of payload added, and the localization of every single linker-payload motif will affect the hydrophobicity of the ADC especially with higher DAR. The hydrophobicity could be further decreased with engineered cysteines allowing site specific conjugations allowing homogenous batches of ADCs, leading to better tolerability (Su et al., 2021). DAR values are typically kept below four to achieve an optimal therapeutic index and to mitigate the adverse effects associated with ADC aggregation caused by hydrophobicity, which can result in accelerated clearance and systemic toxicity. By utilizing innovative stable linkers and less effective payloads, the DAR can be increased, which in turn improves the drug's overall exposure to tumors, leading to enhanced responses. A

notable example of this approach is Enhertu, which features a first-in-class Top1 inhibitor as its payload conjugated via a stable tetrapeptide linker with a homogenous DAR of eight (Metrangolo and Engelholm, 2024).

1.2.3 Payloads

Payloads are the main components responsible for the cytotoxic and anti-proliferative responses to cancer cells. There have been a lot of progress during the last 50 years of ADC development. The first generation consisted of traditional small molecule cancer drugs like methotrexate and doxorubicin, but they were not potent enough, leading to second generation of ADCs with tubulin inhibitors (Wang et al., 2023). Tubulin inhibitors, like monomethyl auristatin E (MMAE) were previously deemed too toxic to be administered systemically, but with advances in linker technologies, conjugating MMAE to an antibody, gave it a better tolerability leading to an acceptable therapeutical window (Riccardi et al., 2023). MMAE and other tubulin inhibitors were potent anti-proliferative agents, but they were lacking efficacy against slow-proliferating cancer cells, which lead to the utilization of DNA damaging agents like topoisomerase 1 (Top1) inhibitors or benzodiazepines (Wang et al., 2023). However, most of the currently FDA approved ADCs use tubulin inhibitors. More about the mechanism of action of Tubulin inhibitors and Top1 inhibitors, in chapter 1.2.4. A variety of new payloads are being investigated, like RNA inhibitors, such as RNA splicing inhibitors or RNA polymerase II inhibitors, and Bcl-xL inhibitors, Nicotinamide phosphoribosyltransferase inhibitors, carmaphycins, immunomodulating payloads like Toll-like receptor agonists and more complex payloads like protein degraders such as proteolysis targeting chimeras (PROTACs) (Wang et al., 2023).

When evaluating these different payloads as viable options for ADCs, there are multiple things to consider. It is essential for the cytotoxicity of the agents to be sufficiently high. The payloads must exhibit low levels of immunogenicity, just like antibodies. To prevent resistance, the payloads shouldn't be substrates of efflux pumps like multidrug resistant protein1. Additionally, these payloads should demonstrate high stability in plasma while conjugated, and within the lysosomes and in the cytosol after the payload has been released. The payload should possess lysosomal escape capability, which is an ongoing study, but is generally achieved with acidic and lipophilic properties (Riehl et al., 2025). Furthermore, it is important that the payloads possess functional groups that can be modified without significantly compromising their efficacy, to enable conjugation to antibodies. Lastly, to tackle the problem of heterogenous antigen expression in tumors, the payloads should exhibit bystander killing effects, without being too hydrophobic to cause aggregation of the ADC, resulting in instability of the ADC (Wang et al., 2023). The bystander effect is the ability of the ADC to induce cytotoxicity in the antigen negative cells surrounding the target positive cells. The bystander effect is achieved

through a lipophilic payload that is able to diffuse through the cell membrane to the surrounding cells after being released from the targeted positive cell (Singh et al., 2016). Mertansine (DM1) and Deruxtecan (DXd) are two examples of successful incorporation of payloads in Kadcyla (Trastuzumab-Emantasine; T-DM1) and Enhertu (Trastuzumab-Deruxtecan; T-DXd) (Figure 2).

1.2.4 Enhertu and Kadcyla

Enhertu and Kadcyla are currently the only ADCs approved by the FDA for the treatment of BC (Figure 2.). Both are approved as a monotherapy for the treatment of adult patients diagnosed with HER2-positive, unresectable, locally advanced, or metastatic BC, provided they have previously undergone treatment with trastuzumab and a Taxane (tubulin stabilizer), either individually or in combination (Kadcyla annex I, 2023; Enhertu annex I, 2024). Kadcyla is approved as a monotherapy for the adjuvant treatment of adult patients diagnosed with HER2-positive early BC, which exhibit residual invasive disease in the breast and/or lymph nodes (Kadcyla annex I, 2023). Enhertu is approved as a monotherapy for adult patients diagnosed with unresectable or metastatic HER2-low BC. Enhertu is also approved for the treatment of HER2 positive advanced non-small cell lung carcinoma and Gastric cancer (Enhertu annex I, 2024). Both ADCs are composed of trastuzumab, which is a humanized anti-HER2 IgG1 monoclonal antibody. The trastuzumab portion of aforementioned ADCs causes ADCC and CDC in cell lines with high HER2 expression (Petricevic et al., 2013). trastuzumab is also responsible for inhibiting the HER2 signalling through phosphatidylinositol 3-kinase (PI3-K) pathway (Kadcyla annex I, 2023; Enhertu annex I, 2024). Enhertu is conjugated with Deruxtecan (DXd) with a tetrapeptide-based cleavable linker (GGFG), which is cleaved by a Cathepsin B and L, which are highly expressed in the lysosomes of cancer cells (Ogitani et al., 2016a; Enhertu annex I, 2024). Kadcyla is conjugated with Emtansine, which is a stable thioether (MCC) linked to DM1, and requires the whole ADC to be degraded to be released. This leads to active metabolites of DM1 (primarily lysine-MCC-DM1) (Kadcyla annex I, 2023). DM1 is a derivative of Maytansine, which belongs to the class of benzoansamacrolide antibiotics (Wang et al., 2023). The N-acetyl group in maytansine was replaced with a 3-methyldithiopropionyl group to produce DM1. DM1 and Maytansine are tubulin inhibitors, which bind to tubulin and disrupt its structure, resulting in the disassembly of the tubulin exoskeleton and the formation of microtubules during mitosis preventing proliferation and causing apoptosis of the cell (Arnst et al., 2019).

DXd is a derivative of Exatecan, which belongs to the class of camptothecins, which inhibit the function of Top1. Top1 is responsible for relaxing the supercoiled DNA during the replication and transcription of DNA, by cleaving and forming a reversible covalent bond with the single strand of DNA and allowing it to straighten out before continuing to religate the strands back

together. Top1 is commonly over expressed in cancer cells, since increased proliferation rate requires higher Top1 activity (Talukdar et al., 2022). DXd binds irreversibly with a covalent bond to the Top1 and DNA causing Top1 cleavage complexes (Top1cc), leading to DNA damage and apoptosis of the cell (Li and Liu, 2016).
DXd has shown good bystander effect in *in vitro* cocultures and spheroid models, unlike the lysine-MCC-DM1, which has no observed bystander effect (Khera et al., 2022).
Trastuzumab is expected to be degraded into small peptides and amino acids via catabolic pathways similar to endogenous IgG through the liver. The half-life of serum trastuzumab ranges from 9 to 11 days, while the half-life of the T-DM1 is around 4 days. The half-life of T-DXd is around 7 days (Enhertu annex I, 2024). Both DXd and DM1 undergo metabolism primarily via the CYP3A4 oxidative pathway, with DM1 also being metabolized to a lesser degree by CYP3A5 (Kadcyla annex I, 2023; Enhertu annex I, 2024). DXd is a substrate for various efflux pumps, including P-glycoprotein (P-gp), OATP1B1, OATP1B3, MATE2-K, MRP1, and BCRP. DM1 is recognized as a substrate of P-gp (Kadcyla annex I, 2023; Enhertu annex I, 2024).

1.3 Preclinical models for testing ADC efficacy

Once an ADC target has been selected to be pursued into validation, the development starts with production of antibodies targeting the chosen ECD. After selecting the antibody candidates for further testing based on their adequate affinity and stability, the next step is to conduct internalization studies. Once an antibody is identified with a sufficient internalization activation, it will be conjugated with payloads to start efficacy studies. These studies are typically initiated with *in vitro* monolayer cultures and subsequently followed by *in vivo* models such as mice and rats. If the results are favourable, the research may then advance to more translational models, including monkeys and dogs.

1.3.1 In vitro monolayer models

In vitro monolayer cell cultures are two-dimensional (2D) models, which have traditionally served as the standard in biomedical research for investigating cellular and molecular mechanisms under both physiological and pathological conditions to advance the understanding of the underlying biology as well as to develop novel therapies (Bloise et al., 2024). 2D models have plenty of advantages like their low cost, high throughput, reproducibility, ease of use and maintenance, as well as good interpretability (Kapałczyńska et al., 2016). However, the simplicity of 2D models also contributes to several limitations. The 2D cultures are grown in culture flasks attached to a plastic bottom leading to a dominance of connections between the plastic surface and the cells. The cell-cell connections are limited to horizontal neighboring cells and cell-ECM interactions are confined to a single side of each cell, in contrast to the

conditions found in natural growth environments (Kapałczyńska et al., 2016). These interactions between cells regulate cell differentiation, proliferation, vitality, expression of genes and proteins, response to stimuli, drug metabolism and other cellular functions. The 2D cell culture forces cells to adapt an apical-basal polarity, which has been shown to modulate the sensitivity of cells to apoptosis (Baker and Chen, 2012). The stiffness of the culture plate has been shown to increase sensitivity to Cisplatin and Taxol by increasing the proliferation rate of the cells (Feng et al., 2013). These growth conditions in 2D can change the morphology of the cells, which will lead to changes in the gene expression, RNA and protein levels, which could lead to differences in cell functions like secretion of signal molecules and cell signaling, possibly compromising the validity of the model (Birgersdotter et al., 2005). The flat growth conditions result in a uniform gradient of treatment exposure, oxygen, nutrients, metabolites and signal molecules.

These flat growth conditions may restrict the interpretation of results from treatment modalities such as ADCs, which are influenced by the physical three-dimensional (3D) structures present in a tumor or in cancer, where factors like hypoxia or growth factors could impact treatment efficacy (Berrouet et al., 2020; Bloise et al., 2024; Kapałczyńska et al., 2016).

As previously mentioned, ADCs such as Enhertu have been observed to have a bystander effect thanks to its lipophilic payload. This means that the antigen negative (Ag-) cells neighboring the antigen positive (Ag+) cells, can be killed by the payload released through the Ag+ cells. The bystander effect can help in addressing the issue with tumor cell heterogeneity and the need for deeper ADC penetration within the tumor, as it is not necessary for all cells to be directly exposed to the ADC. In 2D the bystander effect of ADCs, can be investigated through co-culture models with Ag+ and Ag- cell lines with varying ratios or by extracting the medium of treated Ag+ cultures to a Ag- culture (Wu and Shah, 2020). Both of these models can confirm if there is a bystander effect, but they can’t take into account the bad penetration of the ADC (Figure 4). Furthermore, the released payload becomes diluted when it diffuses outside of the cells, to a greater extent than in a tumor environment, where the cells are surrounded by other cells, which helps retain more of the payload within the tumor (Cilliers et al., 2018; Rubahamya et al., 2024).

1.3.2 In vivo studies

Conducting unnecessary *in vivo* studies in any animal model is unethical, time-consuming and expensive and does not comply with the principles of 3Rs (replacement, reduction and refinement). But there are plenty of reasons, why *In vivo* models are required, like capturing the effects of the tumor microenvironment (TME). TME plays a crucial role in cancer physiology, tumor structure, and function. The tumor microenvironment is typically composed of immune cells, stromal cells, blood vessels, and extracellular matrix. Interactions between malignant

cells and TME are vital for the growth, progression, and development of metastases (Anderson and Simon, 2020). The benchmark for *in vivo* studies involves tumor xenograft models in immunocompromised mice (Nayak et al., 2023). Immunocompromised mouse strains, such as NSG mice, are deficient in a variety of immune cells like T and B cells, as well as natural killer cells, due to genetic mutations that affect antibody production and immune cell development. As a result, only neutrophils remain functional, since the activity of other immune cells relies on T and B cells (Kanaji et al., 2014). The deficiency of immune system components limits the effects of tumor-promoting immune cells within the TME to tumors. But, the absence of immune cells promotes the proliferation of cancer cells and a metastatic pattern similar to that observed in human BC patients (Puchalapalli et al., 2016; Lei et al., 2020). Cell inoculations can be performed either subcutaneously, meaning under the skin, or orthotopically to the origin of the cancer site resulting in a more comparable expression profile to that of clinical patients (Gargiulo, 2018). The benefit of cells inoculated subcutaneously is that monitoring the tumors development is more straightforward. *In vivo* models allow evaluation of the systemic effects of the ADCs, providing essential information about the safety and stability of the ADC (Cilliers et al., 2018; Mukherjee et al., 2022; Wang et al., 2023). Certain payloads may need a longer incubation period to be efficacious, such as Top1 inhibitors. Comparable experimental designs cannot be applied to *in vitro*, since cell growth is eventually going to be limited by the dimensions of the culture dish. The continuous growth of cells is essential for evaluating treatment responses.

1.3.3 In vitro spheroid models

Spheroids are 3D cell cultures consisting of one or more cell lines, which form a solid round sphere of cells submerged in culture medium. Currently spheroids have been produced through scaffold-free techniques like microfluidics, hanging drop, liquid overlay with non-adhesive plates, spinner flask and magnetic bioprinting as well as through techniques revolving around different scaffolds like hydrogels and artificial matrixes (Nayak et al., 2023).
Spheroid formation occurs through a three-step process. Initially, long-chain extracellular matrix (ECM) fibers featuring multiple RGD motifs facilitate the swift aggregation of dispersed cells by binding to cell-surface integrins. RGD motif is an amino acid sequences utilized by integrins for cell adhesion. Within the cells, integrins transmit mechanical signals from the extracellular environment to actin filaments, a crucial step for the self-assembly of spheroids. Following the initial aggregation, a delay phase is observed, characterized by an increase in cadherin expression. Finally, strong cell adhesion is established through homophilic binding between cadherins on adjacent cells, results in the formation of spheroids. The reliance on ECM fibers and cadherins may differ among various cell types (Ivascu and Kubbies, 2007; Lin and Chang, 2008). Certain cell lines do not have the inherent ability to spontaneously form

spheroids. Matrigel is a hydrogel rich in ECM proteins as laminin, collagen IV, heparan sulfate proteoglycans, entactin/nidogen, and a number of growth factors, extracted from Engelbreth-Holm-Swarm mouse sarcoma cell line (Kleinman and Martin, 2005). With the help of ECM protein extracts such as Matrigel™, even cell lines without inherit ability for spheroid formation can develop into spheroids in suspension, exhibiting morphology and diffusion characteristics that more closely resemble xenograft tumors derived from the respective tumour cell lines (Shaw et al., 2004).

Spheroids exhibit characteristics like avascular tissues or tumor masses, with a diffusion limitation of approximately 150–200 μm for various molecules, like oxygen, which also contributes to the buildup of metabolic waste within the spheroids. Consequently, spheroids exceeding 500 μm in diameter typically reveal a layered structure, featuring a necrotic core at the center, followed by an inner layer of quiescent cells, and an outer layer of proliferating cells. This structural arrangement may result in varying responses to treatments across the different layers (Lin and Chang, 2008; Malhão et al., 2022; Zanoni et al., 2016).

Spheroids make a good intermediate model between the *in vitro* monolayer models and *in vivo* models. They have similar control of environmental factors and reproducibility as monolayer models, allowing for simple study designs and effective drug screening, while having more tumor characteristics. Cell-cell interactions in spheroid models may more accurately replicate gene expression patterns and physiological responses that influence the secretion of soluble mediators and mechanisms of drug resistance (Antoni et al., 2015; Nayak et al., 2023). When developing ADCs, the efficacy is tied to the kinetics of the ADC inside the tumor, which is better studied in spheroid models instead of monolayer models. The weak penetration to a solid tumor mass caused by the large size of ADCs, can be better modeled inside a spheroid as well as the distribution of the payload following its release (Figure 4) (Khera et al., 2022). The bystander effect described earlier could be indirectly studied in spheroid models as the 3D structure of the spheroid is hypothesized to limit the penetration distance of the ADC compared to the released payload, which could diffuse deeper into the spheroid. Since cells are surrounded by other cells, the payload can diffuse into neighboring cells, rather than escaping into the external environment, as observed in 2D cultures. The 3D structure results in a more realistic accumulation of the payload within the spheroid (Rubahamya et al., 2024).

Spheroids can be cultured for longer time periods compared to 2D cultures, since there confluence is not an issue, which allows for longer experiments (Antoni et al., 2015; Białkowska et al., 2020). The growth rate is generally faster in 2D compared to spheroids, making the efficacy of anti-proliferative agents higher in 2D cultures (Antoni et al., 2015).

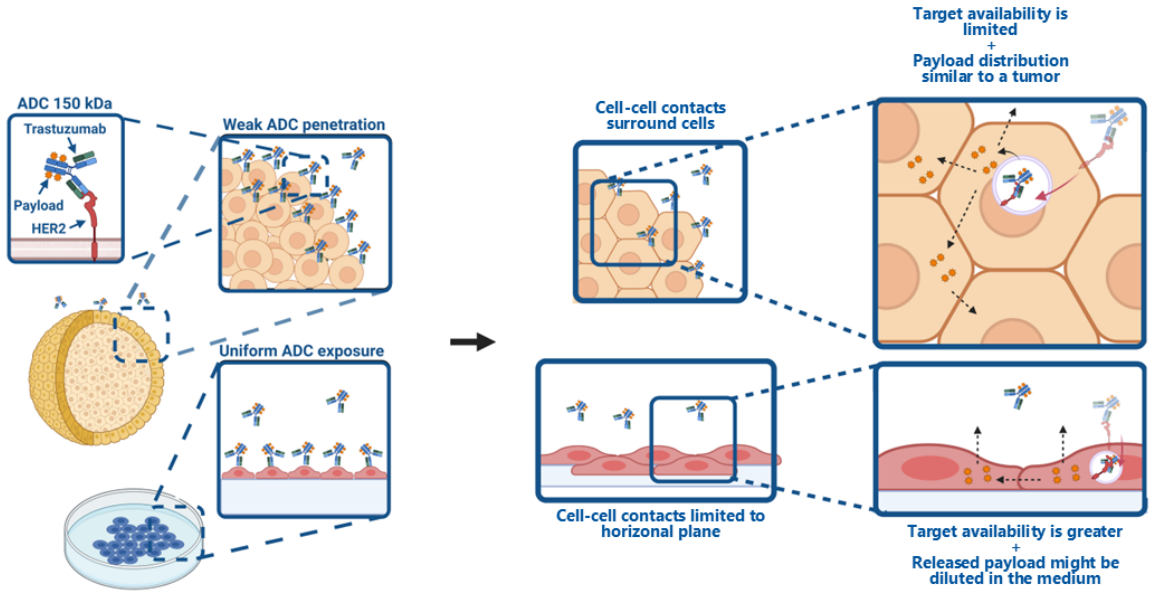

Figure 4. Differences between 2D and 3D culture formats relevant to ADC development

Spheroids can model the efficacy of ADCs more accurately compared to 2D models since the ADC penetration, bystander effect and payload accumulation is similar to tumors. Created with BioRender.com

1.4 Aim of the research project

As the ADCs get more complex during the years, there is a growing demand for more sophisticated models to detect subtle yet potentially significant variations in the characteristics of ADC components. The introduction of Enhertu, a highly effective treatment for advanced BC featuring a first-in-class Top1 inhibitor (DXd) with a high DAR of eight, has generated a significant interest in Top1 inhibitors and in payloads that exhibit a pronounced bystander effect. However, replicating the efficacy of Enhertu has proven challenging with the standard 2D culture formats. Possible reasons for not seeing the full potential of Enhertu in monolayer models, could be due to the monolayer models inability to demonstrate the challenges associated with reduced tumor penetration as well as the benefits of a high DAR and the bystander effect. To address this issue, various spheroid models tailored for different indications were developed. Among these spheroid models, two BC models were investigated more thoroughly by characterizing the HER2 expression, internalization, and dose-response (DR) with Enhertu, Kadcyla, and a research purposed trastuzumab-MMAF. The aim was to develop a more translatable BC model for ADC research and development for Orion Pharma. If successful, the project would allow to bridge the gap between *in vitro* and *in vivo* models and reduce the amount of lead molecules entering the *in vivo* trials. In this work, the models and their differences are discussed with reference to cell lines and culture formats.

The aim of the thesis was to:

- Develop and validate three spheroid models for *in vitro* use.
- Compare the internalization and DR data between the 2D and 3D culture formats.
- Investigate if immunofluorescence staining with confocal imaging could reliably visualize the distribution of ADCs and their payloads inside a spheroid.

The hypothesis for the thesis is that:

- The 3D structure of a spheroid model has a significant effect on the ADC exposure to the cells leading to a significant effect on the efficacy and potency of the ADC.
- There is a significant difference in efficacy and internalization between the 2D and 3D culture formats.
- The immunofluorescence staining with confocal imaging can sufficiently visualize the penetration of the ADC and the bystander effects of different payloads.

2 Results

2.1 Quantification of HER2 in High- and Low-Expressing Cancer Cell lines

The target of Enhertu, Kadcyla and research purposed in-house ADC (trastuzumab-MMAF_DAR2) is HER2. It is essential to determine the HER2 receptor count on the cell surface, as the internalization and efficacy of these ADCs is dependant of the receptor density. To investigate the receptor counts, Quantitative fluorescence-activated cell sorting (qFACS) was conducted with BT-474 (BC), HCC1954 (BC) and 22RV1 (prostate cancer). The ADCs being derived from hIgG, required the evaluation of non-specific FcRn binding associated with hIgG. The mean fluorescence intensity (MFI) values of trastuzumab conjugated fluorochrome and hIgG conjugated fluorochrome were measured (Figure 5.). The MFI was translated to receptor counts using quantitative hIgG binding beads to get the final estimates of the HER2 levels and hIgG background (Figure 5). The HER2 MFI values of BT-474 and HCC1954 were high as expected (Figure 5). 22RV1 had a low HER2 expression, validating its functionality as a negative/ low-expression cell line (Figure 5.). All cell lines had similar HIgG binding (Figure 5.).

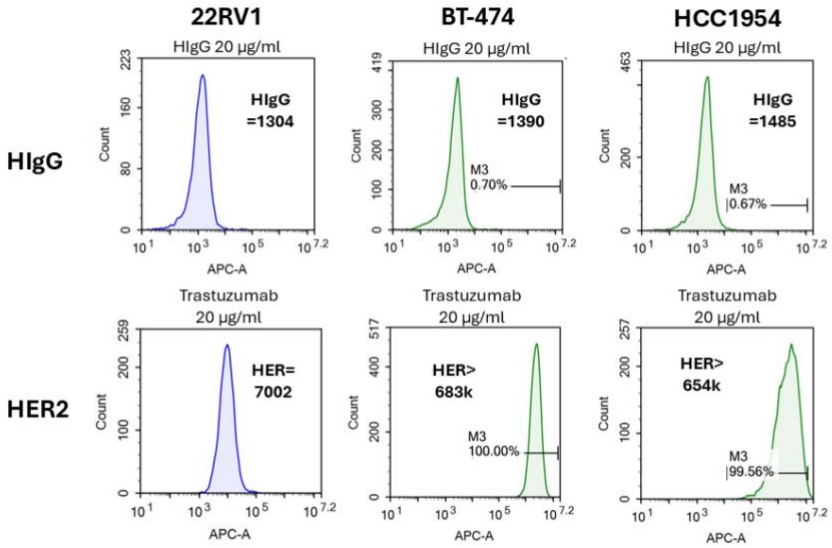

Figure 5. The HER2 receptor counts and unspecific HIgG binding measured with qFACS
The Figure shows the receptor counts of BT-474, HCC1954 and 22RV1 (negative control). All cell lines have a low background of hIgG binding (<1500 receptors). The HER2 expression levels were recorded at 683,000 receptors per cell for BT-474 and 654,000 receptors per cell for HCC1954, while 22RV1 exhibited only 7,002 receptors per cell. The measurements were conducted with 20 µg/mL trastuzumab-AF647 and HIgG-AF647.

2.2 Setting up the spheroid models

The spheroid model optimization started with 22RV1-cells by comparing the different cell seeding amounts. The spheroid model optimizations were conducted with Incucyte®. Incucyte is a device with the capability to image, measure, and analyse cell cultures in real time. Cytotox

green is a reagent used to measure dead cells in cell cultures with Incucyte. Cell death, as indicated by Cytotox green mediated fluorescence, was expected to only occur at the core of the spheroids, given that no treatments were applied during the establishment of the spheroid models. This experiment had samples at the edges of the 96-well plate, but they were excluded due to issues with cell culture media evaporation leading decreased cell viability. Spheroids were generated using the liquid overlay technique on ultra-low attachment (ULA) plates to prevent cell adhesion and promote 3D aggregation. Cell death was first observed to increase at the earliest time point of 144 hours with a seeding density of 5,000 cells per well, and at the latest timepoint of 200 hours with a seeding density of 2,000 cells per well. (Figure 6. A). A reduction in spheroid size was observed to correspond with a decrease in the size of the necrotic core, as well as with delayed time for the necrotic core emergence (Figure 6. A). A lower seeding amount of 1500/well was chosen, knowing that the necrotic core wouldn't appear for at least 200h. The increase in spheroid growth was stable after the first three days of the spheroid formation, and the growth maintained stable throughout the entire experiment duration of 234h with all cell seeding amounts (Figure 6, C). The two concentrations of Cytotox green tested (100 nM and 200 nM) exhibited anticipated differences in the detection sensitivity and intensity of the fluorescence. However, these differences in the detection sensitivity and intensity between 100 nM and 200 nM Cytotox green diminished as the size of the spheroids decreased, ultimately resulting in both concentrations indicating the onset of a necrotic core at the same time point (Figure 6. B). The increase in cell death with the 200 nM could also be associated to the toxicity of the Cytotox green reagent itself. The toxicity of the Cytotox green could have manifested as a decrease in the spheroid sizes, but on the contrary, the spheroid sizes tended to be bigger with the higher Cytotox green concentration compared to the spheroids with lower 100 nM Cytotox green concentration (Figure 6. D). The variance in the sizes of the spheroids, was increased with the 200 nM treated spheroids (Figure 6. D). The 100 nM Cytotox green concentration was selected for the cytotoxicity DR studies.

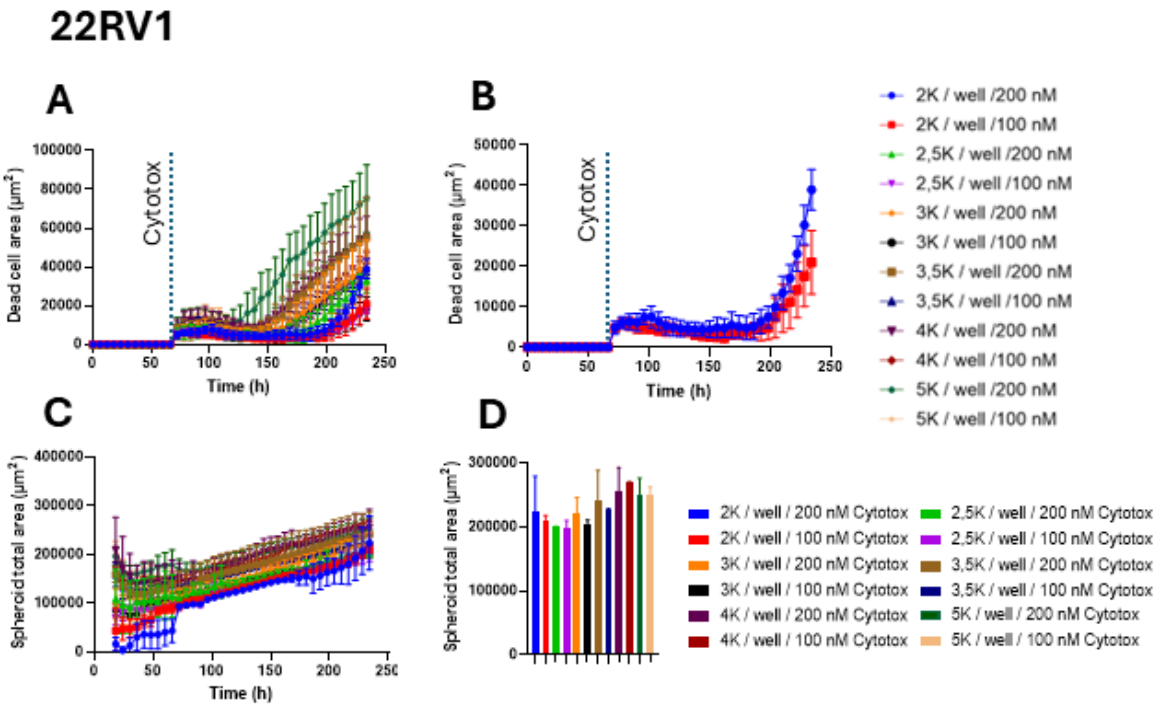

Figure 6. 22RV1 spheroid model optimization

The figure shows the growth between samples with different cell seeding amounts, and two concentrations of Cytotox green reagent. (A) The size of the spheroid influenced the emergence of a necrotic core. A necrotic core developed earlier with the higher seeding amounts. The necrotic core was detected earlier and more intensely with the higher Cytotox green concentrations (200 nM). The difference in Cytotox green concentrations for identifying cell death at the core of the spheroids diminished as the size of the spheroids decreased. (B) There was no distinguishable difference between 200 nM and 100 nM Cytotox green in the detection of the necrotic core with the smallest seeding amount. (C) The spheroid growth was linear after the first three days after plating, except for sample 2K/ well/ 200 nM Cytotox green, which grew faster after 200h. (D) The higher Cytotox green concentration (200 nM) did not appear to affect the spheroid size in a negative fashion compared to the lower concentration (100 nM). There appears to be more variation in the spheroid sizes between 200 nM Cytotox green concentrations.

The next experiments with different cell lines like SK-OV-3, SNU-16 and IM95 (Figure 7.), switched the focus from seeding amounts to Matrigel concentrations to ensure that cell lines formed spheroids. The cell lines were unable to independently generate tight spherical spheroids without the presence of additional supportive matrix proteins. To address the issue with spheroid formation, various concentrations of Matrigel were tested. SNU-16 cells did not aggregate even with Matrigel (Figure 7.). SK-OV-3 cells formed loose aggregates without additives, but with the help of 5% Matrigel, cells formed dense spheroids (Figure 7.). IM95 had similar problems without additives, but with 3% Matrigel the problem was fixed (Figure 7.). However, even if both SK-OV-3 and IM95 cell lines had the ability to form satisfactory spheroids, they both showed high background with Cytotox green. Both the SK-OV-3 and IM95 cell lines exhibited a strong fluorescent readout, suggesting that either the Matrigel influences the Cytotox green, or the viability of the spheroids was decreased, despite the spheroids continued growth (Figure 7.). Cell viability was unfortunately not confirmed with CellTiter-Glo (CTG), which resulted in the discontinuation of the development of SK-OV-3

and IM95 spheroid models. CTG lyses viable cells and binds to the released ATP, resulting in measurable fluorescence. The fluorescence proportional with the quantity of living cells found within the spheroids.

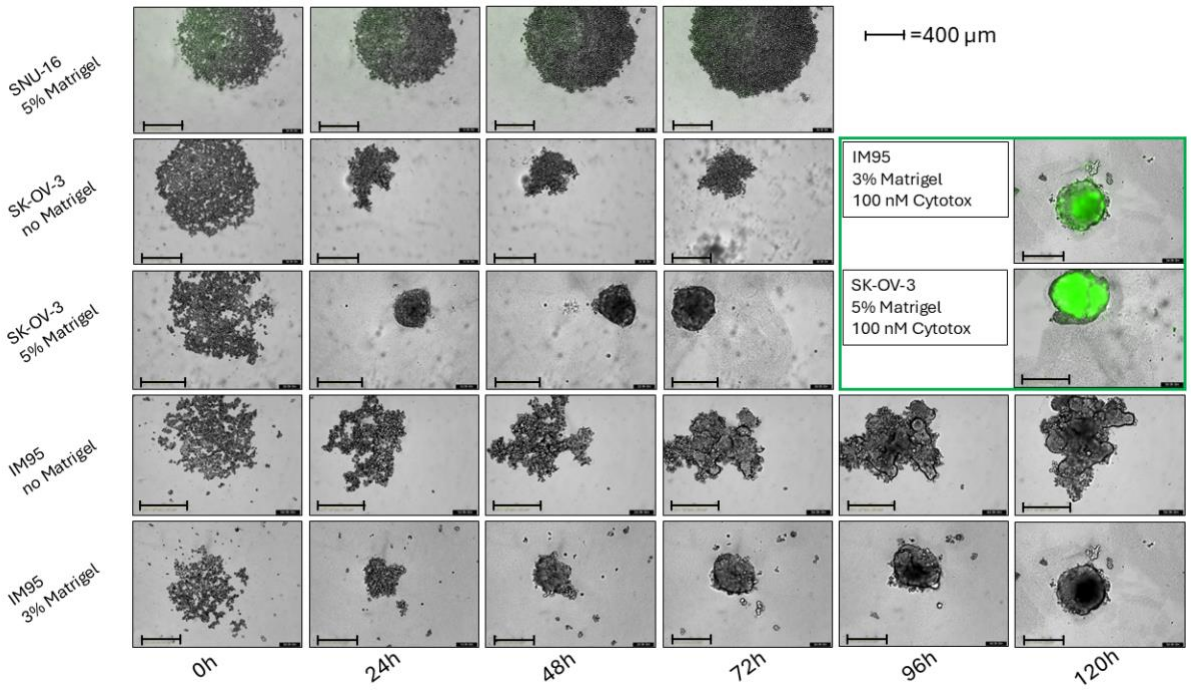

Figure 7. Cell lines assessed for spheroid formation

The figure shows the spheroid formation of three cell lines (SNU-16, SK-OV-4 and IM95). SNU-16 did not aggregate even with the help of 5% Matrigel, which manifested as continuous growth along the bottom of the ULA plate. SK-OV-3 produced loose aggregates without clear boundaries. With the addition of Matrigel, SK-OV-3 was able to form tighter spheroids, with a more distinct outer layer. IM95 also lacked the capability to form spheroids without Matrigel, which resulted in a variety of different shapes and massive sizes (Approx. 1000 µm² in diameter). With 3% Matrigel IM95 formed nice spheroids after 5 days with clear boundaries. The figure also shows how the Matrigel supported spheroids looked after they were treated with 100 nM Cytotox green, which was used to visualize cell death. Spheroids with Matrigel suffered from substantial background fluorescence, making the models not viable for Cytotoxicity studies using Cytotox green as a readout for cell viability.

BT-474 and HCC1954 were selected by literature supporting their utilization as spheroid models. Having gained insights from the experiment with 22RV1 (Figure 6, A and B), a relatively low seeding amount was chosen for HCC1954 and BT-474, while factoring in the growth rate of the cell lines. The emphasis shifted to Matrigel concentrations rather than cell seeding amounts to ensure spheroid formation. Both cell lines formed spheroids without the need for Matrigel addition, which manifested as aggregation of the cell mass after 24h (Figure 8). BT-474 spheroids demonstrated reduced Cytotox green fluorescence in comparison to IM95 and SK-OV-3 cells (Figure 7). Nonetheless, the inclusion of extra procedural steps with Matrigel while introducing a variable in the experiment that could affect the final results was not preferred. The presence of Matrigel also further complicated the focusing of Incucyte imaging.

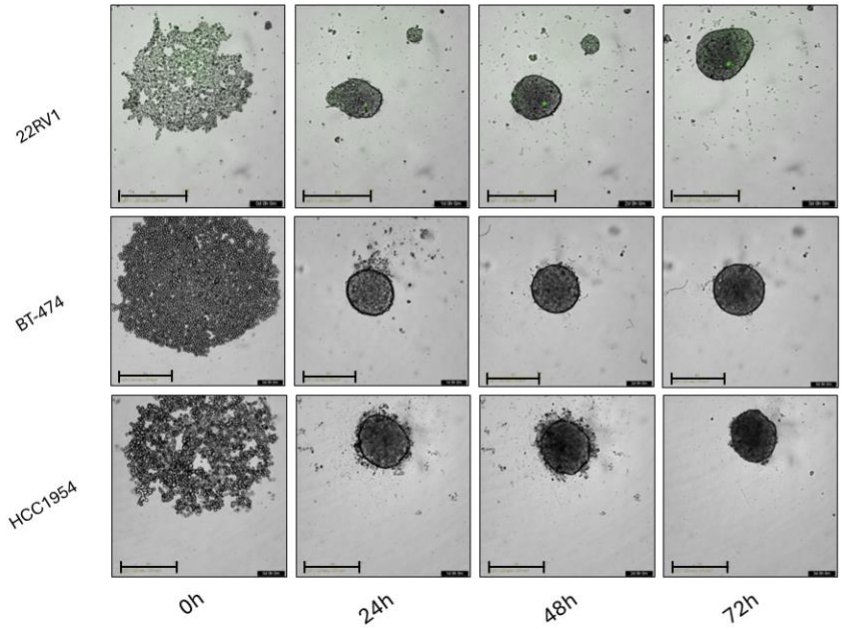

Figure 8. Selected cell lines for the use in spheroids
The Spheroid formation of the selected cell lines (22RV1, BT-474 and HCC1954), which required no use of additives to support the aggregation. BT-474 and HCC1954 cells formed compact spheroids within the initial 24 hours. It was common to observe multiple spheroids with 22RV1 cells that tended to merge during 72 hours of incubation. The pictures are taken from Incucyte brightfield images. The scale bar measures the length of 400 µm.

The growth of BT-474 spheroids was linear for 258h (Figure 9. A). The various conditions did not significantly affect the growth of the spheroids (Figure 9. A-I, II, III, IV, V). There was a lot of background fluorescence from Cytotox green coming outside the spheroid, caused by dying cells that failed to merge with the spheroids. The initial background from the dead cells diminished after 150h timepoint and the fluorescence started to increase after approx. 200h depending on the conditions (Figure 9. B-I). The fluorescence from spheroids treated with Matrigel, was uniformly lower compared to the spheroids without Matrigel (Figure 9. B-I), meaning that the viability of the spheroids either remained higher for longer period of time with the addition of Matrigel or because the focus of the Incucyte images was slightly off caused by the Matrigel.

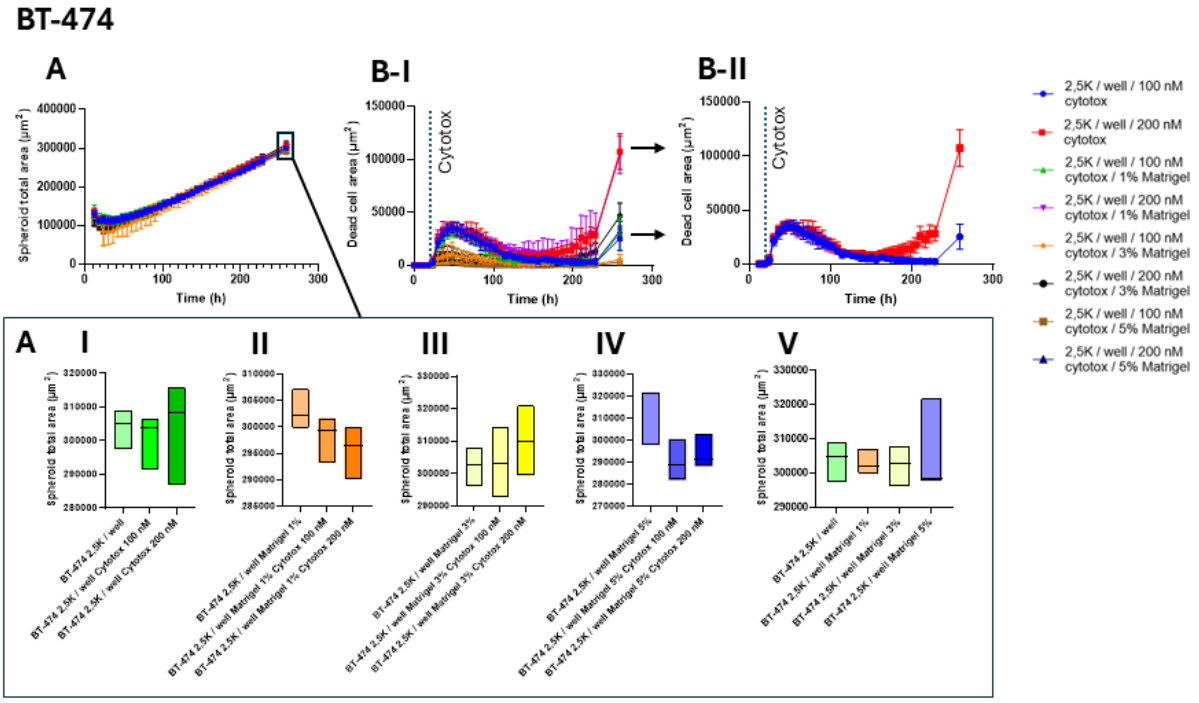

Figure 9. BT-474 spheroid model optimization

(A) The spheroid growth was linear for all treatments. (A-II, III, IV and V) The addition of Cytotox green had no noticeable impact in spheroid sizes between samples with different concentration of Matrigel. (A-V) Matrigel had a positive trend in spheroid size with the 5% Matrigel spheroid samples. (B-I) There was noticeable amount of cell death from the start, caused by cells outside the spheroid. (B-I) The dead cell area decreased after the initial increase in dead cell area, indicating that the cells forming the spheroid were healthy. Cell death starts to increase after 200h, which is detected earliest by the sample without Matrigel that contains 200 nM Cytotox green. (B-I) There was an interruption in the live imaging from 230 hours to 258 hours. A necrotic core developed during the break in imaging, which lead to a sudden increase in cell death once the imaging was resumed. There was an increase in cell death at the final timepoint, with both concentrations of Cytotox green revealing the necrotic core. (B-II) However, the cell death was significantly less pronounced with the 100 nM concentration.

The optimization of HCC1954 cell line was trickier than the other cell lines. A population of cells were observed to stay outside of the spheroids after the initial tightening of the cell mass, causing issues with the spheroid mask. The addition of Cytotox green along with the culture medium caused the cells located outside the spheroids to disperse, resulting in a sudden decrease in spheroid size (Figure 10, A). The decrease in spheroid mask was primarily due to the Incucyte focusing in on the spheroid itself. After the addition of Cytotox green, the spheroid growth was linear (Figure 10, A). There was also increased background with the Cytotox green (Figure 10, B-I). Nevertheless, 100 nM Cytotox green without Matrigel were chosen for HCC1954 cells based on the results from BT-474 and 22RV1 cells. The increase in background fluorescence led to uncertainty of the viability at the later time points (Figure 10, B-II). The spheroid viability was always controlled with untreated spheroids, ruling out the potential of spheroid viability affecting the DR endpoint measurements. There was considerable variation in the spheroid sizes among the different conditions. Nevertheless, none of the conditions

appeared to influence the size of the spheroids (Figure 10, A- I, II, III, IV), except for the observation that the addition of 5% Matrigel resulted in an increased spheroid size (Figure 10, A-V).

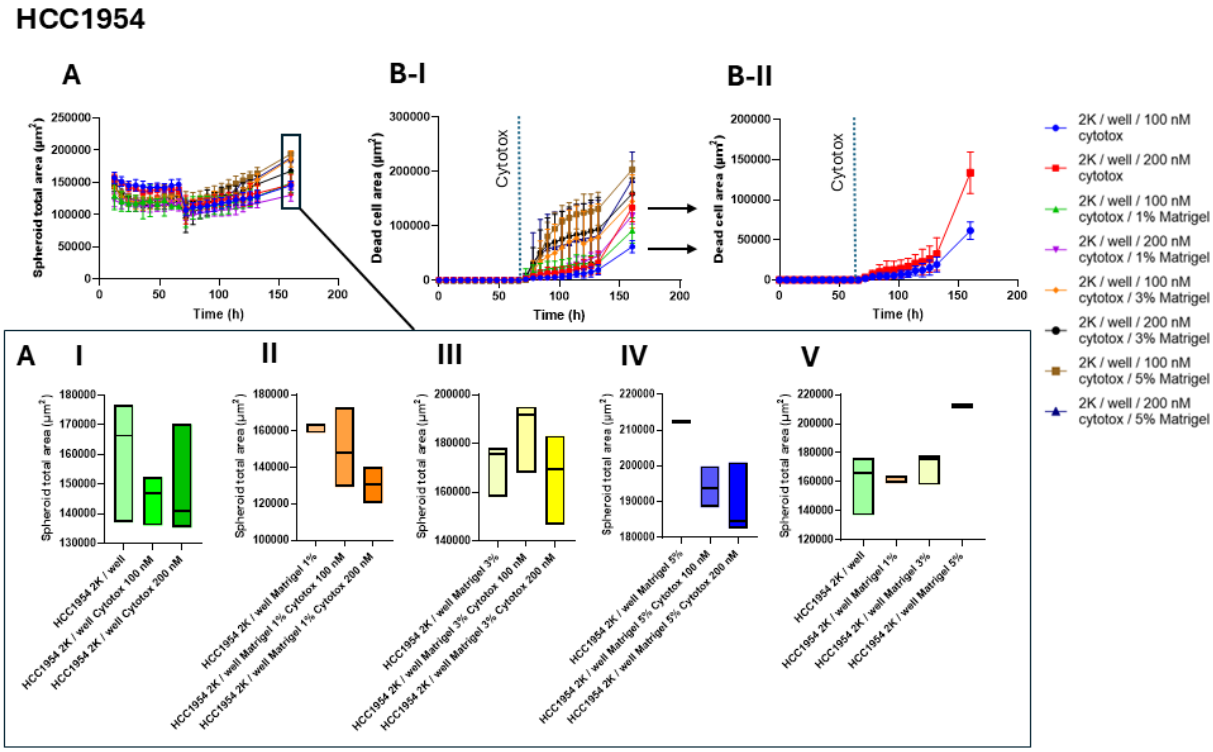

Figure 10. HCC1954 spheroid model optimization

(A) The development of the spheroids exhibited linear growth with variation during the experiment due to complications with the mask used for calculating the spheroid area. Cells located outside the spheroids were mistakenly incorporated into the spheroid area mask, resulting in an inflated measurement of the spheroids' size. Following the addition of Cytotox green with fresh media after 72 hours, the dead cells outside the spheroids were washed away, leading to a reduction in spheroid size, which more accurately reflected the true dimensions of the spheroids (seen as a dip in the total area at 72h timepoint). The growth was linear after 72h with noticeable variation in the spheroid sizes. (A- I, II, III, IV and V) The differences caused by the different conditions were assessed at the last timepoint of the experiment (160h), of which only 5% Matrigel (V) appeared to have a noticeable difference in the spheroid size between the conditions. (B-I) There was also a lot of variances in the dead cell measurements between different conditions. It was anticipated that there would be little to no measurable cell death outside the necrotic core, given that no treatments were applied to the spheroids. However, the early detection of significant fluorescence levels across the spheroids raised concerns about the accuracy of the Cytotox green assay with HCC1954 cells. (B-II) Without Matrigel the cell death levels were lower and started to increase noticeable after 132h.

2.3 The internalization of trastuzumab

The internalization experiments were conducted with Incucyte. The internalization refers here to the net uptake of the mentioned surface protein. Internalization of trastuzumab and hIgG was investigated along an antibody against TfR, which is a highly internalized surface protein expressed across different cancers and cell lines (Daniels et al., 2006). The internalization was studied in both 2D and in 3D to see if there was a difference in the net uptake of trastuzumab. Beginning with the findings from the 2D experiments, it was noted that TfR exhibited a notably high level of internalization across all cell lines (Figure 11, A-I, B-I and C-I). In HCC1954

cells, the internalization begins gradually and accelerates after 36 hours, potentially due to the increase in growth rate of the cells or a threshold effect (Figure 11, A-1). The internalization of trastuzumab can be seen better from (Figure 11, A-II, B-II and C-II) with TfR excluded from the figure. The initial 24 hours in 2D culture are critical for internalization, as this period exhibits the most significant changes, after which the rate of internalization tends to stabilize. The HER2 internalization rates in 22RV1 cells correlate with the low HER2 expression levels, as the internalization rate of 20 nM trastuzumab is almost the same as the 20 nM HIgG control (Figure 11, C-II). BT-474 cells have a high internalization rate for TfR and trastuzumab, which stabilizes after approximately 15h (Figure 11, B-I). The internalization is noticeable decreased with 1 nM trastuzumab compared to the higher doses (Figure 11, A-II and B-II). Internalization in spheroids were tested only with BT-474 and HCC1954 cells (Figure 11, D, E), since the low internalization rate of trastuzumab in 22RV1 cells was already confirmed from 2D studies (Figure 11, C-II) and an even lower internalization rate was expected in 3D. The pHrodo total area between 3D and 2D culture formats cannot be directly compared, as it is not feasible to accurately determine the corresponding 2D area of cells that would match the area of a spheroid. Consequently, the study-focus should be on the kinetic differences between 2D and 3D culture formats, as well as the variations in pHrodo total area in cell lines within same culture formats. Internalization in BT-474 spheroids followed the same trend as in 2D (Figure 11, E). A difference in internalization was observed in HCC1954 cells, where the internalization starts slow, but starts to increase rapidly after 60h with 20 nM trastuzumab and followed up after 100h with 5nM anti-CD71 and 5 nM trastuzumab (Figure 11, D). There is a substantial difference between concentration of 5 nM and 20 nM trastuzumab, which could imply that increasing the dose beyond 20 nM might increase the internalization even more (Figure 11, D).

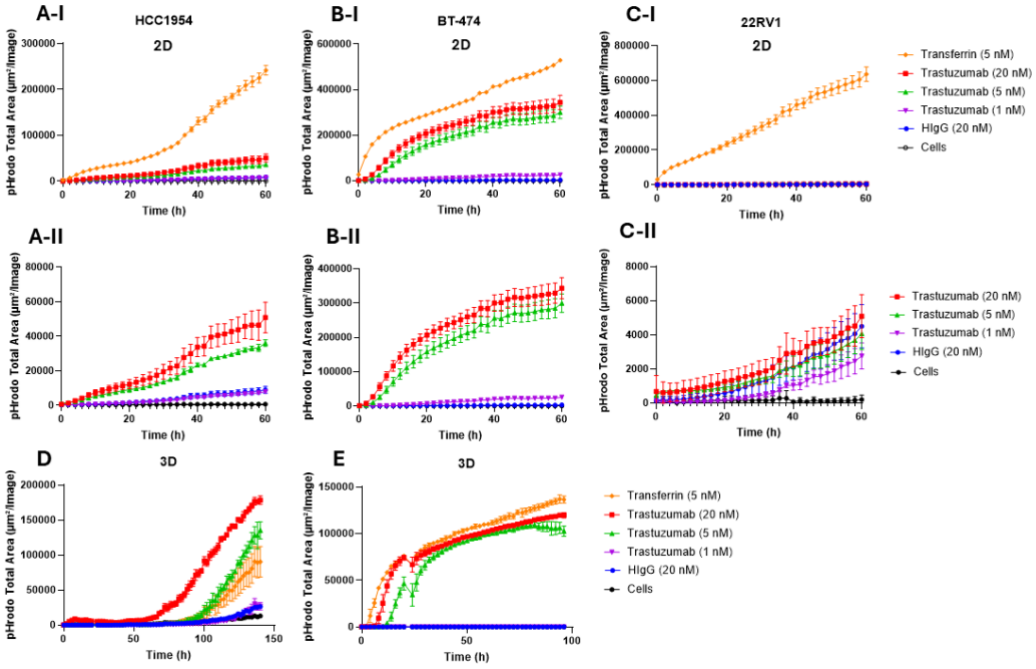

Figure 11. Internalization of HER2 in 2D and 3D culture formats

The graphs illustrate the dose-dependent increase in the internalization of trastuzumab in comparison with TfR and hIgG. TfR is a highly internalized surface protein, establishing a reference for high internalization. HIgG was used to quantify the background fluorescence caused by the target-independent internalization of the antibody isotype. (A-I, B-I and C-I) TfR internalizes highly in all cell lines in 2D culture formats. (A-II and B-II) The internalization rates indicate that a trastuzumab concentration of at least 5 nM is required for the internalization of trastuzumab to significantly exceed the internalization rates observed with the hIgG control. (C-II) The internalization rate of trastuzumab is comparable to that of the hIgG isotype control in 22RV1 cells.
(D) The internalization rates of trastuzumab in HCC1954 cells cultured in 3D increase considerably slower than internalization rates observed in 2D culture (A-I). (D) A dose-dependent relationship was observed in HCC1954 cells, with a trastuzumab concentration of 20 nM exceeding that of 5 nM. (E) The internalization rate of trastuzumab in BT-474 cells cultured in 3D, follows the same pattern as in 2D culture (B-I). The pHrodo total area is not comparable between the 2D and 3D culture formats.

2.4 The start of HER2+ BC spheroid model validation for DR studies

The DR studies were essential for the HER2+ BC models as the primary purpose of the 2D and 3D cytotoxicity models is to be able to rank and screen ADCs in an order of the most to least potent and effective. Any factor that may influence the response independent of the treatment and its properties, has the potential to result in false conclusions regarding the treatment's efficacy. False results could lead to rejection of a promising compound or advancement of ineffective ones into further studies, thereby wasting valuable resources. The DR studies were conducted with free payloads (DXd, Exatecan, DM1, MMAF and MMAE) and ADCs (trastuzumab-DXd_DAR8, trastuzumab-DM1_DAR3,5 and trastuzumab-MMAF_DAR2), to get the complete picture. These investigations were conducted using both 2D and 3D *in vitro* models, which were then compared against each other. All treatments in DR experiments were dosed across a complete logarithmic concentration range, except for MMAE, DM1, and Exatecan, which were tested at only two concentrations in spheroid DR experiments. The focus of these experiments was to measure the differences in IC50 values and maximum inhibitory

rates between different ADCs and payloads. IC50 represents the concentration that induces a 50% inhibitory response. The maximum inhibition rate is the highest response achieved at the peak concentration. Both IC50 and maximum inhibition rate are determined through a non-linear curve fitting process. Potency refers to differences in IC50, while efficacy refers to the maximal inhibition rate.

2.4.1 Monolayer and spheroid model set up using Incucyte

ADC cytotoxicity DR studies were live-imaged with Incucyte for both 2D cultures and spheroids. Live-imaging allowed to measure the cell killing as a function of time. The utility of Incucyte was to aid in choosing the right time for the endpoint measurement, but Incucyte was also used to get preliminary data about the efficacy of the treatments. Only the T-DM1 growth curves are shown as an example, since the Cytotox green measurements from Incucyte were not always as accurate in measuring the cell viability as the CTG endpoint measurements, which is generally a more robust cell viability assay (Figure 12, C). The response to T-DM1 in the 2D cultures appears to begin around 40 hours (Figure 12, A, B), which is also the case for T-MMAF in both cell lines (data not presented). In contrast, the response time for T-DXd in the HCC1954 cell line was observed to occur after 60 hours (data not presented). For the BT-474 cell line, the response time for T-DXd appears to be roughly 40 hours (data not presented). The Cytotox green was also utilized in the 2D studies. However, it was noted that Cytotox green led to a greater deviation in cell viability. As a result, the endpoint measurements using CTG were conducted with cell cultures that did not contain Cytotox green.

The increase in Cytotox green fluorescence was used as an indicator for ADC efficacy in spheroids. The application of Cytotox green was not as effective with the HCC1954 cell line in comparison to the BT-474 cell line, due to problems related to elevated background with HCC1954 cells (Figure 12, C), similar to the challenges encountered in the spheroid setup (Figure 10, B-I). The change in confluence observed in BT-474 cells indicates that T-DM1 begins to exert its effects after 50 hours, while achieving maximal response after 100 hours (Figure 12, B). Outside from the examples presented, the findings obtained with Incucyte were left out from the thesis. There were numerous factors that could have influenced the results, and several inconsistencies with the Cytotox green reagent. Consequently, the primary role of Incucyte was maintained to determine the optimal timepoint for endpoint measurement and to acquire insights regarding the kinetics of ADC efficacy. The endpoint measurement using CTG for both cell lines was determined to be performed at 144 hours, based on the time-dependant inhibition rate (Figure 12, C, D) and cumulative intake of trastuzumab in HCC1954 cells

(Figure 11, D, E).

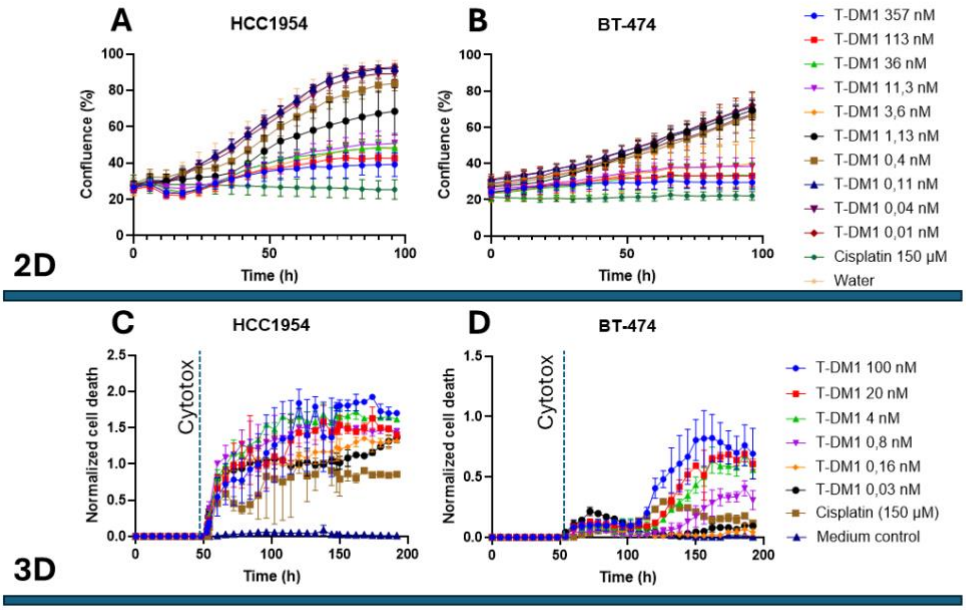

Figure 12. Incucyte as a tool to quantify the cell killing with T-DM1 in 2D and 3D cultures using confluence (%) and Cytotox green as parameters.

Incucyte was used to optimize the time for the endpoint measurement and for preliminary assessment of treatment efficacy. Change in confluence (%) was used to assess the efficacy of different treatments in 2D cultures and Cytotox green was used to assess the ADC efficacy in spheroids. Measuring with Incucyte helped to understand how the efficacy is tied to time (h). Cisplatin was used as a toxic control. **(A)** A response was observed with a concentration above 1.13 nM in HCC1954 cells, while lower concentrations had minimal effect**. (B)** Concentrations below 3,6 nM had no response in BT-474 cells. **(C)** The normalized cell death in HCC1954 cells increased instantaneously with the addition of the treatments along with the Cytotox green, implying that there is a problem with Cytotox green as a death marker. The same is not seen with BT-474 cells, where the response starts at around 50h after the addition of the treatments along with Cytotox green. **(D)** The resistance to Cisplatin in BT-474 cells appears to be elevated in the spheroid culture, as indicated by a decrease in cell death when compared to T-DM1.

2.4.2 Setting up expectations for ADC efficacy with free payloads

Free payloads were dosed in 2D culture format to make sure that the cell lines respond to the payloads used in the studied ADCs. The efficacy of the ADCs and payloads are described as full response, partial response or no response. Full response is categorized as a compound achieving a 90%< inhibition rate. Partial response is defined as a clear response ranging from 30-70% inhibition rate, but with a plateau in the maximum response even at the highest concentrations. No response is when the inhibition rate is close to baseline around 0-20% inhibition rate. Both MMAE and MMAF were used to model the payload efficacy of T-MMAF, since MMAF is a MMAE derivate designed to have decreased membrane permeability. Therefore, it would be inaccurate to assess MMAFs efficacy, given that its exposure to the cells would not correspond with the administered dose. The same philosophy was mistakenly applied to DXd and Exatecan but later found out there isn't much of a

difference in permeability between the two. Exatecan exhibits approximately 10-fold the potency of DXd *in vitro* and demonstrates higher membrane permeability, indicating that free DXd would likely result in lower inhibition rates (Khera et al., 2022). All payloads were studied without the linkers, since linkers would alter the payloads' ability to diffuse through membranes. From payload studies one could draw conclusions about the possible bystander effects of different ADCs and their payloads, since in order to cause cytotoxicity to the cells, the payloads must pass the cell membrane. However, T-DM1 has a non-cleavable linker, which leads to an uncontrolled release of varying versions of DM1-metabolites. This means that even if DM1 can pass through cell membranes, most of the T-DM1 degraded DM1 metabolites containing the linker cannot.

In 2D cultures, MMAE was the most effective and potent in BT-474 and HCC1954 cells (Figure 13, A, B) but not in 22RV1 cells, where MMAE was second to Exatecan (Figure 13, C). 22RV1 cells were more sensitive to each tested payload, including Top1 inhibitors Exatecan and DXd, which had a 100-fold lower potency compared to the other payloads with BT-474 and HCC1954 cells (Figure 13, A B, C). DXd and Exatecan had an especially low efficacy in BT-474 cells (Figure 13, A). DM1 was second in potency behind MMAE in BT-474 and HCC1954 cells (Figure 13, A, B).

There was resistance to the toxic controls in BT-474 cells, causing the inhibition rates to be above 100% on MMAE, DM1 and MMAF (Figure 13, A). The DR curve from 22RV1 cells shows negative values, caused by inconsistent cell seeding amounts when plating cells (Figure 13, C). All tested payloads were effective in 22RV1 cell line, validating it as functional negative control to the other HER2+ cell lines (Figure 13, F). MMAF had good efficacy but low potency in all cell lines, which was expected due to the limited membrane permeability (Figure 13, A, B, C).

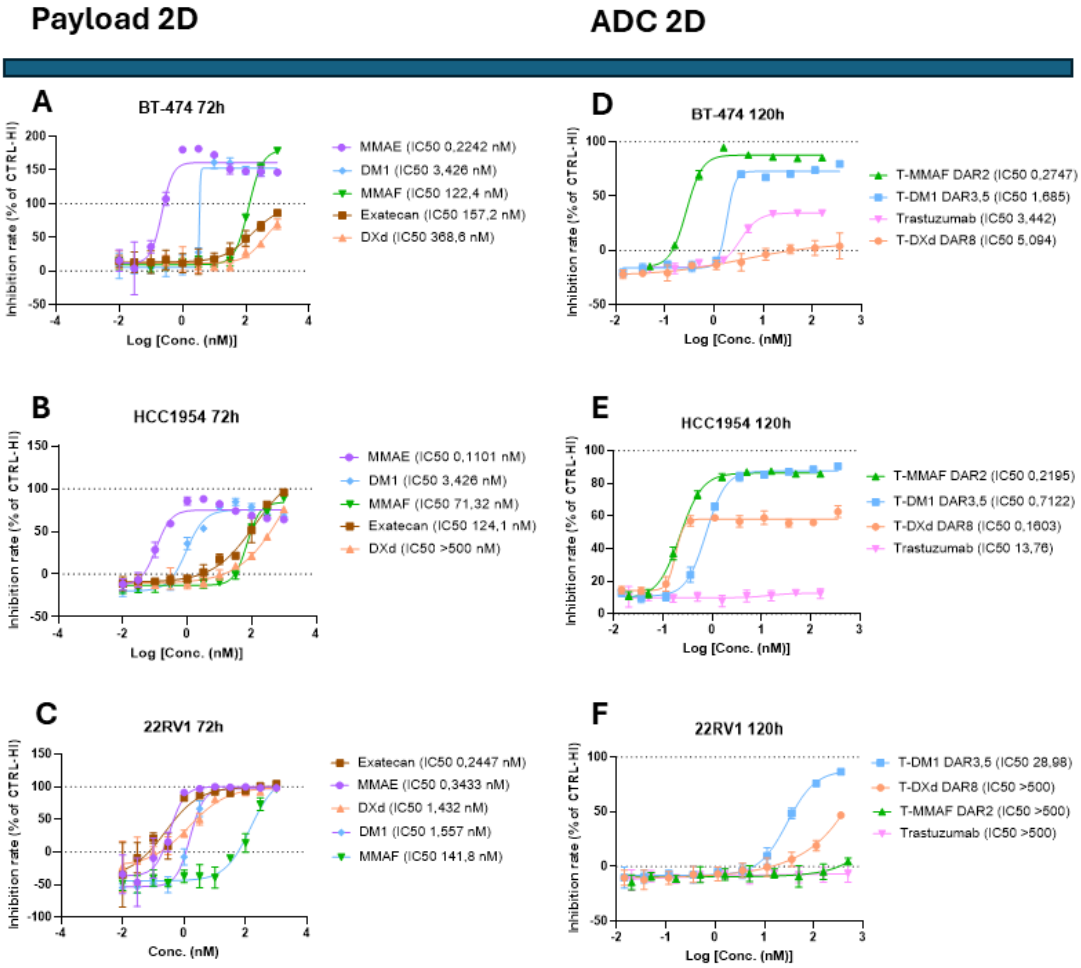

Figure 13. Endpoint measurements from DR studies done in 2D cultures

Figures show payload and ADC inhibition rates in 2D cultures from all cell lines, to illustrate how the ADCs performed in HER2 high (BT-474 and HCC1954) and HER2-low (22RV1) cell lines. Figures (A-C) show payload inhibition rates in 2D cultures from all cell lines, where you can see if there is any resistance to the payloads used in the ADCs. (A-C) Out of Tubulin inhibitors, MMAE was the most potent payload in all cell lines, closely followed by DM1. (A, B) Top1 inhibitors had poor responses in both BT-474 cells and in HCC1954 cells. (C) All of the payloads were effective in 22RV1 cells, validating it as a good negative cell line. (D, E) T-MMAF exhibited the highest levels of potency and efficacy in both BT-474 and HCC1954 cell lines. (E) T-DM1 demonstrated similar efficacy to T-MMAF and the second highest potency in HCC1954 cells. (D) Additionally, T-DM1 ranked second in potency among BT-474 cells, although it did not reach a complete response. (D) T-DXd showed virtually no effect on BT-474 cells, and they displayed a significantly stronger response to trastuzumab than to T-DXd. (E) T-DXd demonstrated high potency in HCC1954 cells but only managed to achieve a partial response. (E, F) As expected, neither HCC1954 nor 22RV1 cells exhibited any response to trastuzumab. The inhibition rates have been derived by subtracting the toxic control values from the raw data, normalizing them to the healthy control values, followed by inverting the results. Values exceeding 100 indicate either resistance or a more effective response of the treatment in comparison to the toxic control.

2.5 ADC DR studies in 2D and 3D cultures

Based on the results from the free payload studies, MMAE and DM1 were expected to be the most effective and potent payloads. Resistance to DXd was observed in BT-474 cells and a lowered potency in both HCC1954 and BT-474 cells. Consequently, it was anticipated that the T-MMAF and T-DM1 would yield similar results, demonstrating strong responses and outperforming T-DXd.

2.5.1 ADC DR studies in 2D cultures were in line with the payload data

The ADCs performed as expected in 2D cultures. T-MMAF had the highest potency and efficacy in both BT-474 and HCC1954 cells. T-DM1 had a similar efficacy as T-MMAF in HCC1954 cells, but a lower potency (Figure 13, D, E). T-DM1 was also second in potency in BT-474 cells, while not resulting in a full response (Figure 13, D). Trastuzumab had a partial response in BT-474 cells with a potency in the range of T-DM1 (Figure 13, D). T-DXd had practically no effect in BT-474 cells (Figure 13, D). BT-474 cells being sensitive to trastuzumab, had a stronger response to trastuzumab than T-DXd (Figure 13, D).
In HCC1954 cells, T-DXd was observed having a high potency, similar to T-MMAF, while only achieving a partial response (Figure 13, E). In the low-expression cell line 22RV1, T-DM1 had the biggest response followed by T-DXd, with T-MMAF having practically no response (Figure 13, F). Neither HCC1954 nor 22RV1 cells responded to trastuzumab, like expected (Figure 13, E, F).

2.5.2 Spheroid cultures did not lead to different outcomes

DR studies were done at two timepoints in spheroids. In BT-474 cells, the endpoint measurements were conducted at 72h and at 144h (Figure 14.). In HCC1954 cells, the endpoint measurements were conducted at 96h and 144h (Figure 14.). The timing of the measurement did not appear to affect the rankings of the treatments in either cell line. In BT-474 cells, the difference between measurements at 72h and 144h was minimal (Figure 14, A, C). The difference between measurements at 96h and 144h in HCC1954, on the other hand were more noticeable (Figure 14, B, D). Both T-MMAF and T-DM1 had only partial responses, while T-DXd had practically no response at 96h (Figure 14, B).
The endpoint measurement at 144h with both spheroid cultures followed the same trend as 2D studies at 120h, where T-MMAF was the most effective, again followed by T-DM1 and T-DXd (Figure 14, C, D). T-DXd continued achieving only a partial response. In Incucyte live-imaging, it looked like T-DXd did not cause cytotoxicity, but more of an anti-proliferative response, limiting the growth of the spheroids, while leaving the spheroid structure completely intact. Trastuzumab was less effective in the spheroids (Figure 14, A, C).

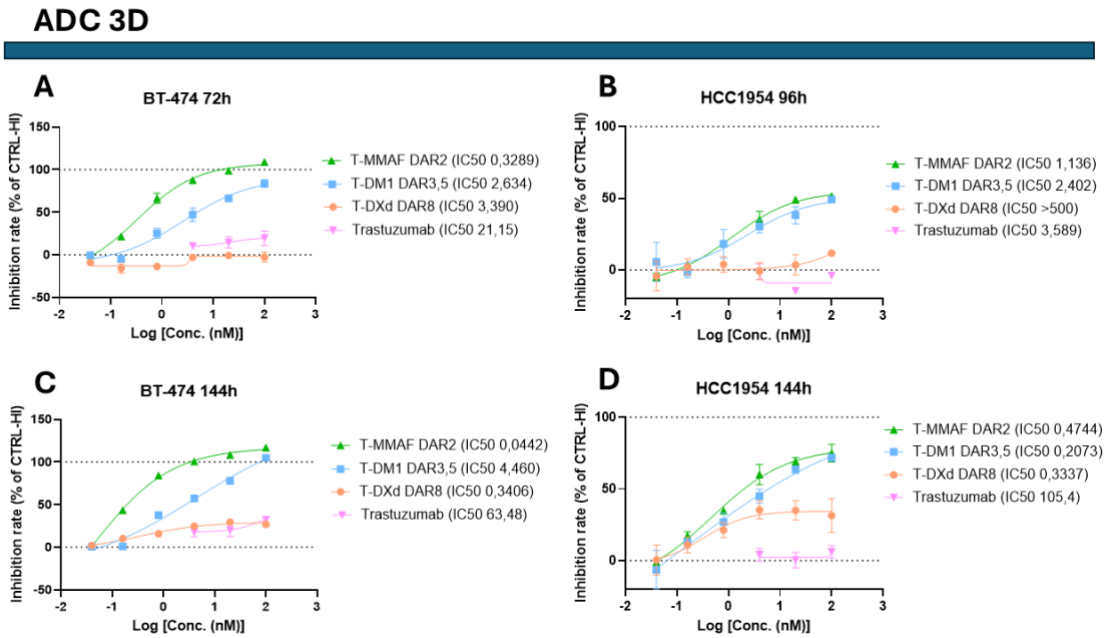

Figure 14. ADC dose response in spheroids at different timepoints

The figure shows how the HER2+ spheroid models respond to HER2 targeted ADCs. (B, D) The graphs show how the endpoint measurement is time-dependent especially with HCC1954 cells, where the response for all ADCs is reduced noticeably at 96h compared to the later timepoint at 144h. (A, C) In the case of BT-474 cells, the distinction does not seem to be as pronounced, except that T-DXd exhibits a marginally greater response at later timepoint (C, D) T-MMAF has the best response in both cell lines, followed by T-DM1 and lastly T-DXd. The difference between T-MMAF and T-DM1 is smaller in HCC1954 cells compared to BT-474 cells.

In the 3D setting, more focus was placed on the ADCs as a delivery mechanism, since the antibody part of the ADC is the main component limiting the ADCs penetration in the 3D environment. To study the effect of ADCs as a delivery mechanism, spheroids were subjected to an equal amount of payload, with one group of payloads conjugated to an antibody and the other as free payload. The concentration of the payloads was calculated by multiplying the ADC concentration with the DAR. Given that T-DXd has a DAR of 8, it means that a 20 nM ADC contains 160 nM of DXd conjugated to it. In a similar manner, T-DM1 has a DAR of 3.5, resulting in a payload concentration of 70 nM per 20 nM ADC, and the same goes for T-MMAF with a DAR of 2. Like previously mentioned, MMAE was used as a proxy for MMAF, and Exatecan for DXd. Since only two concentrations were utilized, the commonly applied four parameter variable slope curve fitting in DR analyses could not be performed. Additionally, the variation in concentrations prevented comparisons of the inhibition rates of the payloads against each other. That being said, MMAE appeared to perform well in the 3D environment, as it was found to be more effective than DM1 in both cell lines, even at lower concentrations. In contrast, Exatecan demonstrated the lowest inhibition rate in both cell lines, despite a significant increase in concentrations compared to MMAE and DM1 (Figure 15). No notable difference in inhibition rates was apparent between ADC and the free payload (Figure 15). A slight trend was noted with BT-474 spheroids, where the free payload demonstrated a greater inhibition rate in comparison to T-MMAF and T-DXd (Figure 15. A, B). However, the trend of

free payload demonstrating a greater inhibition rate was not observed with T-DM1 or any other ADC in HCC1954 spheroids (Figure 15. B, D, E, F).

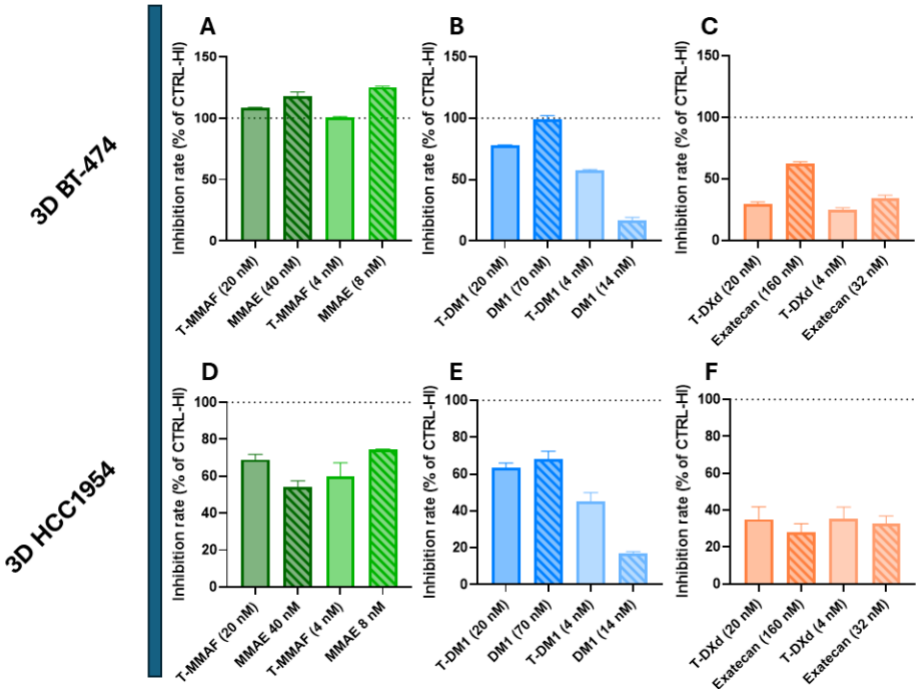

Figure 15. Comparisons between ADCs and payloads in spheroids

The impact of ADCs as a delivery system was studied by administering an equal amount of payload to spheroids with one group of payloads conjugated to an antibody and the other group remaining unconjugated. A concentration of 20 nM T-DXd DAR8 is equivalent to 160 nM DXd, and similarly, this applies to T-DM1 DAR3.5 and T-MMAF DAR2. A slight increase in the inhibition rate associated with free payloads is observed when compared to ADCs in BT-474 spheroids with (A) T-MMAF and MMAE as well as (C) T-DXd and Exatecan. (B) However, the pattern indicating that free payloads exhibit a higher inhibition rate was not as pronounced with T-DM1 and DM1, as this was only evident at elevated concentrations of T-DM1 (20 nM) and DM1 (70 nM), and not at the lower concentrations. (D, E, F) There appears to be no pattern in the favor of ADCs nor payload in the case of HCC1954 spheroids. Free DXd instead of Exatecan should not have resulted in higher inhibition rates, since Exatecan is about 10-fold more potent than DXd *in Vitro* and has a better membrane permeability. The inhibition rates are not comparable between cell lines. The endpoint measurement was performed after 144h.

2.5.3 Comparison between 2D and 3D culture formats was inconclusive

Finally to compare the results between 2D and 3D culture formats, an area under the curve (AUC) was calculated (Figure 16.). The resistance to the toxic control with BT-474 cells increased in 3D culture format, narrowing the assay window compared to the 2D culture format. Since the inhibition rate is normalized to the toxic control, it raises the AUC values of the inhibition rates in 3D culture format, which is why the AUC from BT-474 cells indicate an increased response to ADCs in 3D culture format compared to 2D culture format (Figure 16, A). Differences in the AUC between 2D and 3D culture formats still does not change the rankings of the different ADCs in either cell line.

The assay window in spheroids was also affected in HCC1954 cells by the toxic control, but in the opposite way, by making the cells more sensitive. Because of the differences in the assay windows, the 100% inhibition rate is not the same for both cell lines, which makes the comparison subject for questioning. That in mind, the AUC would indicate that with HCC1954 cell line, the 2D culture format overestimates the efficacy of ADCs comapred to 3D culture format (Figure 16, B). In HCC1954 spheroid model, the difference between T-MMAF and T-DM1 was smaller compared to the difference between the two in 2D culture format (Figure 16, B).

Both 2D and 3D culture formats ranked the ADCs in the same order, with the best being T-MMAF, followed by T-DM1 and T-DXd (Figure 16, A, B).

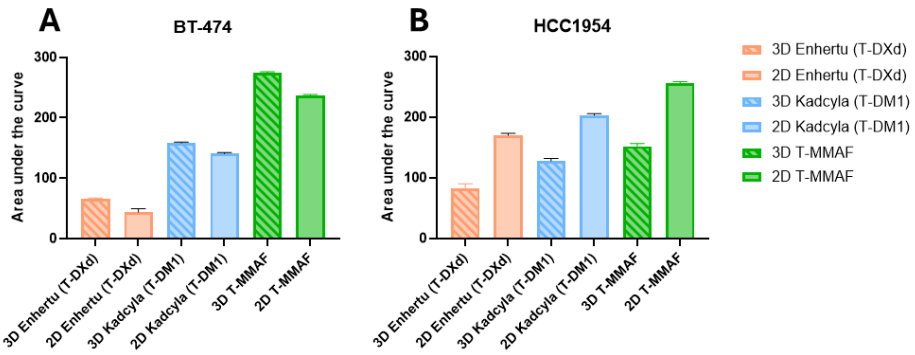

Figure 16. The response to ADCs was different across both cell lines and culture formats

The area under the curve (AUC) was compared between 2D and 3D culture formats. (A) The results showed that ADCs were slightly more efficacious in 3D culture format with BT-474 cells. (B) The opposite was seen with HCC1954 models, where there was a clear trend showing decreased efficacy with ADCs in 3D culture format compared to 2D culture format. T-MMAF (green) was the most efficacious in both cell lines and T-DXd (orange) was the least efficacious. (B) The difference between T-DM1 (blue) and T-MMAF in HCC1954 3D culture format was smaller than in 2D culture format. The contrasting outcomes observed in the BT-474 cell line are likely due to increased resistance to the toxic control (Cisplatin). Since the BT-474 cells did not respond well to the toxic control, the baseline for "maximum effect" was too low. This makes the experimental drugs look more effective than they really are, which can lead to inflated AUC values. Results from HCC1954 cell line are in line with the current literature (Palma Chaundler et al., 2023).

2.6 Visualization of ADC kinetics inside spheroids

The penetration of ADCs and their payloads was imaged with immunofluorescence (IF) staining and confocal microscopy. The ADC penetration was studied in spheroids created with both HCC1954 and BT-474 cell line. The objective was to explore whether the bystander effect of ADCs could be visualized. Previous research has involved the creation of physically cut

slices from treated spheroids, a method that is labour-intensive when compared to confocal imaging techniques (Khera et al. 2022).

The treatment incubation duration was set for 72 hours for T-DXd, while T-MMAF and T-DM1 were incubated for 24 hours. Top1 inhibitors might require a longer period to accumulate sufficient Top1cc on the DNA to induce apoptosis (Tesauro et al., 2019). The mechanism of action for tubulin inhibitors is generally faster, resulting in significant damage to the spheroids already after 72 hours, making it hard to assess the ADC penetration distance from the outer layer. The difference in incubation period was adjusted to enhance the visualization of the payload response when using tubulin inhibitors. The application of antibodies for staining purposes may yield insufficient staining of the spheroid core, since they may struggle penetrating to the core similarly to ADCs, despite the permeabilization of the cell membranes during the staining protocol. Insufficient staining of the spheroid core could lead to false conclusions regarding the depth of payload penetration.

IF staining and imaging was done with all ADCs, but Enhertu was the only ADC exhibiting a bystander effect with DXd, as anticipated (Figure 17). The confocal images were captured at approx. 90 µm from the outer layer of the spheroid. YH2Ax serves as a pharmacodynamic (PD) marker indicating double-stranded breaks induced by DXd. The fluorescence detected from the IF staining of the phosphorylated variant of histone H2AX (yH2Ax) covers almost the entire spheroid, whereas the fluorescence resulting from the IF staining of trastuzumab is limited to the outer layers of the spheroids (Figure 17.). The staining was similar with both BT-474 and HCC1954 spheroids.

The fluorescence measured from the IF staining of trastuzumab with T-MMAF and T-DM1 was strong, but the IF staining of the payload PD marker Phospho-histone H3 (pH3) was lower than anticipated in both cell lines (Figure 18.). PH3 is a PD marker for mitosis and cell mitotic arrest. During cell division and chromatin condensation, pH3 becomes phosphorylated at Serine 10, which can be targeted. IF staining allowed visualization of ADC penetration depth, whereas the released payload was less clearly defined (Figure 18.). The IF staining of trastuzumab was weaker in HCC19554 compared to BT-474 (Figure 18.) The payload staining was expected to follow the staining of trastuzumab. In couple cases, there are so few stained cells that it could be just healthy cells undergoing mitosis. The lack of fluorescence from DAPI at the boundaries where trastuzumab is stained may suggest that the nucleuses of the cells are disintegrated and the pH3 signal is already lost. HCC1954 spheroids were observed being asymmetrical and irregularly shaped, unlike in the images from incucyte (data not presented), possibly implying that the outer layer has degraded away (Figure 17.) But then again, one would expect the trastuzumab staining to be affected as well, so you would expect both to be eroded away.

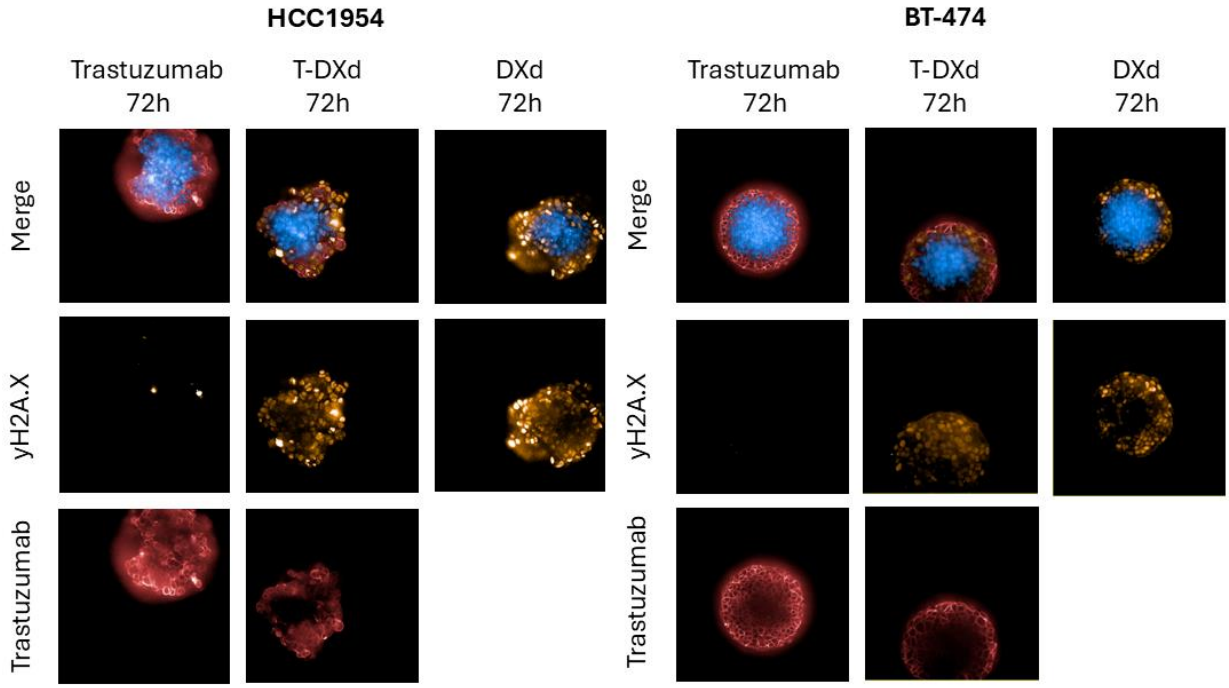

Figure 17. T-DXd penetration and DXd bystander effect visualized

IF stained spheroids imaged with confocal microscopy shows the penetration of T-DXd (red) and the PD effect of the DXd (yellow) and the nucleus of intact cells (blue). T-DXd appears to penetrate only to the superficial layers of the spheroid. DXd on the other hand appears to penetrate deeper, allowing the ADC to target cells deeper in the tumour. The depth of the trastuzumab staining is indirectly validated by the yH2A.x staining depth. This provides confidence to the trastuzumab staining, but the payload penetration visualized through yH2A.x staining could be affected by the penetration of the labelling antibody itself. The cells with an intact nucleus (blue) visualize the zone where the payload did not enter or where the exposure of the payload was too low to cause Cytotoxicity. The slide is approx. 90 µm from the outer layer of the spheroid.

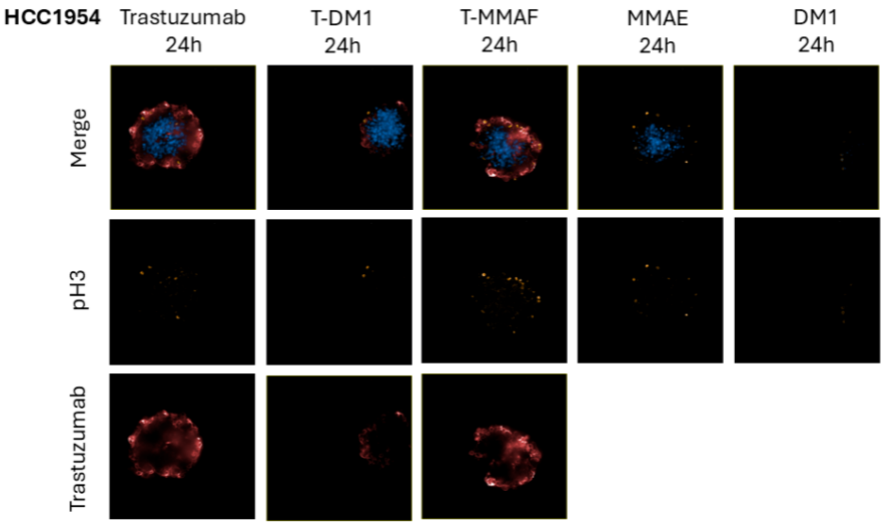

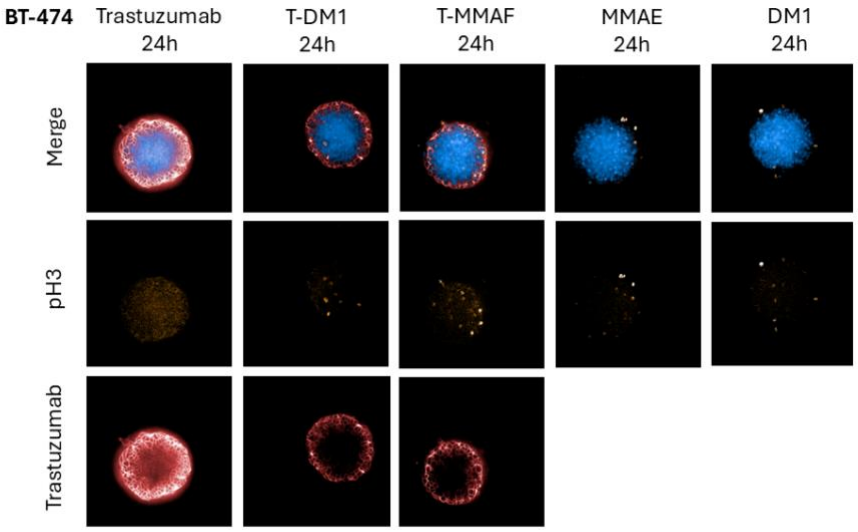

Figure 18. Penetration of T-MMAF and T-DM1

IF stained spheroids imaged with confocal microscopy shows the penetration of T-MMAF and T-DM1 (red) and the PD effect of the tubulin inhibitors (yellow) and the nucleus of intact cells (blue). The IF staining of trastuzumab was strong in BT-474 with trastuzumab, T-DM1 and T-MMAF. The IF staining of trastuzumab was sufficient in HCC1954 with trastuzumab and T-MMAF but not with T-DM1. The weak pH3 staining in both cell lines could indicate a weak response to the treatments with the current time window or problem with the staining protocol. The slides are approx. 90 µm from the outer layer of the spheroid.

3 Discussion

The aim of this thesis was to develop, characterize and validate BC spheroid models for ADC research and development. There are multiple studies that have investigated how different ADCs penetrate into the tumour tissue and how different payloads diffuse into the tumour tissue based on their physicochemical characteristics (Cilliers et al., 2018; Khera et al., 2022; Ogitani et al., 2016b; Palma Chaundler et al., 2023; Thurber et al., 2008). There has been an ongoing effort to identify an *in vitro* model that can effectively demonstrate the efficacy of Enhertu and its active component, Deruxtecan. It was hypothesized that the 3D structure of a spheroid model, would give a more relevant picture of the ADC efficacy and help distinguishing between differences in ADC drug to antibody ratios and payload bystander effect. The impact of these characteristics on ADC efficacy is more challenging to model in a 2D culture format.

3.1 HER2+ BC spheroid optimization

A model is a simplified representation of reality. While it is not necessary for a model to perfectly mirror the disease, especially in the context of an *in vitro* model, it should be capable of addressing fundamental scientific questions and the findings should be applicable to clinical settings. There needs to be a dose-dependent relationship between the measured parameters. A model needs to be able to reliably and confidently distinguish between compounds and rank them in an order of superiority. The ranking shouldn't be affected by the model inherently or if the model does, it needs to be controlled for, which could lead to a narrowed assay window. It's in cancer cells' nature that they are adaptable, which is why every pathway to cause stress is subject for change and needs to be always considered and preferably controlled as well as possible, to allow for informed decisions about the future of the investigated compounds or a pursued novel target. Good models are the cornerstone of a drug development project, and all the results rely on the models, giving results that can be later translated into clinical efficacy.
A variety of different cell lines such as 22RV1 (Prostate cancer), HCC1954 (BC), BT-474 (BC), IM95 (Gastric cancer), SNU-16 (Gastric cancer) and SK-OV-3 (Ovarian cancer) and their inherit capability for spontaneous and extracellular matrix assisted spheroid formation were investigated during the thesis. There are multiple ways to produce spheroids, but one of the easiest and most reproducible way has been utilizing ultra-low attachment plates (Malhão et al., 2022). Out of these cell lines, only SNU-16 did not lead to any aggregation, which could be due to them being a non-adherent cell line. Other groups have managed to produce clustered aggregates with SNU-16, using 1% agarose coated 24-well plates (Mayer et al., 2001).
The model development using Incucyte and Cytotox green reagent was found very helpful and informative. The development of a necrotic core at around 8 days in spheroids with a diameter

of 400-500 µm is consistent with the literature, validating the sensitivity of the Cytotox green as an indicator of cell death (Malhão et al., 2022; Zanoni et al., 2016).

HCC1954 exhibited inconsistencies in spheroid formation. While optimizing the concentrations of Matrigel and Cytotox green with a constant spheroid size across all samples, it raised concerns when the Cytotox green fluorescence observed in Matrigel samples was significantly higher than that in spheroids without Matrigel. The Cytotox green fluorescence appeared to increase with higher concentrations of Matrigel (Figure 10, B-I). However, since the same Matrigel was utilized for BT-474 spheroids, one would anticipate a similar background level for BT-474 cells. BT-474 spheroids embedded in Matrigel exhibited significantly reduced Cytotox green fluorescence when compared to spheroids without Matrigel (Figure 9, B-I). The reduction in Cytotox green fluorescence may be due to optical interference caused by Matrigel scattering or it absorbing the fluorescence emitted by Cytotox green. Additionally, the decrease in fluorescence could result from the Incucyte not properly focusing on the spheroids due to the presence of Matrigel. The increased fluorescence observed in HCC1954 spheroids is likely due to an increased number of cells dying outside the spheroid, which is evident as an elevated background even in the absence of Matrigel, as shown in the DR studies (Figure 12, C). The number of dying cells could be further exacerbated by Matrigel trapping the cells, preventing their dispersion from the spheroid periphery, thereby leading to an increase in Cytotox green fluorescence.

The inability of a population of HCC1954 cells to merge with other HCC1954 cells to form a spheroid may be due to the heterogeneity of the cell line, as observed by the 2D culture morphology (not shown) and the variability in HER2 expression (Figure 5.). The inconsistencies with the spheroid formation could also be due to the aggressive and poorly differentiated phenotype of HCC1954, leading to an irregular structure (de Abreu Pereira et al., 2022). The established treatment windows for all cell lines except HCC1954, were sufficient for internalization and DR studies (Figure 6, 9, 10). The high background observed HCC1954 made it hard to assess the treatment window with Cytotox green. However, the viability of spheroids showed no issues in the later experiments and was always controlled with untreated spheroids, allowing to distinguish difference between treatments and background.

The use of Cytotox green as a measure of cell death proved to be quite practical, although it does have certain limitations. One of them being the plateauing of the response with high concentrations, while the lagging Cytotox green measurement from lower concentrations could ultimately exceed the measurement obtained from higher concentrations. This might be due to the Cytotox green assay exclusively quantifying dying cells, which could lead to a situation where a high ADC concentration kills the cells quickly, resulting in a significant increase in Cytotox green mediated fluorescence in a small area. However, the earlier the cell killing starts and the more intense the cell killing is, the less time there is for the cells to grow. This could

manifest as a low concentration causing steady killing of the cells, while still allowing for the majority of cells to grow, leading to growth of the Cytotox green mediated fluorescence surpassing the peak fluorescence from the higher concentrations. The response with lower ADC concentration could be falsely interpreted as stronger efficacy, since the fluorescence signal is higher in the latter case. Secondly, the Cytotox green does not allow to detect the anti-proliferative effects of payloads, meaning that if there is a cytostatic effect leading to a halt in cell proliferation without inducing cell death, there would essentially be no detectable signal. In contrast, the CTG assay is regarded as more accurate, because it measures viable cells, thereby enabling the quantification of changes in the proliferation rate. CTGs application as an endpoint measurement reagent for spheroids has been established as the most reliable and reproducible method (Zanoni et al., 2016).

3.2 HER2 internalization characterization

Both established spheroid models demonstrated significantly different internalization rates with 5 nM and 20 nM antibody concentrations, despite of the similar HER2 expression levels (Figure 11; Figure 5; DepMap, 2024). The changes in internalization could be due to variety of different reasons specific to each cell line, like differences in expression of adaptor proteins (AP) or endocytic accessory proteins (EAP) in the clathrin-dependent internalization pathway (Mettlen et al., 2018). The internalization rate of HER2 in HCC1954 cells has been observed to exceed that of BT-474 cells (Ram et al., 2014b), which contradicts current findings (Figure 11.). Ram et al. focused on assessing the overall alterations in HER2 surface levels with trastuzumab through flow cytometry, rather than examining the entry of the antibody-HER2 complex into the lysosomes. In their study, a concentration of 15 mg/mL was administered to the cells every 24 hours, with HER2 surface levels being evaluated at 24, 48, and 72 hours. According to the trastuzumab titration curve performed for the present study (data not included) to investigate the HER2 surface expression levels, even a concentration of 20 µg/mL was insufficient to fully saturate the HER2 receptors in either of the investigated cell lines. This discrepancy between results may arise from the application of varying methodologies and different concentrations of trastuzumab.

The internalization was significantly reduced with a 1 nM trastuzumab concentration when compared to the higher concentrations across BT-474 and HCC1954 cells, potentially indicating a threshold effect related to the antibody concentration (Figure 11, A-II and B-II). A restriction point for endocytosis has been documented in existing literature (Loerke et al., 2009). Progression through the restriction point is dependent on the concentration of cargo receptors, which is HER2-antibody complex in this scenario, as well as AP2 adaptors. An increase in cargo concentration significantly improves the maturation efficiency of productive

clathrin-coated pits, preventing them from being aborted and allowing them to develop into clathrin-coated vesicles, which progress to endosomes (Loerke et al., 2009).

TfR is widely expressed receptor on the surface of different cancers including BT-474, HCC1954 and 22RV1 cell lines (DepMap, 2024). TfR is recognized for its significant recycling within different cell lines (Daniels et al., 2006; Cullen and Steinberg, 2018). In the BT-474 cell line, trastuzumab exhibited kinetics similar to TfR (Figure 11, B-I) seen as a plateau of internalization after the first 24h. Trastuzumab exhibiting similar kinetics to TfR may indicate that the ADC-target complex is also influenced by a degree of recycling back to the cell surface. Recycling of the receptor-ADC complex could explain why T-DM1 exhibited a lower efficacy compared to T-MMAF in BT-474 cells (Figure 13, D; Figure 14, C), but not in HCC1954 cells (Figure 13, E; Figure 14, D). T-MMAF features a cleavable linker (PEG4-Val-Cit-PAB) that allows for the release of the drug without requiring the complete degradation of the ADC-target complex. In contrast, T-DM1 is ineffective if the complex is recycled back to the cell surface (Hunter et al., 2020). However, confirming the recycling rate of the ADC-target complex aspect requires separate investigation using a distinct internalization assay capable of detecting early endosomal pH, as the current assay is limited to examining later stages of the endocytic pathway. Based on the literature, the recycling of HER2 in HCC1954 cells could be expected to be the same, which means that the differences in responses to T-DM1 between BT-474 and HCC1954 could be due to some other factors (Ram et al., 2014).

The hypothesized rapid turnover rate of HER2 in BT-474 cells combined with the high receptor expression appears to result in a binding site barrier effect. The turnover refers here to the rapid internalization and recycling of the surface protein. This phenomenon prevents the antibody from effectively penetrating further to activate additional receptors, possibly manifesting as incapability of the antibodies to penetrate any deeper even with the 20 nM concentration (Figure 11, E). The slow additional increase in the internalization could be partly due to the expansion of the outer layer of the spheroid, increasing its surface area. In HCC1954 cells, the turnover rate of HER2 is suspected to be slow, leading to receptor saturation and improved penetration within the spheroid as described by previous publications (Thurber et al., 2008). Improved penetration ultimately contributes to an increased level of internalization, which is further amplified by higher concentrations of trastuzumab (Figure 11, D). The internalization of TfR being decreased to the same levels in spheroids as trastuzumab, could indicate that the decrease is caused by the 3D structure (Figure 11, D, E). The threshold for internalization signal is increased in the 3D culture format, accounting for the high internalization of the first layer. This means that the antibody needs to penetrate deeper into the spheroid to expose multiple cells. When enough cells are internalizing the target, the fluorescence is high enough to surpass the threshold, leading to a readout.

The threshold for internalization may explain the observed DR relationship with trastuzumab, despite the 2D nature of the readout. The enhanced penetration is attributed to a higher concentration. Although TfR facilitates significant uptake in 2D environments, the low concentration of 5 nM restricts penetration in 3D culture format, resulting in uptake levels comparable to those seen with 5 nM trastuzumab (Figure 11, D.).
The IF staining of ADC penetration in HCC1954 and BT-474 spheroids does not indicate a noticeable deeper penetration in HCC1954 spheroids (Figure 17.), which is contradicting to the earlier conclusion. One potential explanation may be the erosion of the outer layer caused by ADC toxicity, which could result in a perceived reduction in antibody penetration distance. Nevertheless, spheroids treated with trastuzumab appeared similar in terms of antibody penetration to those treated with ADCs, despite the fact that trastuzumab was not toxic to HCC1954 cells, which contradicts the earlier claim. Additionally, the incubation period of 72 hours might have been insufficient, as the internalization rate indicated that both internalization and penetration were low to none before 60 hours (Figure 11, D). HCC1954 cells could also exhibit greater heterogeneity in HER2 expression, as indicated by the broader spike in HER2 expression (Figure 5.) and the inconsistent trastuzumab staining when compared to the staining observed in BT-474 spheroids (Figure 17.).

3.3 HER2 ADC cytotoxicity DR characterization

Increased internalization is expected to result in greater exposure to the ADCs. Due to the differences in internalization between HCC1954 and BT-474 cells, it would be reasonable to anticipate a variation in ADC cell killing potency between these cell lines. Certainly, the disparity in internalization begins to diminish after approximately 100 hours, suggesting that the response in HCC1954 spheroids may require a longer duration to develop. Based on that, it could be expected that the response observed before 100 hours would be significantly weaker than at 150 hours. On the other hand, considering the internalization rate in BT-474 spheroids, it could be expected that the effectiveness of ADCs would likely become apparent almost immediately. These differences in the cumulative intake of trastuzumab can be proven by HCC1954 spheroids having only a partial response with T-MMAF and T-DM1 at 96h, while BT-474 spheroids have a full response with same ADCs already at 72h (Figure 14). The slower internalization rate in HCC1954 spheroids could explain why neither T-MMAF nor T-DM1 had sufficient time to achieve a maximal inhibition rate at the highest concentrations (Figure 14, H). This highlights that the endpoint measurement should be cell line and culture format specific. Overall, the results between 2D and 3D culture formats are generally consistent with each other at the final measured timepoint. Payload inhibition rate in 2D cultures suggests tolerance affecting potency and efficacy of Top1 inhibitors in BT-474 cells (Figure 13, A), which correlates with the findings from 2D cultures (Figure 13, D) and 3D ADC studies (Figure 14,

A, C). The lack of difference in AUC values from ADC DR studies between the 3D and 2D culture formats in BT-474 could probably be explained by the similar internalization kinetics (Figure 16.). Additionally, the reduced disparity in AUC values between the 2D and 3D models could be stemming from the 3D culture formats heightened insensitivity to Cisplatin, resulting in a limited assay window that influences the maximal inhibition rates. The superiority of T-MMAF compared to T-DM1 in BT-474 cells is likely due to the higher potency of MMAF, along with the effective internalization of HER2, which allows for significant exposure rates of MMAF to the cells, despite the lower DAR of 2. Conversely, even with high internalization of HER2, T-DM1, which has a less effective payload but a higher DAR of 3.5, may not undergo adequate cleavage. Insufficient cleavage would result in reduced levels of DM1 exposure, thereby limiting its maximum inhibition rate, as has been previously indicated (Figure 13, A; Figure 14, A). The sensitivity of BT-474 cells to trastuzumab indicates that any efficacy observed with T-DXd is most likely due to the trastuzumab component of T-DXd, rather than the payload component.

The DR of ADCs with HCC1954 cells in 2D culture format exhibits a similar pattern to that seen in 3D cultures, with T-DXd resulting in a partial inhibition rate, while T-DM1 and T-MMAF exhibit significantly higher inhibition rates. Despite the low potency of DXd as a free payload (Figure 10, B), T-DXd demonstrates significant potency similar to other ADCs in HCC1954 cells (Figure 13, E). However, the maximal inhibition rate of T-DXd in 3D culture format is lower compared to the maximal inhibition rate in 2D culture. The lower potency of DXd and Exatecan should not be caused by issues with permeability, since both are lipophilic compounds (Khera et al., 2022). The higher potency of T-DXd compared to DXd, is likely due to the increased accumulation of DXd, facilitated by the ADC delivery system, which transports eight payloads per ADC to the spheroid, resulting in increased cellular exposure.

It is important to recognize that a high level of efficacy observed in *in vitro* studies does not necessarily ensure superior outcomes in clinical settings, nor does low efficacy guarantee inferior results. Utilizing a highly potent payload, can lead to decreased tolerability.

In a clinical setting, the major adverse events of T-DM1 are thrombocytopenia and peripheral neuropathy as typical toxicities of tubulin inhibitors. A decrease in platelet count was observed in a monkey study with T-DM1, which correlates with thrombocytopenia, thereby restricting the maximum tolerated dose (MTD) of T-DM1 to 3.6 mg/kg every three weeks in clinical settings (Ogitani et al., 2016a).

A corresponding experimental design administering T-DXd to monkeys induced no toxicities indicative of thrombocytopenia or peripheral neuropathy, which were observed in the monkey studies with T-DM1. Gastrointestinal toxicity and bone marrow toxicity are typical dose-limiting factors in the clinical use of topoisomerase I inhibitors. The effects of T-DXd on the intestines were very slight and the bone marrow toxicity observed as reductions in erythrocyte

production, was only observed at a dosage of 78.8 mg/kg (Ogitani et al., 2016a). The enhanced tolerability of T-DXd permits the administration of higher doses, which typically results in improved patient outcomes.

The disparity in AUC values from ADC DR studies between 3D and 2D culture formats involving HCC1954 cells (Figure 16.) aligns with existing literature, which indicates a reduction in AUC values in 3D cultures (Palma Chaundler et al., 2023).

Resistance to Top1 inhibitors such as DXd and Exatecan in both BT-474 and HCC1954 cell lines may arise from several factors. One potential explanation is that these compounds get transported out of the cells before they can elicit a therapeutic response, which could have been the case, as DXd is a substrate of a variety of different efflux proteins like P-gp, OATP1B1, OATP1B3, MATE2-K, MRP1, and BCRP (Enhertu, Annex I, 2024). That being said, the IF staining of T-DXd and DXd show yH2Ax activation, which signifies the presence of double-stranded DNA breaks (Figure 17.). It is possible that the DNA repair mechanisms are more robust in BT-474 and HCC1954 cell lines than usual. BRCA2 reversion may serve as a potential mechanism of resistance to topoisomerase I inhibitors, as BRCA2 plays a crucial role in homologous recombination and has been associated with resistance to cisplatin, which was also noticed with BT-474 cells (Sakai et al., 2008). The effectiveness of Top1 inhibitors is also linked to the expression levels of Top1, which are together responsible for forming the DNA-Top1 cleavage complexes, which could be saturated. If the forming of Top1cc is slower than the repair mechanisms, then it could lead to a partial response (Kumar and Sherman, 2023; Tesauro et al., 2019). Based on the gene expression levels from Depmap, the expression of Top1 in BT-474 cells is 5,19 log2 (TPM+1) and in HCC1954 cells 6,19 log2 (TPM+1) and in 22RV1 cells it is 6,0 log2 (TPM+1), which could indicate that BT-474 cells are less sensitive to Top1 inhibitors (DepMap, 2024).

The internalization of trastuzumab in 22RV1 cells in the context of trastuzumab expression rate implies that there is barely any difference between endogenous unspecific internalization of hIgG and trastuzumab (Figure 5. & Figure 11, C-II). Knowing this, it is pretty alarming that T-DM1 causes such a high response in 22RV1 cells, while T-DXd has much lower response even with the DAR of eight and a similar potency of the free payload (Figure 13, C, F). The observed unspecified toxicity may result from the instability of the linker utilized in T-DM1, leading to a premature release of the payload. This highlights the benefit of utilizing a hydrophilic payload, such as MMAF, which is unable to diffuse across membranes if released prematurely in the plasma. In instances of early payload release, this characteristic will prevent systemic toxicity.

3.4 Immunofluorescence staining combined with confocal imaging as a tool to study ADC distribution inside a spheroid

The IF staining and confocal imaging worked successfully with T-DXd, but not so well with T-DM1 and T-MMAF. The PD marker yH2Ax, serving as an indicator for the response to topoisomerase I inhibitors, exhibited staining across a wide area of the spheroid cells. In contrast, the PD marker pH3, which indicated the response to tubulin inhibitors, was observed to be stained in only a few cells. Only T-DXd was expected to exhibit a bystander effect from the three previously mentioned ADCs, which would manifest as a diffused PD response across the spheroid, while the ADCs with no bystander effect would only show a strong fluorescent signal at the edges of the spheroid, corresponding to the depth of ADC staining. (Khera et al., 2022). Although this was true for T-DXd and the staining of yH2Ax, a strong staining at the edges of the spheroid was not seen with pH3. This discrepancy may arise from the degradation of dying cells before the spheroids are fixed, caused by the rapid effect of tubulin inhibitors. However, it would be reasonable to anticipate that the remaining cells, which show trastuzumab staining, would also exhibit staining for the PD marker. The low fluorescence observed from pH3 staining raises the question of whether the staining is a result of false positives from dividing cells (Hans and Dimitrov, 2001). It is worth noting that the 24-hour time point for HCC1954 cells is quite early, which may contribute to the reduced staining of pH3 as a result of the low accumulation of trastuzumab (Figure 11, D). However, a response could be expected with BT-474 cells owing to their higher uptake of trastuzumab (Figure 11, E). The pH3 staining was performed with a 72-hour incubation period, resulting in increased quantity of stained cells. Nevertheless, the level of staining remained below expectations. This calls for further optimization of the staining for ADCs with Tubulin inhibitors. The experiment did not include an ADC that utilizes a bystander effect facilitated by a tubulin inhibitor. The absence of a membrane permeable tubulin inhibitor is noteworthy, as it leaves the possibility that minimal payload diffusion to neighboring cells could lead to decreased toxicity while still producing a detectable staining, similar to T-DXd, which, although less toxic, resulted in quantifiable levels of DSBs.

3.5 Solutions to the limitations of the spheroid models

Although the spheroid models appeared consistent and reliable, they did not provide increased translational value regarding the examined ADCs. The inferior inhibition rate of T-DXd is mostly due to the cell lines exhibiting insensitivity towards Top1 inhibitors. It is also possible that comparing Top1 inhibitors and tubulin inhibitors in a similar time window is inherently flawed. Top1 inhibitors require the accumulation of DNA damage to cause cell death, which might take longer to take effect compared to tubulin inhibitors. Enhertu is dosed on three-week intervals in the clinical studies, which last from months to years allowing the full effect of Top1

inhibitors to emerge (Mosele et al., 2023). Time window is an unfortunate limitation in preclinical *in vitro* models, especially in the 2D cell cultures, since the growth is limited to the area of the culture plate. The cell growth is faster in 2D cultures, which can lead to increased efficacy of Tubulin inhibitors (Antoni et al., 2015). Spheroid culture format allows for longer culture periods, since the growth is not limited to a culture plate or scaffold. The growth is only limited by the concentration of nutrients to the cells, which emerges as larger necrotic core, which can be controlled through untreated spheroid controls. In this study, Top1 inhibitors and Tubulin inhibitors were compared in the same time window, which should perhaps be reconsidered in the future. Spheroids could allow for multiple dose studies, similar to *in vivo* studies done in mice, which could better highlight the efficacy of Top1 inhibitors.
There has been a growing interest in utilizing dual payloads in ADCs. One of the reasons for dual payloads would be the possibility of using two compounds with synergy, like a DNA damaging compound with a DNA damage response inhibitor. BT-474 cells could work well as a model with resistance to TOP1 inhibitors, to assess the rationale for such combination, as it has been hypothesized that the DNA damage repair mechanism is responsible for the resistance to Top1 inhibitors (D. Thakkar et al. ACCR 2024). Research indicates that the outer layer of the spheroid is mostly responsible for the spheroid growth, while the inner layers remain quiescent and not proliferating due to increasing hypoxia and accumulation of waste products (Lin and Chang, 2008; Malhão et al., 2022). The endocytosis mediated by clathrin, recognized as the predominant internalization pathway for ADCs, remains unaffected under hypoxic conditions (A. Naveena and Bhatia, 2023). Similar internalization kinetics across the layers, combined with the understanding that Tubulin inhibitors may not effectively target both layers, could support the rationale for combining Top1 inhibitors with Tubulin inhibitors.

3.6 Future of spheroids

Many groups have started investigating how the ADCs tumor penetration could be improved, as currently the challenge of low penetration, is limiting the ADC exposure to the outer layers of the tumours. With a better tumor penetration, more cells would get exposed to the ADC, leading to more cell death. The ADC penetration is affected by the antibody affinity, target expression, internalization and antibody size. There has been attempts through development of biparatopic antibodies that have low affinity but high avidity, binding to two epitopes in the same target protein to get better antibody penetration (Evans and Thurber, 2022). High avidity is the phenomena where multiple low-affinity interactions to the same target can result in a strong overall binding. There has been also attempts to increase the penetration by saturating the targets with naked antibodies and then dosing with an ADC binding to the same target, or dosing them at the same time in a ratio of example 1:8 (Cilliers et al., 2018). Both approaches

in attempt to enhance antibody penetration require a model with a 3D structure, thereby making spheroid models an excellent choice.

Tumors have a varying amount of heterogeneity in terms of antigen positive (Ag+) and antigen negative cells (Ag-). Tumor target heterogeneity has a high relevancy in the context of ADC penetration. BC spheroid models composed of two or more cell lines, which vary in target expression, would provide more support for the selection of payload, DAR and dosage, along with insights into how these factors influence efficacy. In low target expression tumors or highly heterogenous tumors, it's advantageous to have a high DAR since the ADCs tumor penetration will not pose a problem. The low target expression allows for lower doses to effectively saturate the receptors, thereby facilitating the further distribution of the ADC. To compensate the lower ADC dose, a higher DAR is necessary to ensure that cancer cells receive adequate amounts of the payload to induce cell death in both target-positive and target-negative cells.

In high target expression tumors, it would make sense to use a high ADC concentration to help with the tumor penetration. A high ADC dose combined with a low DAR would prevent excessively high payload concentrations resulting from increased ADC internalization, which could result in unnecessary systemic toxicity. Also, a less toxic payload could be better when combined with a higher DAR, while a more potent payload would be optimal for lower DAR. One of the reasons for Enhertus success is it high DAR combined with a less toxic payload, which works well in low expression tumors and in tumors with high target heterogeneity (Modi et al., 2022)

One method to introduce heterogeneity into the spheroids, while simultaneously supporting cell lines that cannot independently form spheroids, is to incorporate fibroblasts into the cultures. Addition of fibroblasts to the culture would create a more authentic ECM for the spheroids (Flörkemeier et al., 2024). Cancer-associated fibroblasts have been linked to increased metastasis and drug resistance in BC, making the treatment responses more translatable to the clinics (Luo et al., 2015). But it would require further studies to generalize a level of heterogeneity in a spheroids that would correspond with the most common HER2-enriched invasive ductal carcinoma and their heterogeneity. To achieve a more authentic representation of tumor cellular heterogeneity, it is also feasible to create patient-derived spheroids. These spheroids can preserve the same cellular heterogeneity in the context of HER2 positive and negative cells, closely resembling the original tumor tissue (Hofmann et al., 2022).

Additional research aimed at creating more sophisticated spheroid models that are more translatable to humans would further reduce the reliance on animal studies, in accordance with the principles of the 3Rs in animal research.

3.7 Conclusions

The target expression was found not to be the sole factor to consider when selecting a cell line for ADC research and development. Variations in internalization may exist even among cell lines exhibiting comparable target expression, as well as between 2D and 3D cultures. Additionally, different cell lines may exhibit varying responses to treatments, and sensitivity levels may differ between 2D and 3D culture formats.

From the characterized BC spheroid models, HCC1954 cell line made the best model, since the model did not struggle with the same issues as BT-474 cell line. Cytotox green alone as a primary endpoint, would not provide sufficient and reliable data for ADC cytotoxicity DR studies. BT-474 cell line had more factors that affected the results, like sensitivity towards trastuzumab and resistance towards Top1 inhibitors and toxic controls Cisplatin and AZD 4573. Further optimization of these spheroid models would require the inclusion of multiple other toxic controls instead of the Cisplatin and AZD 4573.

Both spheroid models are able to rank ADCs with tubulin inhibitors as payloads, but not Top1 inhibitors. If the assumption holds that recycling influences the effectiveness of T-DM1 in the BT-474 cell line, then BT-474 spheroid model demonstrated a superior ability to distinguish between ADCs with cleavable linkers and those with non-cleavable linkers.

The IF staining combined with confocal imaging was successfully implemented and able to visualize the bystander effect of Enhertu, but the protocol for ADCs utilizing tubulin inhibitors, requires further optimization.

4 Materials and methods

4.1 Cell culture

Experiments were mainly performed with BT-474, HCC1954 and 22RV1 cell lines but also with IM95, SKOV3 and SNU-16 cell lines to a lesser extent. BT-474 (HTB-20™, ATCC®), is a cell line isolated from a solid, invasive ductal carcinoma of the breast obtained from a 60-year-old, White, female BC patient. BT-474 cell line represents the luminal B subtype with ER+/PR+/HER2+ expression. BT-474 cells were cultured in DMEM, low glucose, GlutaMAX™ Supplement, pyruvate (Gibco, Cat. No. 21885-025) supplemented with Human insulin 10 mg/l (I9278-5mL, Sigma-Aldrich). HCC1954 (CRL-2338 ™, ATCC®) is an epithelial cell line isolated from a primary stage IIA, grade 3 invasive ductal carcinoma. HCC1954 cell line represents the HER2 enriched subtype with ER-/PR-/HER2+ expression. HCC1954 cells were cultured in RPMI-1640 (ATCC, Cat. No. 30-2001). 22RV1 (CRL-2505 ™, ATCC®) is a human prostate carcinoma epithelial cell line. 22RV1 cells were cultured in RPMI 1640 Medium, GlutaMAX™ Supplemented (Cat.No. 61870-010, Gibco). IM95 (NIBIOHN JCRB cell bank, Cat. No. JCRB1075.0) is a human gastric cancer cell line derived from moderately differentiated adenocarcinoma, originating from a 63-year-old Japanese male. IM95 cells were cultured in DMEM, high glucose, GlutaMAX™ Supplement (Cat.No. 61965, Gibco) supplemented with 10 mg/L Human insulin (I9278-5mL, Sigma). SK-OV-3 (HTB-77™, ATCC®) is a cell line with epithelial morphology that was isolated from the ovary of a 64-year-old, White, female with ovarian adenocarcinoma. SK-OV-3 cells were cultured in McCoy's 5a Medium Modified (ATCC, Cat. 30-2007). SNU-16 (CRL-5974™, ATCC®) is a suspension cell line exhibiting epithelial morphology that was isolated in 1987 from ascites derived from a 33-year-old, female, Asian, stomach cancer patient prior to chemotherapy. SNU-16 cells were cultured in RPMI-1640 Medium (ATCC, Cat. No. 30-2001). All mediums were supplemented with 10% FBS (Sigma-aldrich, Cat.No. F7524) and 1% penicillin/streptomycin (Cat. No. 15140-122, Gibco). Cells were subcultured every 3-5 days. All cells were checked for mycoplasma every other week.

4.2 Spheroid culture

All spheroid cultures were produced with ULA plates (Cat No. 7007, Corning). The surface of the plates prevents cells from attaching to the bottom of the wells, while the circular shape of the wells facilitates the aggregation of cells into a spheroid through centrifugation and the passage of time. All spheroids were cultured with the same media as in 2D cultures. Spheroids formed from BT-474 and HCC1954 cell lines were cultured for a period of 1 to 3 days prior to the experiments, while 22RV1 spheroids were cultured for 3 days. These spheroids remained

viable, showing no detectable necrotic core for approximately eight days. The established treatment window was supported by a preliminary study that examined how various factors influenced spheroid size and the development of a necrotic core. The only treatment applied was Cytotox green, a reagent utilized to assess cell death within the spheroids. Cytotox green was dosed with a final concentration of 100 nM and 200 nM in 150 µl of medium. The diameter of the spheroids was around 300-500 µm, which was achieved by seeding 1500 cells/well for 22RV1, 2000 cells/well for HCC1954 and 2500 cells/well for BT-474 in 100 µl culture medium specific for each cell line. Cell lines utilizing Matrigel (Corning, Cat. No. 356231, Lot 0027004) were applied with 1-5% (v/v) Matrigel straight to the cell suspension in the seeding process. Cells were held on ice, while working with Matrigel to avoid spontaneous polymerization, which starts at 10°C. Cells were centrifuged with 150-300 RCF for 5 min.

4.3 Quantitative flow cytometry

QFACS was used to determine the cell surface expression level of HER2, which is the target for Enhertu (T-DXd), Kadycla (T-DM1) and T-MMAF. Herceptin (trastuzumab, Roche, Lot N3032H26) and a humane IgG isotype control (ThermoFisher, Cat, No. 31154) were labeled with Alexa Fluor® Antibody Labeling Kit (Invitrogen, A20186) according to the instructions provided by the manufacturer. Antibody labeling resulted in a degree of labeling of 4,6 for trastuzumab and 5,4 for hIgG, which was measured with DS-11 Series Spectrophotometer (DeNovix) and calculated according to the manufacturer's protocol. The titration curve was prepared with concentrations ranging from 20 µg/mL to 0.04 µg/mL (20, 15, 10, 5, 1, 0.2, and 0.04 µg/mL). Based on previous unpublished internal data, it was predicted that saturating the HER2 receptors would require a high amount of antibody. This resulted in an emphasis on the elevated concentrations of 20 µg/mL and 15 µg/mL, of which 20 µg/mL was the concentration utilized for beads 1-4 (Quantum™ Simply Cellular® quantification beads, Sigma-Aldrich) to translate the Alexa fluor (AF) fluorescence intensity into a receptor count according to the manufacturer’s protocol. Antibodies and beads were both incubated for 45 min with the AF647 conjugated antibodies. The experiment was conducted with all cell lines, including the 22RV1, which based on the literature was a low HER2 expressive cell line (DepMap, 2024)**.** Inclusion of 22RV1 cell line would later allow comparisons between the results of a low expression cell line and two high expression cell lines: BT474 and HCC1954 (DepMap, 2024).
The acquisition of the fluorescence was executed with Novocyte Quanteon (MilliQuest) with 10 000 events on gate 1 for cells and 2000 events for beads. Fast flowrate was used for cells and medium flowrate for beads. Dot plot consisted of the fluorescence (647 nm), forward-scattered light (FSC-A) and side-scattered light (SSC-A). Density plot was used to screen out

attached cells and density plot to screen out unviable cells. The exact gatings are in the supplementary data.

4.4 Live cell imaging with Incucyte

Spheroids and 2D cultures were imaged at six-hour intervals with Incucyte (Incucyte® SX5, Sartorius, software 2023A). Incucyte recorded cell confluency % and dead cell area for 2D cell cultures. For spheroids, the total spheroid area, dead cell area and green mean intensity were recorded. Green channel (488 nm) was used for Cytotox green (Incucyte® Cytotox Green, Cat. No. 4633) and phase- contrast for spheroid structure. Images were recorded with a 10x objective and an acquisition time of 300 ms. Cytotox green dye is a reagent developed by Sartorius to track dead cells inside spheroids. The reagent works by binding to DNA inside the cells once the membrane wall has been disrupted, leading to an increase in fluorescence (Incucyte® Cytotox Dyes for Detection of Cell Membrane Integrity Disruption). The Cytotox green dye facilitated the assessment of cell death within the spheroids, enabling the determination of a treatment window prior to the development of a necrotic core. Cytotox green was used at a concentration of 100 nM, which was optimized based on the preliminary experiments. Combination of Incucyte with Cytotox green enabled the evaluation of the efficacy of ADCs and free payloads, in addition to determining the optimal time for endpoint measurements.

The total spheroid area and the spheroid dead cell area were used as measurements for the DR studies. There were difficulties associated with readouts from lower concentrations exceeding those from higher concentrations when quantifying dead cells with Cytotox green, potentially due to the continuous growth of the spheroids during the experiment. This growth alone could result in inflated readings of cell death, a scenario that was worsened when evaluating the efficacy of the treatments, as the fluorescence from dying cells at the beginning will be less than the fluorescence from, for instance, 50% of cells dying at a later time point. To mitigate the effect of spheroid growth, the results were adjusted based on the size of the spheroids to generate the normalized cell death -parameter. The Cytotox green derived measurements were not as reliable, which required the endpoint measurement of cell viability at the end of the study with CTG.

4.4.1 Incucyte analysis for cell viability and necrotic core

Most of the DR results were produced through Incucyte, which analyzed the real time images collected throughout the experiments, although not utilized for the thesis. The mask for the spheroids was done individually for all cell lines as they acted differently. The mask was generated with a segmentation between cells and background while utilizing minimum area and eccentricity filters. There were scenarios where the focus of the images or cell debris caused

errors in the mask, which were taken into consideration when analysing the spheroid area and normalized cell death.

The normalized cell death parameter derived from the Cytotox green fluorescence was measured by Incucyte as green calibrated units (GCU). Based on the preliminary experiments, a threshold of 500 GCU was applied for the cell death. The cell death area was quantified by the area (μm^2) where the fluorescence was above the threshold. The cell death area was then normalized with the total spheroid area to create the normalized cell death parameter. The normalized cell death parameter encountered issues, particularly regarding spheroid degradation. The spheroid area mask could misinterpret the expansion of cell debris surrounding the spheroid as part of the total spheroid, resulting in inflated spheroid sizes. This issue with cell debris was particularly significant for HCC1954 cells, rendering the analysis challenging and once again highlighting the necessity for CTG measurements.

4.5 Internalization assay with Incucyte

The internalization of trastuzumab, which served as the backbone of the ADCs used in this study, was examined in both 2D and 3D culture formats. The internalization of the ADCs was assumed to be similar to that of trastuzumab. In 2D cultures the seeding amount was 10 000 cells/well/50 µl for BT-474, 3000 cells/well/50 µl and 6000 cells/well/5V1 in phenol-free medium into a 96-well TC-plate (Revvity, Cat. No. 6055302). All treatments were added in phenol-free medium with added supplements for each cell line based on their needs mentioned in 2.1 cell culture. The internalization experiment with 2D cultures were carried out for 60h. The spheroids were grown with the same seeding amounts as in other experiments but in phenol-free medium and similarly in a 96-well ULA plate (Cat No. 7007, Corning). The internalization experiment was carried out for 150h with HCC1954 cells. The time frame for BT-474 cells was limited to 100h, as significant levels of non-specific fluorescence began to rise from the spheroid core with extended incubation periods. Trastuzumab and anti-CD71 was administered in combination with a secondary FAB fragment that was conjugated with pHrodo deep red, a pH-sensitive fluorophore intended for studying the later phases of the endocytic pathway (InVitrogen, pHrodo™ Antibody Labeling Kits, Cat. No. P35355). An anti-human FAB was used for trastuzumab and anti-mouse FAB for anti-CD71. The pH-sensitive fluorophore is designed to be detected when the antibody reaches the late endosome or lysosome. The linkers used by the ADCs, require enzymes like cathepsin B or the degradation of the ADC, which both happen in the lysosomes and to a degree in late endosomes. The assay basically measures how many antibodies reach the part of the endocytic pathway, where the payload would get released. Both secondary FABs were labeled according to the manufactures protocol, which resulted in a degree of labeling of 0,7 for both anti-human FAB and anti-mouse FAB. Trastuzumab (Roche, Lot N3032H26) was dosed with a final concentration of 20 nM, 5

nM and 1 nM and anti-CD71 (Thermofisher, Cat. No.14-0719-82) with a concentration of 5 nM, which was used as a positive control. HIgG (ThermoFisher, Cat, No. 31154) was dosed with 20 nM as a negative control matching the highest concentration of trastuzumab. The FAB-pHrodo was dosed in a 1:3 ratio to the primary antibody.

4.5.1 Incucyte internalization analysis

The internalization measurement was conducted using Incucyte at two-hour intervals. The same principle as with the analysis of Cytotox green, was applied in the analysis of the internalization of trastuzumab. The pHrodo total area from FAB-pHrodo indicates the area of the spheroid where the fluorescence intensity has exceeded the established threshold. The pHrodo total area parameter was derived from the pHrodo fluorescence and measured by Incucyte as red calibrated unit (RCU). The thresholds used for 2D studies were 0,2 RCU for all cell lines and for 3D 1,4 RCU for BT474 and 0,5 RCU for HCC1954. The total pHrodo area between 3D and 2D culture formats should not be directly compared, since determining accurately the corresponding 2D area of cells that would match with the area of a spheroid is not feasible. Therefore, the emphasis should be on the differences in pHrodo total area within the cell lines and in time window between the 2D and 3D culture formats.

4.6 Cytotoxicity DR studies

Cytotoxicity DR studies were done in both 2D and in 3D culture formats with payloads or ADCs. The studies were performed using BC cell lines BT-474 and HCC1954, along with 22RV1 serving as a negative control cell line. The treatments were dispensed with the help of Labcyte Echo 650 Acoustic Liquid Handlers (Beckman Coulter) in the 2D culture format to 384 well plates in 25 µl of culture medium. ADCs were diluted in sterile mQ H2O and payloads in sterile DMSO. All treatments are listed in table 2.

In 2D payload plates, assay-ready plates were able to be prepared by adding the treatments at the bottom of the wells, without concerns regarding solution evaporation, and allowing the plates to be stored in a freezer for future use. The concentrations ranged from 999 nM to 0.01 nM (999, 299.7, 99.9, 31.6, 10.0, 3.2, 1.0, 0.3, 0.1, 0.03, 0.01 nM). AZD 4573 (AstraZeneca) was used as the toxic control, and DMSO as the negative control in the payload DR experiments. AZD 4573 is a Cyclin-dependent kinase 9 selective inhibitor with high potency and efficacy across multiple cancer cell lines (Cidado et al., 2020).

In the 2D ADC DR experiment, the cells were seeded onto the plates in 25 µl of medium and allowed to adhere overnight, prior to the addition of ADCs in 25 µl of medium on top of them. The concentrations ranged from 500 nM to 0.01 nM (500, 100, 20, 4, 0.8, 0.16, 0.03 and 0.01 nM). Cisplatin (150 µM) was included as a cytotoxic control in the ADC plates and sterile mQ water as negative control.

The 384 well plates were seeded with 3000 22RV1 cells/25µl/well, 4000 HCC1954 cells/25µl/well and 4000 BT-474 cells/25µl/well. All cell lines were seeded to the same 384 TC-plates (Revvity, Cat. No. 6057302). The incubation period was around 4-6 days in culture conditions.

In the 3D cytotoxicity DR studies, the spheroids were seeded with the values mentioned in the 2.2 Spheroid culture. Experiments with spheroids required the treatments to be dispensed manually by pipetting due to the incompatibility of the 96-well ULA plates with the Echo dispenser. ADCs and payloads were added to the same plates. The concentrations ranged from 100 nM to 0.03 nM (100, 100, 20, 4, 0.8, 0.16 and 0.03 nM). The concentrations of the payloads varied based on the ADC DAR. DM1 was dosed with concentrations of 70 and 14 nM. Exatecan was dosed with concentrations of 160 and 32 nM. MMAF was dosed with concentrations of 40 and 8 nM. Cisplatin (150 µM) was included as a cytotoxic control and culture medium as a negative control.

Both 3D and 2D ADC DR plates were imaged with Incucyte™ every at six-hour intervals. The experiments included two technical replicate plates for each cell line, where one plate contained Cytotox green reagent (1:10000, 100 nM) (Sartorius Cat. No. 4633) while the other not.

All cytotoxicity DR studies had an endpoint measurement conducted using CellTiter-Glo (Promega, Cat. No. G9683), which lyses viable cells and binds to the released ATP, resulting in measurable fluorescence. This fluorescence correlates with the number of living cells present within the spheroids or at the bottom of the wells. The fluorescence was quantified using CLARIOstar Plus (BMG Labtech), which is a luminescence plate reader. Cytotoxicity DR studies with payloads had only endpoint measurement with CTG.

Table 2: Treatments used during the experimental part

Treatment, ADCs	Manufacturer/Supplier	Batch/lot/product code	Buffer
Enhertu (T-DXd)	Daiichi Sankyo, AstraZeneca	-	50 mM His-Acetate pH 6
Kadcyla (T-DM1)	Genentech, Roche	-	50 mM His-Acetate pH 6
T-MMAF	in-house	-	50 mM His-Acetate pH 6
Treatment, Payload			
DXd	MedChem Express	HY-13631D	DMSO
Exatecan	MedChem Express	HY-13631A	DMSO
MMAE	BroadPharm	BP-22278	DMSO
MMAF	BroadPharm	BP-22316	DMSO
DM1	BroadPharm	BP-23648	DMSO
Cytotoxic controls			

Cisplatin	MedChem Express	HY-17394	DMSO
AZD 4573	MedChem Express	HY-112088	DMSO

4.7 Immunofluorecence staining and confocal imaging

Spheroids were treated with 20 nM and 4 nM ADC or with payloads with the concentration representing the amount of payload per every ADC. The payload concentration was determined by multiplying the concentration of the ADC by the DAR. Since T-DXd has a DAR of 8, this indicates that a 20 nM ADC contains 160 nM of DXd attached to it. Similarly, T-DM1 has a DAR of 3.5, leading to a payload concentration of 70 nM for every 20 nM of ADC, and the same applies to T-MMAF, which has a DAR of 2. Spheroids were treated with ADCs for a duration of 24 or 72 hours, depending on the type of payload, as the response to tubulin inhibitors was rapid, leading to the lysis of the spheroid structures with the 72h timepoint. ADCs that included a tubulin inhibitor as their payload (such as T-DM1 and T-MMAF) were incubated for 24 hours and subsequently stained with a primary mouse antibody that target the PD marker pH3. In contrast, ADCs with a Top1 inhibitor as the payload (like T-DXd) were incubated for 72 hours and stained with a primary mouse antibody targeting the PD marker yH2Ax. The objective was to assess what was happening inside the spheroids and to study the ADC and payload distribution inside the spheroid. The plan was also to compare the intensity of free-payload and ADC on the PD marker. The protocol was modified from (Bergdorf et al., 2021) with exceptions of using DPBS as a buffer and adjusting the volumes for a 96-well plate.

4.7.1 Fixing of the spheroids.

The spheroids were first washed by continuous aspiration and dispensing with DPBS. Spheroids were fixed with 4% electron microscopy grade paraformaldehyde (Thermofisher, Cat. No.199983) with an incubation time of 30 min in RT and then washed again and left in DPBS and stored in 4 degrees.

4.7.2 Immunofluorescent staining

After the spheroids were fixed, they were permeabilized with 0,5% TritonX (Cat. No. I8896-50ML) in DPBS for 30 min and then blocked with Antibody dilution buffer (ADB, 0,1% Triton X-100, 2% BSA (Sigma-Aldrich Cat. No. A2153) in DPBS) for 1h.
Antibodies were added with final ratio being 1:400 for anti-pH3 (ThermoFisher, Cat. No. 9706) and 1:800 for anti-yH2A.x (ThermoFisher, Cat. No. 560443) and incubated for 16h in a tilter in 4 degrees. Trastuzumab was stained with an AF647 anti-human secondary antibody (ThermoFisher, Cat. No. A21445) with a final ratio of 1:400. Both PD markers were stained with the same AF568 anti-mouse (ThermoFisher, Cat. No. A11004) with final ratio of 1:400.

The secondary antibodies were incubated for 3h in room temperature protected from light. Hoechst 33342 (Invitrogen Cat. No. H3570) was added to the spheroids with ratio of 1:1000 for the last 30 min of incubation. Confocal imaging was performed using Operetta CLS High-Content Analysis System (Revvity) using PhenoPlate™ microplates (Revvity, Cat. No. 6055302) for imaging and the Harmony® high-content imaging and analysis software (Revvity) for analysis. The fluorescence of the IF stainings were acquired with the same intensity (100%) and acquisition time (500 ms). DAPI was acquired with intensity (50%) and acquisition time (20 ms). The final exposure settings of the pictures, with Top1 inhibitor treated spheroids, are adjusted for T-DXd sample. The exposure settings for Tubulin inhibitor treated spheroids, are adjusted for T-MMAF. All images shown are captured from a focal plane positioned 90 µm from the bottom of the spheroid.

4.8 Data analysis

All data analysis was done in Excel and Prism (version 10.3.1). In excel the CTG raw fluorescence measurements were first subtracted with the values from the toxic control, and then normalized to the healthy controls, which were treated with fresh medium. To convert the data from cell viability to cell inhibition rate, the normalized values were subtracted from 1 and then multiplied by 100 to express the results as a percentage (%). In prism the cell inhibition rate and concentrations were transformed to a logarithmic scale and then analysed with a four-parameter variable slope model analysis. The IC50 of the different treatments were calculated from the nonlinear curve fit. AUC was calculated from the nonlinear curves to compare the cytotoxicity DR results between 2D and 3D culture formats. The cytotoxicity DR experiments involving 3D cultures did not utilize a complete set of concentrations for the payloads, which is necessary to calculate the IC50 and AUC values for the free payloads.

4.9 Limitations

The objective of this thesis was to set up BC spheroid models and get preliminary results for the future projects. The experiments were carried out without any biological replicates and solely two technical replicates for the spheroid DR studies. As a result, no statistical analysis could be performed on the results. The comparison of AUC calculations between 2D and 3D culture formats is once more founded on individual DR experiments, rendering the comparison subject for questioning. Furthermore, variations in the assay window were noted between 2D and 3D cultures. In the case of HCC1954 2D cultures, the ratio of fluorescence between healthy and toxic control was 75:1, whereas in 3D cultures, this ratio increased to 118:1. For BT-474 cells, the ratio in 2D cultures was 7:1, but in 3D cultures, it decreased to just 3:1, which could impact the comparison of AUC calculations between the two culture formats.

A greater variation in CTG values from ADC DR experiments was observed in 2D cultures utilizing Cytotox green when compared to the technical replicates which did not include Cytotox green. Consequently, the data presented in the thesis is derived from cultures that were without Cytotox green. However, in the case of spheroids, Cytotox green was administered to the 144-hour samples. Cytotox green may have influenced the results. Nevertheless, the 144-hour ADC DR CTG spheroid data aligns with the corresponding CTG data obtained from earlier time points which were without Cytotox green.

Concerning the IF staining and confocal imaging, there is a possibility that the antibodies used for staining, couldn't penetrate and stain all cells properly. The resolution from the confocal images decreased noticeably after 100 µm from the bottom of the spheroid, which means that the core of the spheroid was never able to be imaged. This limitation was especially relevant for the payload staining and imaging, since DXd was expected to diffuse deeper into the spheroid, and possibly all the way to the core. HER2 could have been stained separately from the ADC, to confirm that the IF staining depth is sufficient for imaging the ADC penetration. The IF staining depth of the payload PD marker could have been verified using an antibody that targets structures within the cell nucleus, such as heterochromatin or the nucleolus.

Given that the Incucyte data is derived from 2D images, all research involving spheroids is subject to uncertainty. The 2D nature of these images introduces ambiguity concerning the fluorescence depth within the spheroid. The threshold set during data analysis, which seeks to differentiate signals from different depths of the spheroid, has a substantial effect on the final results. Differences in threshold could have resulted in different outcomes, which could lead to different interpretation of the data.

Acknowledgements

A big thanks goes to the supervisors Antti Arjonen and Reetta Riikonen for their guidance with conceptualization, data analysis and writing of the project work. Reetta Riikonen had a large contribution in the confocal imaging and Antti Arjonen in the internalization studies and interpretation. A thanks for Marcin Chrusciel for pushing for more and emphasizing the bigger picture. The author would also like to thank the whole ADC research team for all help, especially Shaoxia wang and Camilla Ahlquist for their help with qFACS and continuous support with the experimental work. Thanks for Simo Vainionpää for all the help with ECHO drug dispenser. Thanks for Ilona Arnkil and Sonja Vahlman for the initial help with the Spheroid cultures.

And lastly a big thanks for all the lovely coworkers at Orion and at the University of Turku, who made the journey more enjoyable with their presence.

Abbreviations

ADC	Antibody Drug Conjugate
ADCC	Antibody dependant cellular cytotoxicity
ADB	Antibody dilution buffer
AF	Alexa fluor
Ag+/-	Antigen positive/negative
AUC	Area under the curve
BC	Breast cancer
CDC	Complement dependant cytotoxicity
CME	Clathrin-mediated endocytosis
CavME	Caveolae-mediated endocytosis
CTG	CellTiter-Glo
DAR	Drug antibody ratio
DR	Dose-response
DM1	Mertansine
DSB	Double stranded breaks
DXd	Deruxtecan
ER	Estrogen receptor
ECD	Extracellular domain
FDA	Federal drug administration
FcRn	The neonatal Fc receptor
FAB	Antigen binding fragment
GCU	Green calibrated units
HER2	Human epidermal growth factor receptor 2
IC50	50% inhibitory concentration
IF	Immunofluorescence
MoA	Mechanism of action
MMAE	Monomethyl auristatin E
MMAF	Monomethyl auristatin F
pH3	Phospho-histone H3
PR	Progesterone receptor
PD	Pharmacodynamic
QFACS	Quantitative fluorescence-activated cell sorting
RCU	Red calibrated units
TNBC	Triple-negative breast cancer

Top1	Topoisomerase 1
Top1cc	Top1 cleavage complexes
TfR	Transferrin receptor
ULA	Ultra-low adhesion
yH2AX	phospho-Ser139-H2AX

References

A. Naveena, H., and D. Bhatia. 2023. Hypoxia Modulates Cellular Endocytic Pathways and Organelles with Enhanced Cell Migration and 3D Cell Invasion**. *ChemBioChem*. 24:e202300506. doi:10.1002/cbic.202300506.

de Abreu Pereira, D., V. Sandim, T.F.B. Fernandes, V.H. Almeida, M.R. Rocha, R.J.F.C. do Amaral, M.I.D. Rossi, D.E. Kalume, and R.B. Zingali. 2022. Proteomic Analysis of HCC-1954 and MCF-7 Cell Lines Highlights Crosstalk between αv and β1 Integrins, E-Cadherin and HER-2. *Int. J. Mol. Sci.* 23:10194. doi:10.3390/ijms231710194.

Anderson, N.M., and M.C. Simon. 2020. The tumor microenvironment. *Curr. Biol.* 30:R921–R925. doi:10.1016/j.cub.2020.06.081.

Antoni, D., H. Burckel, E. Josset, and G. Noel. 2015. Three-dimensional cell culture: a breakthrough in vivo. *Int. J. Mol. Sci.* 16:5517–5527. doi:10.3390/ijms16035517.

Arnst, K.E., S. Banerjee, H. Chen, S. Deng, D.-J. Hwang, W. Li, and D.D. Miller. 2019. Current advances of tubulin inhibitors as dual acting small molecules for cancer therapy. *Med. Res. Rev.* 39:1398–1426. doi:10.1002/med.21568.

Austin, C.D., A.M. De Mazière, P.I. Pisacane, S.M. Van Dijk, C. Eigenbrot, M.X. Sliwkowski, J. Klumperman, and R.H. Scheller. 2004a. Endocytosis and Sorting of ErbB2 and the Site of Action of Cancer Therapeutics Trastuzumab and Geldanamycin. *Mol. Biol. Cell*. 15:5268–5282. doi:10.1091/mbc.e04-07-0591.

Austin, C.D., A.M. De Mazière, P.I. Pisacane, S.M. Van Dijk, C. Eigenbrot, M.X. Sliwkowski, J. Klumperman, and R.H. Scheller. 2004b. Endocytosis and Sorting of ErbB2 and the Site of Action of Cancer Therapeutics Trastuzumab and Geldanamycin. *Mol. Biol. Cell*. 15:5268–5282. doi:10.1091/mbc.e04-07-0591.

Badve, S., D.J. Dabbs, S.J. Schnitt, F.L. Baehner, T. Decker, V. Eusebi, S.B. Fox, S. Ichihara, J. Jacquemier, S.R. Lakhani, J. Palacios, E.A. Rakha, A.L. Richardson, F.C. Schmitt, P.-H. Tan, G.M. Tse, B. Weigelt, I.O. Ellis, and J.S. Reis-Filho. 2011. Basal-like and triple-negative breast cancers: a critical review with an emphasis on the implications for pathologists and oncologists. *Mod. Pathol.* 24:157–167. doi:10.1038/modpathol.2010.200.

Baker, B.M., and C.S. Chen. 2012. Deconstructing the third dimension – how 3D culture microenvironments alter cellular cues. *J. Cell Sci.* jcs.079509. doi:10.1242/jcs.079509.

Baldassarre, T., P. Truesdell, and A.W. Craig. 2017. Endophilin A2 promotes HER2 internalization and sensitivity to trastuzumab-based therapy in HER2-positive breast cancers. *Breast Cancer Res.* 19:110. doi:10.1186/s13058-017-0900-z.

Barr, D.J., A.G. Ostermeyer-Fay, R.A. Matundan, and D.A. Brown. 2008. Clathrin-independent endocytosis of ErbB2 in geldanamycin-treated human breast cancer cells. *J. Cell Sci.* 121:3155–3166. doi:10.1242/jcs.020404.

Batra, H., J.A. Mouabbi, Q. Ding, A.A. Sahin, and M.G. Raso. 2023. Lobular Carcinoma of the Breast: A Comprehensive Review with Translational Insights. *Cancers*. 15:5491. doi:10.3390/cancers15225491.

Bergdorf, K.N., C.J. Phifer, M.E. Bechard, M.A. Lee, O.G. McDonald, E. Lee, and V.L. Weiss. 2021. Immunofluorescent staining of cancer spheroids and fine-needle aspiration-derived organoids. *STAR Protoc.* 2:100578. doi:10.1016/j.xpro.2021.100578.

Berrouet, C., N. Dorilas, K.A. Rejniak, and N. Tuncer. 2020. Comparison of drug inhibitory effects (IC_{50}) in monolayer and spheroid cultures. doi:10.1101/2020.05.05.079285.

Bertelsen, V., and E. Stang. 2014. The Mysterious Ways of ErbB2/HER2 Trafficking. *Membranes*. 4:424–446. doi:10.3390/membranes4030424.

Białkowska, K., P. Komorowski, M. Bryszewska, and K. Miłowska. 2020. Spheroids as a Type of Three-Dimensional Cell Cultures-Examples of Methods of Preparation and the Most Important Application. *Int. J. Mol. Sci.* 21:6225. doi:10.3390/ijms21176225.

Birgersdotter, A., R. Sandberg, and I. Ernberg. 2005. Gene expression perturbation in vitro—A growing case for three-dimensional (3D) culture systems. *Semin. Cancer Biol.* 15:405–412. doi:10.1016/j.semcancer.2005.06.009.

Biswas, S.K., S. Banerjee, G.W. Baker, C.-Y. Kuo, and I. Chowdhury. 2022. The Mammary Gland: Basic Structure and Molecular Signaling during Development. *Int. J. Mol. Sci.* 23:3883. doi:10.3390/ijms23073883.

Blair, H.A. 2018. Pyrotinib: First Global Approval. *Drugs*. 78:1751–1755. doi:10.1007/s40265-018-0997-0.

Bloise, N., M. Giannaccari, G. Guagliano, E. Peluso, E. Restivo, S. Strada, C. Volpini, P. Petrini, and L. Visai. 2024. Growing Role of 3D In Vitro Cell Cultures in the Study of Cellular and Molecular Mechanisms: Short Focus on Breast Cancer, Endometriosis, Liver and Infectious Diseases. *Cells*. 13:1054. doi:10.3390/cells13121054.

Bombonati, A., and D.C. Sgroi. 2011. The molecular pathology of breast cancer progression. *J. Pathol.* 223:307–317. doi:10.1002/path.2808.

Cheng, J., M. Liang, M.F. Carvalho, N. Tigue, R. Faggioni, L.K. Roskos, and I. Vainshtein. 2020. Molecular Mechanism of HER2 Rapid Internalization and Redirected Trafficking Induced by Anti-HER2 Biparatopic Antibody. *Antibodies Basel Switz.* 9:49. doi:10.3390/antib9030049.

Cidado, J., S. Boiko, T. Proia, D. Ferguson, S.W. Criscione, M. San Martin, P. Pop-Damkov, N. Su, V.N. Roamio Franklin, C. Sekhar Reddy Chilamakuri, C.S. D'Santos, W. Shao, J.C. Saeh, R. Koch, D.M. Weinstock, M. Zinda, S.E. Fawell, and L. Drew. 2020. AZD4573 Is a Highly Selective CDK9 Inhibitor That Suppresses MCL-1 and Induces Apoptosis in Hematologic Cancer Cells. *Clin. Cancer Res.* 26:922–934. doi:10.1158/1078-0432.CCR-19-1853.

Cilliers, C., B. Menezes, I. Nessler, J. Linderman, and G.M. Thurber. 2018. Improved Tumor Penetration and Single-Cell Targeting of Antibody-Drug Conjugates Increases Anticancer Efficacy and Host Survival. *Cancer Res.* 78:758–768. doi:10.1158/0008-5472.CAN-17-1638.

Cullen, P.J., and F. Steinberg. 2018. To degrade or not to degrade: mechanisms and significance of endocytic recycling. *Nat. Rev. Mol. Cell Biol.* 19:679–696. doi:10.1038/s41580-018-0053-7.

Daniels, T.R., T. Delgado, J.A. Rodriguez, G. Helguera, and M.L. Penichet. 2006. The transferrin receptor part I: Biology and targeting with cytotoxic antibodies for the treatment of cancer. *Clin. Immunol.* 121:144–158. doi:10.1016/j.clim.2006.06.010.

DepMap, B. 2024. DepMap 24Q4 Public. 30825074613 Bytes. doi:10.25452/FIGSHARE.PLUS.27993248.V1.

Drago, J.Z., S. Modi, and S. Chandarlapaty. 2021. Unlocking the potential of antibody–drug conjugates for cancer therapy. *Nat. Rev. Clin. Oncol.* 18:327–344. doi:10.1038/s41571-021-00470-8.

Economopoulou, P., V.G. Kaklamani, and K. Siziopikou. 2012. The role of cancer stem cells in breast cancer initiation and progression: potential cancer stem cell-directed therapies. *The Oncologist*. 17:1394–1401. doi:10.1634/theoncologist.2012-0163.

Elkin, S.R., A.M. Lakoduk, and S.L. Schmid. 2016. Endocytic pathways and endosomal trafficking: a primer. *Wien. Med. Wochenschr.* 166:196–204. doi:10.1007/s10354-016-0432-7.

Erber, R., and A. Hartmann. 2020. Histology of Luminal Breast Cancer. *Breast Care*. 15:327–336. doi:10.1159/000509025.

Evans, R., and G.M. Thurber. 2022. Design of high avidity and low affinity antibodies for in situ control of antibody drug conjugate targeting. *Sci. Rep.* 12:7677. doi:10.1038/s41598-022-11648-0.

Feng, J., Y. Tang, Y. Xu, Q. Sun, F. Liao, and D. Han. 2013. Substrate stiffness influences the outcome of antitumor drug screening in vitro. *Clin. Hemorheol. Microcirc.* 55:121–131. doi:10.3233/CH-131696.

Flörkemeier, I., L.K. Antons, J.P. Weimer, N. Hedemann, C. Rogmans, S. Krüger, R. Scherließ, A. Dempfle, N. Arnold, N. Maass, and D.O. Bauerschlag. 2024. Multicellular ovarian cancer spheroids: novel 3D model to mimic tumour complexity. *Sci. Rep.* 14:23526. doi:10.1038/s41598-024-73680-6.

Fridolfsson, H.N., D.M. Roth, P.A. Insel, and H.H. Patel. 2014. Regulation of intracellular signaling and function by caveolin. *FASEB J.* 28:3823–3831. doi:10.1096/fj.14-252320.

Gargiulo, G. 2018. Next-Generation in vivo Modeling of Human Cancers. *Front. Oncol.* 8:429. doi:10.3389/fonc.2018.00429.

Gilboa, L., R. Ben-Levy, Y. Yarden, and Y.I. Henis. 1995. Roles for a Cytoplasmic Tyrosine and Tyrosine Kinase Activity in the Interactions of Neu Receptors with Coated Pits. *J. Biol. Chem.* 270:7061–7067. doi:10.1074/jbc.270.13.7061.

Girish, S., M. Gupta, B. Wang, D. Lu, I.E. Krop, C.L. Vogel, H.A. Burris Iii, P.M. LoRusso, J.-H. Yi, O. Saad, B. Tong, Y.-W. Chu, S. Holden, and A. Joshi. 2012. Clinical pharmacology of trastuzumab emtansine (T-DM1): an antibody-drug conjugate in development for the treatment of HER2-positive cancer. *Cancer Chemother. Pharmacol.* 69:1229–1240. doi:10.1007/s00280-011-1817-3.

Goldhirsch, A., E.P. Winer, A.S. Coates, R.D. Gelber, M. Piccart-Gebhart, B. Thürlimann, H.-J. Senn, K.S. Albain, F. André, J. Bergh, H. Bonnefoi, D. Bretel-Morales, H. Burstein, F. Cardoso, M. Castiglione-Gertsch, A.S. Coates, M. Colleoni, A. Costa, G. Curigliano, N.E. Davidson, A. Di Leo, B. Ejlertsen, J.F. Forbes, R.D. Gelber, M. Gnant, A. Goldhirsch, P. Goodwin, P.E. Goss, J.R. Harris, D.F. Hayes, C.A. Hudis, J.N. Ingle, J. Jassem, Z. Jiang, P. Karlsson, S. Loibl, M. Morrow, M. Namer, C. Kent Osborne, A.H. Partridge, F. Penault-Llorca, C.M. Perou, M.J. Piccart-Gebhart, K.I. Pritchard, E.J.T. Rutgers, F. Sedlmayer, V. Semiglazov, Z.-M. Shao, I. Smith, B. Thürlimann, M. Toi, A. Tutt, M. Untch, G. Viale, T. Watanabe, N. Wilcken, E.P. Winer, and W.C. Wood. 2013. Personalizing the treatment of women with early breast cancer: highlights of the St Gallen International Expert Consensus on the Primary Therapy of Early Breast Cancer 2013. *Ann. Oncol.* 24:2206–2223. doi:10.1093/annonc/mdt303.

Hammood, M., A.W. Craig, and J.V. Leyton. 2021. Impact of Endocytosis Mechanisms for the Receptors Targeted by the Currently Approved Antibody-Drug Conjugates (ADCs)-A Necessity for Future ADC Research and Development. *Pharm. Basel Switz.* 14:674. doi:10.3390/ph14070674.

Hans, F., and S. Dimitrov. 2001. Histone H3 phosphorylation and cell division. *Oncogene*. 20:3021–3027. doi:10.1038/sj.onc.1204326.

Harbeck, N., F. Penault-Llorca, J. Cortes, M. Gnant, N. Houssami, P. Poortmans, K. Ruddy, J. Tsang, and F. Cardoso. 2019. Breast cancer. *Nat. Rev. Dis. Primer*. 5:66. doi:10.1038/s41572-019-0111-2.

Harper, J., S. Mao, P. Strout, and A. Kamal. 2013. Selecting an optimal antibody for antibody-drug conjugate therapy: internalization and intracellular localization. *Methods Mol. Biol. Clifton NJ.* 1045:41–49. doi:10.1007/978-1-62703-541-5_3.

Haslekås, C., K. Breen, K.W. Pedersen, L.E. Johannessen, E. Stang, and I.H. Madshus. 2005. The Inhibitory Effect of ErbB2 on Epidermal Growth Factor-induced Formation of Clathrin-coated Pits Correlates with Retention of Epidermal Growth Factor Receptor-ErbB2 Oligomeric Complexes at the Plasma Membrane. *Mol. Biol. Cell*. 16:5832–5842. doi:10.1091/mbc.e05-05-0456.

Herschkowitz, J.I., K. Simin, V.J. Weigman, I. Mikaelian, J. Usary, Z. Hu, K.E. Rasmussen, L.P. Jones, S. Assefnia, S. Chandrasekharan, M.G. Backlund, Y. Yin, A.I. Khramtsov, R. Bastein, J. Quackenbush, R.I. Glazer, P.H. Brown, J.E. Green, L. Kopelovich, P.A. Furth, J.P. Palazzo, O.I. Olopade, P.S. Bernard, G.A. Churchill, T. Van Dyke, and C.M. Perou. 2007. Identification of conserved gene expression features between murine mammary carcinoma models and human breast tumors. *Genome Biol.* 8:R76. doi:10.1186/gb-2007-8-5-r76.

Hofmann, S., R. Cohen-Harazi, Y. Maizels, and I. Koman. 2022. Patient-derived tumor spheroid cultures as a promising tool to assist personalized therapeutic decisions in breast cancer. *Transl. Cancer Res.* 11:134–147. doi:10.21037/tcr-21-1577.

Hunter, F.W., H.R. Barker, B. Lipert, F. Rothé, G. Gebhart, M.J. Piccart-Gebhart, C. Sotiriou, and S.M.F. Jamieson. 2020. Mechanisms of resistance to trastuzumab emtansine (T-DM1) in HER2-positive breast cancer. *Br. J. Cancer*. 122:603–612. doi:10.1038/s41416-019-0635-y.

Ivascu, A., and M. Kubbies. 2007. Diversity of cell-mediated adhesions in breast cancer spheroids. *Int. J. Oncol.* doi:10.3892/ijo.31.6.1403.

Jain, N., S.W. Smith, S. Ghone, and B. Tomczuk. 2015. Current ADC Linker Chemistry. *Pharm. Res.* 32:3526–3540. doi:10.1007/s11095-015-1657-7.

Jatoi, I., S.G. Hilsenbeck, G.M. Clark, and C.K. Osborne. 1999. Significance of Axillary Lymph Node Metastasis in Primary Breast Cancer. *J. Clin. Oncol.* 17:2334–2334. doi:10.1200/JCO.1999.17.8.2334.

Jin, Y., S. Edalatian Zakeri, R. Bahal, and A.J. Wiemer. 2022. New Technologies Bloom Together for Bettering Cancer Drug Conjugates. *Pharmacol. Rev.* 74:680–713. doi:10.1124/pharmrev.121.000499.

Kanaji, N., A. Tadokoro, K. Susaki, S. Yokokura, K. Ohmichi, R. Haba, N. Watanabe, S. Bandoh, T. Ishii, H. Dobashi, and T. Matsunaga. 2014. Higher susceptibility of NOD/LtSz-scid Il2rg-/- NSG mice to xenotransplanted lung cancer cell lines. *Cancer Manag. Res.* 431. doi:10.2147/CMAR.S71185.

Kang, J.C., W. Sun, P. Khare, M. Karimi, X. Wang, Y. Shen, R.J. Ober, and E.S. Ward. 2019. Engineering a HER2-specific antibody–drug conjugate to increase lysosomal delivery and therapeutic efficacy. *Nat. Biotechnol.* 37:523–526. doi:10.1038/s41587-019-0073-7.

Kapałczyńska, M., T. Kolenda, W. Przybyła, M. Zajączkowska, A. Teresiak, V. Filas, M. Ibbs, R. Bliźniak, Ł. Łuczewski, and K. Lamperska. 2016. 2D and 3D cell cultures – a comparison of different types of cancer cell cultures. *Arch. Med. Sci.* doi:10.5114/aoms.2016.63743.

Khera, E., S. Dong, H. Huang, L. De Bever, F.L. Van Delft, and G.M. Thurber. 2022. Cellular-Resolution Imaging of Bystander Payload Tissue Penetration from Antibody-Drug Conjugates. *Mol. Cancer Ther.* 21:310–321. doi:10.1158/1535-7163.MCT-21-0580.

Kirkham, M., A. Fujita, R. Chadda, S.J. Nixon, T.V. Kurzchalia, D.K. Sharma, R.E. Pagano, J.F. Hancock, S. Mayor, and R.G. Parton. 2005. Ultrastructural identification of uncoated caveolin-independent early endocytic vehicles. *J. Cell Biol.* 168:465–476. doi:10.1083/jcb.200407078.

Kiss, A.L., and E. Botos. 2009. Endocytosis via caveolae: alternative pathway with distinct cellular compartments to avoid lysosomal degradation? *J. Cell. Mol. Med.* 13:1228–1237. doi:10.1111/j.1582-4934.2009.00754.x.

Kleinman, H.K., and G.R. Martin. 2005. Matrigel: Basement membrane matrix with biological activity. *Semin. Cancer Biol.* 15:378–386. doi:10.1016/j.semcancer.2005.05.004.

Knudson, A.G. 1971. Mutation and Cancer: Statistical Study of Retinoblastoma. *Proc. Natl. Acad. Sci.* 68:820–823. doi:10.1073/pnas.68.4.820.

Kumar, S., and M.Y. Sherman. 2023. Resistance to TOP-1 Inhibitors: Good Old Drugs Still Can Surprise Us. *Int. J. Mol. Sci.* 24:7233. doi:10.3390/ijms24087233.

Lei, X., Y. Lei, J.-K. Li, W.-X. Du, R.-G. Li, J. Yang, J. Li, F. Li, and H.-B. Tan. 2020. Immune cells within the tumor microenvironment: Biological functions and roles in cancer immunotherapy. *Cancer Lett.* 470:126–133. doi:10.1016/j.canlet.2019.11.009.

Leyton, J.V. 2020. Improving Receptor-Mediated Intracellular Access and Accumulation of Antibody Therapeutics-The Tale of HER2. *Antibodies Basel Switz.* 9:32. doi:10.3390/antib9030032.

Li, J.Y., S.R. Perry, V. Muniz-Medina, X. Wang, L.K. Wetzel, M.C. Rebelatto, M.J.M. Hinrichs, B.Z. Bezabeh, R.L. Fleming, N. Dimasi, H. Feng, D. Toader, A.Q. Yuan, L. Xu, J. Lin, C. Gao, H. Wu, R. Dixit, J.K. Osbourn, and S.R. Coats. 2016. A Biparatopic HER2-Targeting Antibody-Drug Conjugate Induces Tumor Regression in Primary Models Refractory to or Ineligible for HER2-Targeted Therapy. *Cancer Cell*. 29:117–129. doi:10.1016/j.ccell.2015.12.008.

Li, M., and Y. Liu. 2016. Topoisomerase I in Human Disease Pathogenesis and Treatments. *Genomics Proteomics Bioinformatics*. 14:166–171. doi:10.1016/j.gpb.2016.02.004.

Li, Z., B.-F. Krippendorff, and D.K. Shah. 2017. Influence of Molecular size on the clearance of antibody fragments. *Pharm. Res.* 34:2131–2141. doi:10.1007/s11095-017-2219-y.

Lin, R., and H. Chang. 2008. Recent advances in three-dimensional multicellular spheroid culture for biomedical research. *Biotechnol. J.* 3:1172–1184. doi:10.1002/biot.200700228.

Loerke, D., M. Mettlen, D. Yarar, K. Jaqaman, H. Jaqaman, G. Danuser, and S.L. Schmid. 2009. Cargo and dynamin regulate clathrin-coated pit maturation. *PLoS Biol.* 7:e57. doi:10.1371/journal.pbio.1000057.

LoRusso, P.M., D. Weiss, E. Guardino, S. Girish, and M.X. Sliwkowski. 2011. Trastuzumab Emtansine: A Unique Antibody-Drug Conjugate in Development for Human Epidermal Growth Factor Receptor 2–Positive Cancer. *Clin. Cancer Res.* 17:6437–6447. doi:10.1158/1078-0432.CCR-11-0762.

Łukasiewicz, S., M. Czeczelewski, A. Forma, J. Baj, R. Sitarz, and A. Stanisławek. 2021. Breast Cancer-Epidemiology, Risk Factors, Classification, Prognostic Markers, and Current Treatment Strategies-An Updated Review. *Cancers*. 13:4287. doi:10.3390/cancers13174287.

Luo, H., G. Tu, Z. Liu, and M. Liu. 2015. Cancer-associated fibroblasts: A multifaceted driver of breast cancer progression. *Cancer Lett.* 361:155–163. doi:10.1016/j.canlet.2015.02.018.

Malhão, F., A.C. Macedo, A.A. Ramos, and E. Rocha. 2022. Morphometrical, Morphological, and Immunocytochemical Characterization of a Tool for Cytotoxicity Research: 3D Cultures of Breast Cell Lines Grown in Ultra-Low Attachment Plates. *Toxics*. 10:415. doi:10.3390/toxics10080415.

Mayer, B., G. Klement, M. Kaneko, S. Man, S. Jothy, J. Rak, and R.S. Kerbel. 2001. Multicellular gastric cancer spheroids recapitulate growth pattern and differentiation phenotype of human gastric carcinomas. *Gastroenterology*. 121:839–852. doi:10.1053/gast.2001.27989.

Meijer, I.M.J., and J.E.M. Van Leeuwen. 2011. ERBB2 is a target for USP8-mediated deubiquitination. *Cell. Signal.* 23:458–467. doi:10.1016/j.cellsig.2010.10.023.

Metrangolo, V., and L.H. Engelholm. 2024. Antibody-Drug Conjugates: The Dynamic Evolution from Conventional to Next-Generation Constructs. *Cancers*. 16:447. doi:10.3390/cancers16020447.

Mettlen, M., P.-H. Chen, S. Srinivasan, G. Danuser, and S.L. Schmid. 2018. Regulation of Clathrin-Mediated Endocytosis. *Annu. Rev. Biochem.* 87:871–896. doi:10.1146/annurev-biochem-062917-012644.

Moasser, M.M. 2007. The oncogene HER2: its signaling and transforming functions and its role in human cancer pathogenesis. *Oncogene*. 26:6469–6487. doi:10.1038/sj.onc.1210477.

Modi, S., W. Jacot, T. Yamashita, J. Sohn, M. Vidal, E. Tokunaga, J. Tsurutani, N.T. Ueno, A. Prat, Y.S. Chae, K.S. Lee, N. Niikura, Y.H. Park, B. Xu, X. Wang, M. Gil-Gil, W. Li, J.-Y. Pierga, S.-A. Im, H.C.F. Moore, H.S. Rugo, R. Yerushalmi, F. Zagouri, A. Gombos, S.-B. Kim, Q. Liu, T. Luo, C. Saura, P. Schmid, T. Sun, D. Gambhire, L. Yung, Y. Wang, J. Singh, P. Vitazka, G. Meinhardt, N. Harbeck, and D.A. Cameron. 2022. Trastuzumab Deruxtecan in Previously Treated HER2-Low Advanced Breast Cancer. *N. Engl. J. Med.* 387:9–20. doi:10.1056/NEJMoa2203690.

Molica, M., S. Perrone, C. Mazzone, P. Niscola, L. Cesini, E. Abruzzese, and P. de Fabritiis. 2021. CD33 Expression and Gentuzumab Ozogamicin in Acute Myeloid Leukemia: Two Sides of the Same Coin. *Cancers*. 13:3214. doi:10.3390/cancers13133214.

Mosele, F., E. Deluche, A. Lusque, L. Le Bescond, T. Filleron, Y. Pradat, A. Ducoulombier, B. Pistilli, T. Bachelot, F. Viret, C. Levy, N. Signolle, A. Alfaro, D.T.N. Tran, I.J.

Garberis, H. Talbot, S. Christodoulidis, M. Vakalopoulou, N. Droin, A. Stourm, M. Kobayashi, T. Kakegawa, L. Lacroix, P. Saulnier, B. Job, M. Deloger, M. Jimenez, C. Mahier, V. Baris, P. Laplante, P. Kannouche, V. Marty, M. Lacroix-Triki, V. Diéras, and F. André. 2023. Trastuzumab deruxtecan in metastatic breast cancer with variable HER2 expression: the phase 2 DAISY trial. *Nat. Med.* 29:2110–2120. doi:10.1038/s41591-023-02478-2.

Mukherjee, P., S. Roy, D. Ghosh, and S.K. Nandi. 2022. Role of animal models in biomedical research: a review. *Lab. Anim. Res.* 38:18. doi:10.1186/s42826-022-00128-1.

Nayak, P., V. Bentivoglio, M. Varani, and A. Signore. 2023. Three-Dimensional In Vitro Tumor Spheroid Models for Evaluation of Anticancer Therapy: Recent Updates. *Cancers*. 15:4846. doi:10.3390/cancers15194846.

Ogitani, Y., T. Aida, K. Hagihara, J. Yamaguchi, C. Ishii, N. Harada, M. Soma, H. Okamoto, M. Oitate, S. Arakawa, T. Hirai, R. Atsumi, T. Nakada, I. Hayakawa, Y. Abe, and T. Agatsuma. 2016a. DS-8201a, A Novel HER2-Targeting ADC with a Novel DNA Topoisomerase I Inhibitor, Demonstrates a Promising Antitumor Efficacy with Differentiation from T-DM1. *Clin. Cancer Res. Off. J. Am. Assoc. Cancer Res.* 22:5097–5108. doi:10.1158/1078-0432.CCR-15-2822.

Ogitani, Y., K. Hagihara, M. Oitate, H. Naito, and T. Agatsuma. 2016b. Bystander killing effect of DS-8201a, a novel anti-human epidermal growth factor receptor 2 antibody-drug conjugate, in tumors with human epidermal growth factor receptor 2 heterogeneity. *Cancer Sci.* 107:1039–1046. doi:10.1111/cas.12966.

Palma Chaundler, C.S., H. Lu, R. Fu, N. Wang, H. Lou, G.S. De Almeida, L.M. Hadi, E.O. Aboagye, and S. Ghaem-Maghami. 2023. Kinetics and efficacy of antibody drug conjugates in 3D tumour models. doi:10.1101/2023.02.14.528517.

Parker, J.S., M. Mullins, M.C.U. Cheang, S. Leung, D. Voduc, T. Vickery, S. Davies, C. Fauron, X. He, Z. Hu, J.F. Quackenbush, I.J. Stijleman, J. Palazzo, J.S. Marron, A.B. Nobel, E. Mardis, T.O. Nielsen, M.J. Ellis, C.M. Perou, and P.S. Bernard. 2009. Supervised Risk Predictor of Breast Cancer Based on Intrinsic Subtypes. *J. Clin. Oncol.* 27:1160–1167. doi:10.1200/JCO.2008.18.1370.

Paul, D., O. Stern, Y. Vallis, J. Dhillon, A. Buchanan, and H. McMahon. 2023. Cell surface protein aggregation triggers endocytosis to maintain plasma membrane proteostasis. *Nat. Commun.* 14:947. doi:10.1038/s41467-023-36496-y.

Pedersen, N.M., I.H. Madshus, C. Haslekås, and E. Stang. 2008. Geldanamycin-Induced Down-Regulation of ErbB2 from the Plasma Membrane Is Clathrin Dependent but Proteasomal Activity Independent. *Mol. Cancer Res.* 6:491–500. doi:10.1158/1541-7786.MCR-07-0191.

Pereira, P.M.R., S.K. Sharma, L.M. Carter, K.J. Edwards, J. Pourat, A. Ragupathi, Y.Y. Janjigian, J.C. Durack, and J.S. Lewis. 2018. Caveolin-1 mediates cellular distribution of HER2 and affects trastuzumab binding and therapeutic efficacy. *Nat. Commun.* 9:5137. doi:10.1038/s41467-018-07608-w.

Perou, C.M., T. Sørlie, M.B. Eisen, M. Van De Rijn, S.S. Jeffrey, C.A. Rees, J.R. Pollack, D.T. Ross, H. Johnsen, L.A. Akslen, Ø. Fluge, A. Pergamenschikov, C. Williams, S.X. Zhu, P.E. Lønning, A.-L. Børresen-Dale, P.O. Brown, and D. Botstein. 2000. Molecular portraits of human breast tumours. *Nature*. 406:747–752. doi:10.1038/35021093.

Petricevic, B., J. Laengle, J. Singer, M. Sachet, J. Fazekas, G. Steger, R. Bartsch, E. Jensen-Jarolim, and M. Bergmann. 2013. Trastuzumab mediates antibody-dependent cell-

mediated cytotoxicity and phagocytosis to the same extent in both adjuvant and metastatic HER2/neu breast cancer patients. *J. Transl. Med.* 11:307. doi:10.1186/1479-5876-11-307.

Puchalapalli, M., X. Zeng, L. Mu, A. Anderson, L. Hix Glickman, M. Zhang, M.R. Sayyad, S. Mosticone Wangensteen, C.V. Clevenger, and J.E. Koblinski. 2016. NSG Mice Provide a Better Spontaneous Model of Breast Cancer Metastasis than Athymic (Nude) Mice. *PLOS ONE*. 11:e0163521. doi:10.1371/journal.pone.0163521.

Pust, S., T.I. Klokk, N. Musa, M. Jenstad, B. Risberg, B. Erikstein, L. Tcatchoff, K. Liestøl, H.E. Danielsen, B. Van Deurs, and K. Sandvig. 2013. Flotillins as regulators of ErbB2 levels in breast cancer. *Oncogene*. 32:3443–3451. doi:10.1038/onc.2012.357.

Rädler, P.D., B.L. Wehde, A.A. Triplett, H. Shrestha, J.H. Shepherd, A.D. Pfefferle, H. Rui, R.D. Cardiff, C.M. Perou, and K.-U. Wagner. 2021. Highly metastatic claudin-low mammary cancers can originate from luminal epithelial cells. *Nat. Commun.* 12:3742. doi:10.1038/s41467-021-23957-5.

Ram, S., D. Kim, R.J. Ober, and E.S. Ward. 2014a. The level of HER2 expression is a predictor of antibody-HER2 trafficking behavior in cancer cells. *mAbs*. 6:1211–1219. doi:10.4161/mabs.29865.

Ram, S., D. Kim, R.J. Ober, and E.S. Ward. 2014b. The level of HER2 expression is a predictor of antibody-HER2 trafficking behavior in cancer cells. *mAbs*. 6:1211–1219. doi:10.4161/mabs.29865.

Riccardi, F., M. Dal Bo, P. Macor, and G. Toffoli. 2023. A comprehensive overview on antibody-drug conjugates: from the conceptualization to cancer therapy. *Front. Pharmacol.* 14:1274088. doi:10.3389/fphar.2023.1274088.

Ritchie, M., L. Tchistiakova, and N. Scott. 2013. Implications of receptor-mediated endocytosis and intracellular trafficking dynamics in the development of antibody drug conjugates. *mAbs*. 5:13–21. doi:10.4161/mabs.22854.

Riehl, P.S., M.Y. Zhang, P. Dhar, Z. Wang, J. Pan, K. Mansfield, W.L. Johnson, Q. Zhang, Y. Li, R. D'Souza, J. Zhang, J. Olsen, M. Deshpande, S. Kotapati, S.A. Hollingsworth, I. Verma, Y. Li, Y. Su, Q. Cheng, S. Yamazoe, L. Micci, M. Broz, J. Janc, E.P. Chekler, and J.C. Lo. 2025. Antibody-Drug Conjugates of NLRP3 Agonists: How Overcoming Lysosomal Accumulation Necessitated Noncanonical Linker Attachments. *J. Med. Chem.* 68:9799–9810. doi:10.1021/acs.jmedchem.5c00596.

Rubahamya, B., S. Dong, and G.M. Thurber. 2024. Clinical translation of antibody drug conjugate dosing in solid tumors from preclinical mouse data. *Sci. Adv.* 10:eadk1894. doi:10.1126/sciadv.adk1894.

Rudnick, S.I., J. Lou, C.C. Shaller, Y. Tang, A.J.P. Klein-Szanto, L.M. Weiner, J.D. Marks, and G.P. Adams. 2011. Influence of Affinity and Antigen Internalization on the Uptake and Penetration of Anti-HER2 Antibodies in Solid Tumors. *Cancer Res.* 71:2250–2259. doi:10.1158/0008-5472.CAN-10-2277.

Ryman, J.T., and B. Meibohm. 2017. Pharmacokinetics of Monoclonal Antibodies. *CPT Pharmacomet. Syst. Pharmacol.* 6:576–588. doi:10.1002/psp4.12224.

Sakai, W., E.M. Swisher, B.Y. Karlan, M.K. Agarwal, J. Higgins, C. Friedman, E. Villegas, C. Jacquemont, D.J. Farrugia, F.J. Couch, N. Urban, and T. Taniguchi. 2008. Secondary

mutations as a mechanism of cisplatin resistance in BRCA2-mutated cancers. *Nature*. 451:1116–1120. doi:10.1038/nature06633.

Samantasinghar, A., N.P. Sunildutt, F. Ahmed, A.M. Soomro, A.R.C. Salih, P. Parihar, F.H. Memon, K.H. Kim, I.S. Kang, and K.H. Choi. 2023. A comprehensive review of key factors affecting the efficacy of antibody drug conjugate. *Biomed. Pharmacother.* 161:114408. doi:10.1016/j.biopha.2023.114408.

Sharma, D.K., A. Choudhury, R.D. Singh, C.L. Wheatley, D.L. Marks, and R.E. Pagano. 2003. Glycosphingolipids Internalized via Caveolar-related Endocytosis Rapidly Merge with the Clathrin Pathway in Early Endosomes and Form Microdomains for Recycling. *J. Biol. Chem.* 278:7564–7572. doi:10.1074/jbc.M210457200.

Shaw, K.R.M., C.N. Wrobel, and J.S. Brugge. 2004. Use of three-dimensional basement membrane cultures to model oncogene-induced changes in mammary epithelial morphogenesis. *J. Mammary Gland Biol. Neoplasia*. 9:297–310. doi:10.1007/s10911-004-1402-z.

Siegel, R.L., T.B. Kratzer, A.N. Giaquinto, H. Sung, and A. Jemal. 2025. Cancer statistics, 2025. *CA. Cancer J. Clin.* 75:10–45. doi:10.3322/caac.21871.

Singh, A.P., S. Sharma, and D.K. Shah. 2016. Quantitative characterization of in vitro bystander effect of antibody-drug conjugates. *J. Pharmacokinet. Pharmacodyn.* 43:567–582. doi:10.1007/s10928-016-9495-8.

Sørlie, T., C.M. Perou, R. Tibshirani, T. Aas, S. Geisler, H. Johnsen, T. Hastie, M.B. Eisen, M. van de Rijn, S.S. Jeffrey, T. Thorsen, H. Quist, J.C. Matese, P.O. Brown, D. Botstein, P.E. Lønning, and A.L. Børresen-Dale. 2001. Gene expression patterns of breast carcinomas distinguish tumor subclasses with clinical implications. *Proc. Natl. Acad. Sci. U. S. A.* 98:10869–10874. doi:10.1073/pnas.191367098.

Su, Z., D. Xiao, F. Xie, L. Liu, Y. Wang, S. Fan, X. Zhou, and S. Li. 2021. Antibody–drug conjugates: Recent advances in linker chemistry. *Acta Pharm. Sin. B*. 11:3889–3907. doi:10.1016/j.apsb.2021.03.042.

Swain, S.M., M. Shastry, and E. Hamilton. 2023. Targeting HER2-positive breast cancer: advances and future directions. *Nat. Rev. Drug Discov.* 22:101–126. doi:10.1038/s41573-022-00579-0.

Talukdar, A., B. Kundu, D. Sarkar, S. Goon, and M.A. Mondal. 2022. Topoisomerase I inhibitors: Challenges, progress and the road ahead. *Eur. J. Med. Chem.* 236:114304. doi:10.1016/j.ejmech.2022.114304.

Tesauro, C., A.K. Simonsen, M.B. Andersen, K.W. Petersen, E.L. Kristoffersen, L. Algreen, N.Y. Hansen, A.B. Andersen, A.K. Jakobsen, M. Stougaard, P. Gromov, B.R. Knudsen, and I. Gromova. 2019. Topoisomerase I activity and sensitivity to camptothecin in breast cancer-derived cells: a comparative study. *BMC Cancer*. 19:1158. doi:10.1186/s12885-019-6371-0.

The Cancer Genome Atlas Network. 2012. Comprehensive molecular portraits of human breast tumours. *Nature*. 490:61–70. doi:10.1038/nature11412.

Thurber, G.M., M.M. Schmidt, and K.D. Wittrup. 2008. Antibody tumor penetration: Transport opposed by systemic and antigen-mediated clearance. *Adv. Drug Deliv. Rev.* 60:1421–1434. doi:10.1016/j.addr.2008.04.012.

Wang, J., and S.-G. Wu. 2023. Breast Cancer: An Overview of Current Therapeutic Strategies, Challenge, and Perspectives. *Breast Cancer Dove Med. Press*. 15:721–730. doi:10.2147/BCTT.S432526.

Wang, Z., H. Li, L. Gou, W. Li, and Y. Wang. 2023. Antibody–drug conjugates: Recent advances in payloads. *Acta Pharm. Sin. B*. 13:4025–4059. doi:10.1016/j.apsb.2023.06.015.

WHO Classification of Tumours Editorial Board, 2019 ed. . Breast tumours. 5th ed. OMS, Geneva.

Wu, J. 2021. The Enhanced Permeability and Retention (EPR) Effect: The Significance of the Concept and Methods to Enhance Its Application. *J. Pers. Med.* 11:771. doi:10.3390/jpm11080771.

Wu, S., and D.K. Shah. 2020. Determination of ADC Cytotoxicity in Immortalized Human Cell Lines. *Methods Mol. Biol. Clifton NJ*. 2078:329–340. doi:10.1007/978-1-4939-9929-3_23.

Xiong, X., L.-W. Zheng, Y. Ding, Y.-F. Chen, Y.-W. Cai, L.-P. Wang, L. Huang, C.-C. Liu, Z.-M. Shao, and K.-D. Yu. 2025. Breast cancer: pathogenesis and treatments. *Signal Transduct. Target. Ther.* 10:49. doi:10.1038/s41392-024-02108-4.

Xu, S. 2015. Internalization, Trafficking, Intracellular Processing and Actions of Antibody-Drug Conjugates. *Pharm. Res.* 32:3577–3583. doi:10.1007/s11095-015-1729-8.

Zanoni, M., F. Piccinini, C. Arienti, A. Zamagni, S. Santi, R. Polico, A. Bevilacqua, and A. Tesei. 2016. 3D tumor spheroid models for in vitro therapeutic screening: a systematic approach to enhance the biological relevance of data obtained. *Sci. Rep.* 6:19103. doi:10.1038/srep19103.

Zhao, Y.-Y., O. Feron, C. Dessy, X. Han, M.A. Marchionni, and R.A. Kelly. 1999. Neuregulin Signaling in the Heart: Dynamic Targeting of erbB4 to Caveolar Microdomains in Cardiac Myocytes. *Circ. Res.* 84:1380–1387. doi:10.1161/01.RES.84.12.1380.

D. Thakkar, B. Dharmadhikari, O. Zharkova, S. Paliwal, W. Toy, G. Khoo, S. Guan, S. Chen, C.T. Ng, B. Ayers, R. Srinivasan, X.L. Sim, A. Bansal, P. Ingram, J. Boyd-Kirkup *A novel HER2 targeted dual-payload ADC, HMBD-802 overcomes resistance to topoisomerase 1 inhibitor ADC* San Diego ACCR 2024

Incucyte® Cytotox Dyes for Detection of Cell Membrane Integrity Disruption Product Guide

European Medicines Agency. 2024. Kadcyla: Summary of Product Characteristics. Amsterdam (NL)

European Medicines Agency. 2025. Enhertu: Summary of Product Characteristics. Amsterdam (NL)

BioRender.com. (2025). BioRender [Online software].

AI was used to polish the language and structure of the writing.

Supplementary data

22RV1 qFACS gating

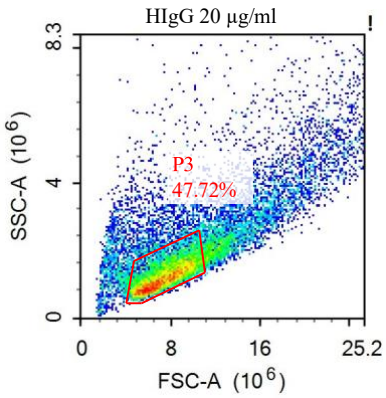

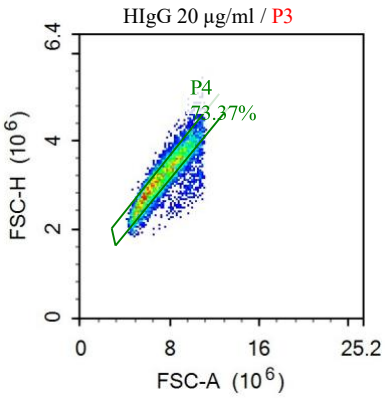

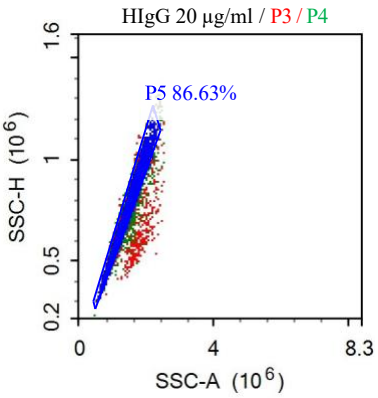

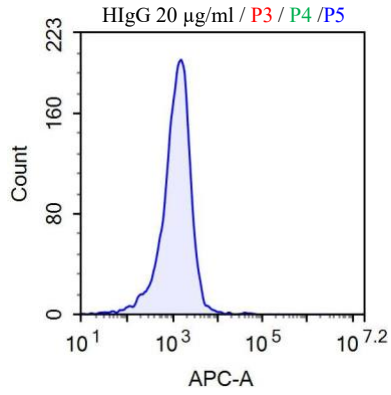

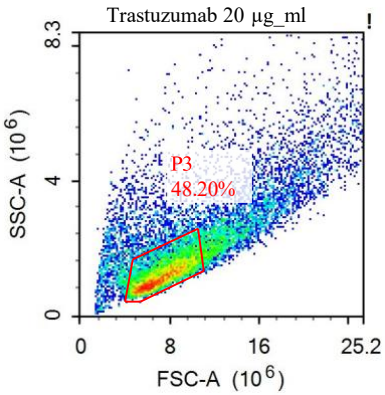

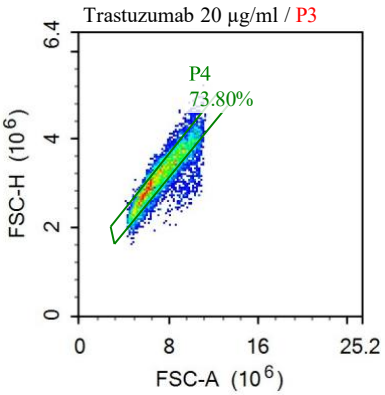

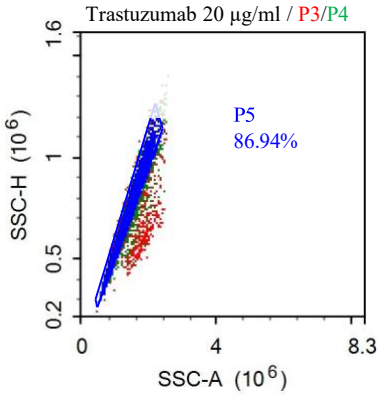

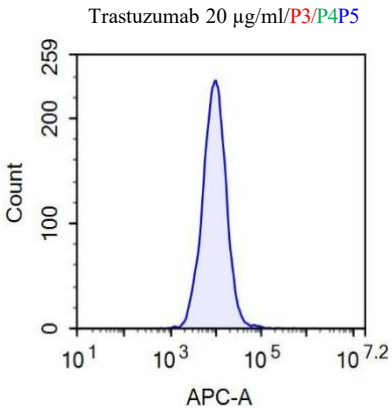

BT-474 qFACS gating

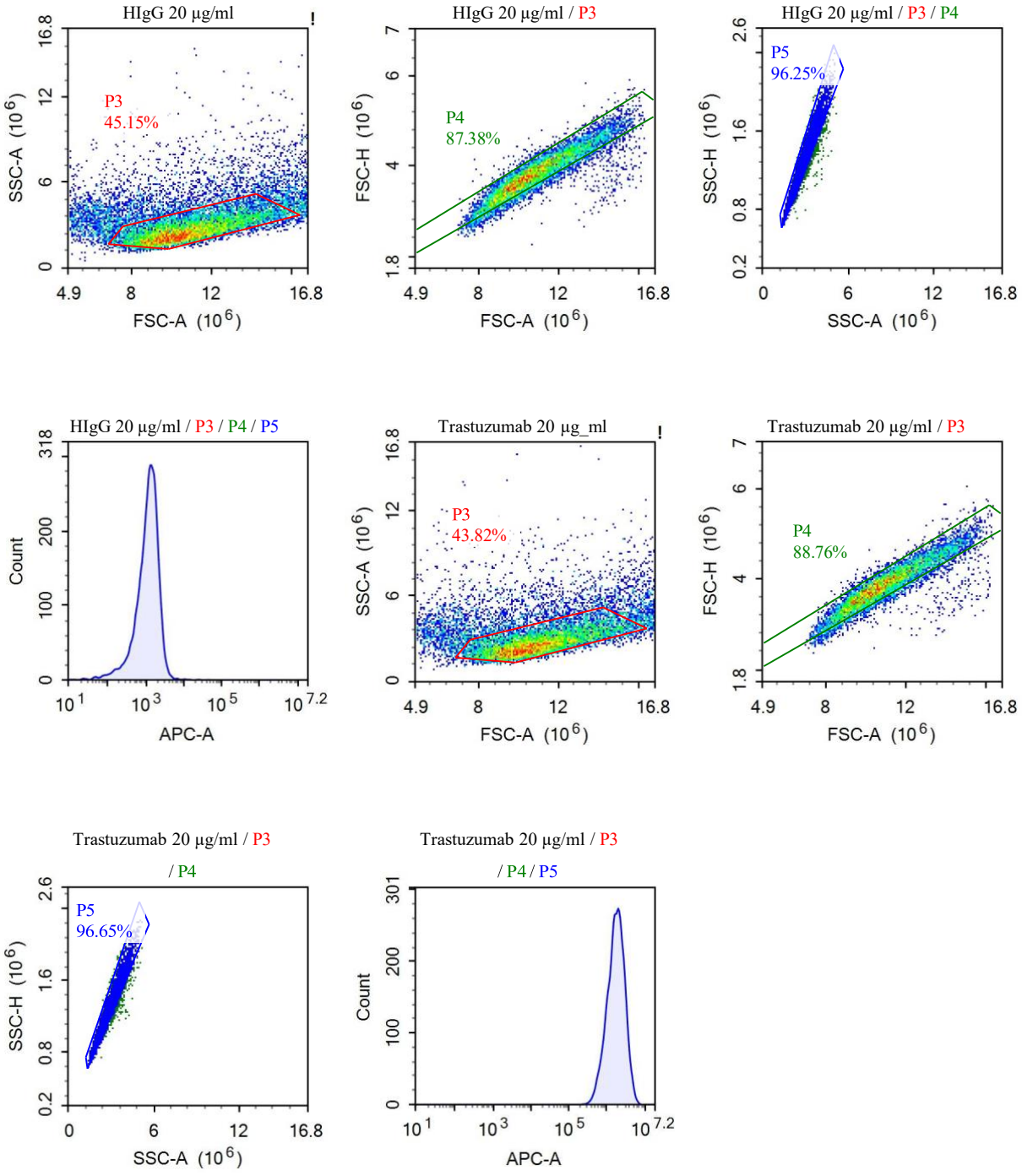

HCC1954 qFACS gating